Nanoparticle-mediated drug therapy against tuberculosis in the zebrafish embryo model

Nils-Jørgen Knudsen Dal

Thesis for the Master of Science degree in Molecular Biosciences

Department of Biosciences
Faculty of Mathematics and Natural Sciences

UNIVERSITY OF OSLO

May 2018

2018

Nanoparticle-mediated drug therapy against tuberculosis in the zebrafish embryo model

Nils-Jørgen Knudsen Dal

http://www.duo.uio.no/

Trykk: Reprosentralen, Universitetet i Oslo

Acknowledgements

First and foremost, I would like to express my sincere gratitude to my main supervisor, Professor Gareth Griffiths. Thank you for giving me the opportunity to do my master's degree in your group and for inspiring me to pursue a career within science. I would also like to express my appreciation to my co-supervisor, Dr. Federico Fenaroli. Thank you for all the help, instructions, inspiration, as well as all the exciting and challenging discussions on various topics we have had. Thanks also to Dr. Martin Speth for teaching me how to work with mammalian cells and for challenging my thought processes with your natural skepticism. Thank you Dr. Julien Resseguier, for the beautiful cryostat-images of zebrafish you provided, a great contribution. I am also grateful to all that have been a member of the Griffiths group during my time here. Thank you Urska Repnik, Bård Mathiesen, Matthew Yoke Wui NG and Agnese Kocere for your contributions. In addition, a big thanks to the EM-imaging facility here at UiO, especially Norbert Roos and Antje Hofgaard.

This thesis is based on a collaboration project and all that play a part deserves my gratitude. I would especially express my appreciation to Matthias Barz and Kerstin Johann for making the polymeric micelle nanoparticles, to Bruno De Geest and Simon Van Herck for making the polymeric nanoparticles, to David Russell and Yitian Xu for performing the mouse experiments. Thank you Dr. Andrew Thompson, for synthesizing the novel-drugs used, helping me understand them and for being so kind to read my thesis and always offer answers when I ask questions.

Big thanks to my friends that I have got to know over the last five years, you are amazing!

At the end, I would like to express my appreciation to my family that always support and encourage me. A warm thanks to my parents Irene and Gard, my grandparents Britt and Nils, and of course my brothers John-Kristian and Jostein.

Finally, Christina, thank you for putting up with me, for all your love, support, conversations as well as discussions. I am incredibly grateful for having you in my life.

Abstract

Mycobacterium tuberculosis (*M.tb*), the primary agent of human tuberculosis (TB), is a global problem of pandemic dimensions, despite the introduction of antibiotics against the disease happened more than 70 years ago. Today TB is the largest cause of death by a single infectious agent. Harsh and inadequate treatment often associated with lack of patient compliance, has in the past two decades led to the emergence of drug-resistant TB, which is hard to treat successfully. However, this negative development has in turn attracted significant attention in the field and consequently resulted in an increase in funding and research of new antibiotics against TB. One of the new drugs developed is pretomanid, a hydrophobic compound formerly known as PA-824. The drug is currently in phase III clinical trials and have displayed great promise. An important property of pretomanid is its ability to kill replicating, as well as non-replicating bacteria. The latter, being associated with persister bacilli, the main reason for why it is so difficult to eradicate TB completely. With the aim of improving the effectiveness of pretomanid against TB, in the last decade, approximately one thousand second-generation analogues have been synthesized and evaluated. The work described in this thesis investigates the therapeutic effect of a selection of these analogues, and more specifically the potential benefit of nanoparticle (NP) encapsulation. Although NP-based delivery of drugs is a relatively new field, there are several studies reporting on improved therapeutic outcome and lowering of toxicity when compared to free drug delivery. The NP-based approach is especially interesting with respect to hydrophobic compounds with poor oral bioavailability.

Our work is performed using the embryonic zebrafish model for fish-TB (caused by *Mycobacterium marinum*, *M.m*) as an initial platform for rapid screening of the efficacy and general safety of the compounds. Based on these results, testing is then moved on to preclinical model, the mouse. In the zebrafish embryo, we observed a significant therapeutic effect when the compounds were in NP formulation. The free form of the hydrophobic drugs was extremely difficult to administer, and therefore only one of the compounds could be thoroughly examined as a free drug. Nevertheless, for this compound, the NP formulation was superior in fighting against the infection. Finally, this thesis describes the establishment of a new model for studying the fitness of *M.m* during TB infection by using the zebrafish embryo in combination with *M.m* expressing two fluorescent proteins.

Selected abbreviations

ATc (Anhydrotetracycline)

BCG (Bacille Calmette-Guérin)

BSA (Bovine serum albumin)

BSL (Biosafety level)

CFU (Colony forming units)

CMC (Critical micelle concentration)

DLS (Dynamic light scattering)

DMSO (Dimethyl sulfoxide)

Dox (Doxycycline)

Emb (Ethambutol)

FDA (American food and drug administration)

FPC (Fluorescence pixel count)

GFP (Green fluorescent protein)

INF + UT (Infected and untreated zebrafish embryos)

Inh (Isoniazid)

M.m (*Mycobacterium marinum*)

MPEO-b-PCL (Monomethoxypoly(ethylene oxide)-block- polycaprolactone)

M.tb (*Mycobacterium tuberculosis*)

MDR-TB (Multi-drug resistant tuberculosis)

MIC (Minimum inhibitory concentration)

mKO (Monomeric Kusabira Orange)

MTBC (*Mycobacterium tuberculosis* complex)

NP (Nanoparticle)

OD_{600} (Optical density at 600 nm)

PBS (Phosphate buffered saline)

PDI (Polydispersity index)

PEG (Poly (ethylene glycol))

PFA (Para-formaldehyde)

PGlu-b-PSar (Poly glutamine-block-poly sarcosine)

PLA (Polylactic acid)

PLGA (Poly (lactic-co-glycolic) acid)

PM (Polymeric micelle)

PNP (Polymeric nanoparticle)

PTU (N-Phenylthiourea)

PVP (Polyvinyl pyrrolidone)

Pza (Pyrazinamide)

Rif (Rifampicin)

SD (Standard deviation)

SEM (Standard error of the mean)

TB (Tuberculosis)

TDR-TB (Totally-drug resistant tuberculosis)

TEM (Transmission electron microscopy)

Tet (Tetracycline)

Tween 80 (Polyoxyethylene (20) sorbitan monooleate)

UF + UT (Uninfected and untreated zebrafish embryos)

WHO (World Health Organization)

Wt (Wild type)

w/v (Weight/volume)

XDR-TB (Extensively-drug resistant tuberculosis)

Table of Contents

1 Introduction

1.1 Tuberculosis

1.1.1 White plague, the history of tuberculosis

For many people living in industrialized countries today the disease known as tuberculosis (TB) may sound like a relic from the last century. This is unfortunately far from the truth.

The history of tuberculosis, as a disease in humans, dates back to the dawn of man. It has been hypothesized that the genus *Mycobacterium* was generated 150 million years ago [1]. However, this timeline is being challenged based on modern genetic analyses [2]. *Mycobacterium tuberculosis* (*M.tb*) is part of the *Mycobacterium tuberculosis* complex (MTBC), a group of genetically related *Mycobacteria* species that are able to cause TB in humans and other animals. In addition to *M.tb*, the members of MTBC are *M. africanum*, *M. bovis*, *M. canettii*, *M. caprae*, *M. microti*, *M. orygis*, *M. pinnipedii*, *M. suricattae* and the recently identified *M. mungi* [3]. By means of genetic analyses, a tubercle bacillus causing TB in humans and found in East Africa, was discovered to represent an extant member of a broader progenitor species from which the MTBC evolved. Estimates based on genetic variation in housekeeping genes suggested that the tubercle bacilli evolved roughly 3 million years ago, and therefore possibly caused TB in early humanoid species [4]. The members of MTBC that exist today share an extensive degree of genetic homogeneity [5, 6], even though they display differences in phenotype characteristics and choice of host. The modern strains of *M.tb*, such as H37Rv and CDC1551, probably evolved from a common progenitor bacteria more than 35,000 years ago [7]. There is clear evidence that TB has plagued humans since ancient times. Morphological and molecular evidence of TB has been found in human remains from ancient civilizations in diverse locations such Syria, Egypt and other Eastern Mediterranean regions and even in Peru, South America [8-11].

The impact of TB on human history is highlighted by its association with myths and superstitions. This is reflected in some of the many names given to the disease over the centuries. For instance, during the Middle Ages in France and England, scrofula, a form of TB affecting the cervical lymph nodes, was referred to as “king’s evil”. It was believed that it could be cured by the touch of a royal [12]. Other historical names given to TB are more poetic, like "white plague" or "consumption" given during the 1700s and "Captain of All These Men of Death" introduced about 100 years later. These names reflected the bizarre romanticizing of the disease that took place at that time, when an epidemic swept over Europe and North America causing thousands of deaths, especially in the major cities [13]. During the 1800s, several strides were taken toward understanding TB and eventually finding a cure. In 1804, the French physician René Théophile Hyacinthe Laennec was the first to suggest that the term "tuberculosis" should be applied to all diseases characterized by the presence of lesions called tubercles, regardless of which organ was affected. In 1819, he published a book where he described in detail the pathology of TB, which provided new and important insights about the disease [14]. Another landmark in understanding the pathology of TB was the evidence provided by the French military surgeon Jean-Antoine Villemin that TB was an infectious, and not a hereditary disease. In 1865, he injected a rabbit with a liquid, extracted from the lung of an infected person that had succumbed to TB. The rabbit was found to be infected when it was later sacrificed and autopsied [13]. The major breakthrough came in 1882, when Robert Koch found *M.tb* to be the causative agent of TB [15]. He was later (1905) awarded the Noble Prize in Medicine or Physiology for this discovery.

After Koch's discoveries, progress within the TB field continued further. At the beginning of the 20th century, a new technique was developed to diagnose TB [13], which today is referred to as the tuberculin skin test (TST). The method is based on a sub-cutaneous injection of tuberculin, a purified protein derivative (PPD) isolated from *M.tb* [16]. A person infected with TB will show a larger skin reaction, because of a greater immune response against tuberculin, compared to a non-infected individual [16]. The only vaccine against TB was also developed in the first part of the 20th century. The vaccine strain was generated from the bovine pathogen *M. bovis*, which was attenuated by continuous culturing for more than a decade. This vaccine strain was named Bacille Calmette-Guérin (BCG) in honor of the two Paris microbiologists who made the new vaccine [17]. It was showed to be non-virulent in all animal models tested and displayed protection against TB infection [17]. In 1921, BCG was tested for the first time in a human. This was a baby boy whose mother died of TB shortly after birth and who was then handed over to his grandmother, who also suffered from TB. The baby survived, and showed no signs of TB growing up, and in the following years several clinical trials were conducted using the vaccine [17]. The attenuated phenotype of BCG was later determined to have occurred because of deletions of several genomic regions responsible for virulence [18]. In particular, the Region of Difference 1 (RD1), that encodes for the secreted virulence factors ESAT-6 and

CFP-10, including the secretion system ESX-1 that is essential for virulence, which is absent in all sub-strains of BCG [19, 20].

At the beginning of the second half of the 20th century, a new revolution took place with the discoveries of several antibiotics against TB. During World War II, the first antibiotic against TB was introduced, para-amino salicylic acid (PAS), which was later found to be bacteriostatic and not very effective by itself [13]. The first effective bactericidal TB-antibiotic was isolated in 1944 and named streptomycin (SM) [21]. This was followed by the discovery of isoniazid (INH) in 1952 [13]. A new chapter in the history of TB had started.

1.1.2 Global burden of tuberculosis today

Improved living standards, e.g. better housing, nutrition and hygiene, combined with the introduction of effective antibiotic treatments against *M.tb* in the mid-1900s, drastically reduced the global burden of TB [22]. Despite this progress, poor diagnostics, lack of sufficient medical treatment, failure of compliance in use of the antibiotics provided, and development of drug resistance are problems associated with TB today. Consequently, TB is still one of the major health threats among infectious diseases worldwide. It is the ninth largest cause of death in the world, and the leading cause when it comes to death by a single infectious agent [23].

According to the World Health Organization (WHO), Global TB Report 2017, 10.4 million people fell ill from TB in 2016. Out of this number, 90 % were adults, 65 % were male and 10 % were HIV-positive. The latter group is much larger in Africa and Asia compared to the world overall [23]. Estimates say that close to 1.7 million succumbed to the disease in 2016; 20 % of these patients were co-infected with the HIV virus, a situation that makes treatment even more difficult [23]. The highest incidence rates of TB infection are found in developing countries, especially in sub-Saharan Africa and Southeast Asia (Fig. 1.1). In addition it is estimated that 25-30 % of the human population are carriers of latent TB [24], which is defined as positivity to an immunologic test for *M.tb*, e.g., TST or the newer interferon gamma release assay, without displaying any symptoms of the disease. There is a consensus among scientists that, during latent TB, the bacterial population is usually in a low metabolic state and does not replicate [25]. However, it is difficult to find direct evidence supporting this hypothesis.

According to the consensus, 5-10 % of individuals infected by *M.tb* develop active primary (first infection) TB shortly after exposure [26]. The majority of infected individuals are able to contain the infection in the presumed latent stage, with a lifetime risk of 10 % for reactivation and development of secondary TB (see next paragraph) [25, 27, 28]. The risk of active primary TB or secondary TB, either through reactivation of latent stage, or reinfection, increases among groups that are immunocompromised, e.g., HIV-positive individuals [29].

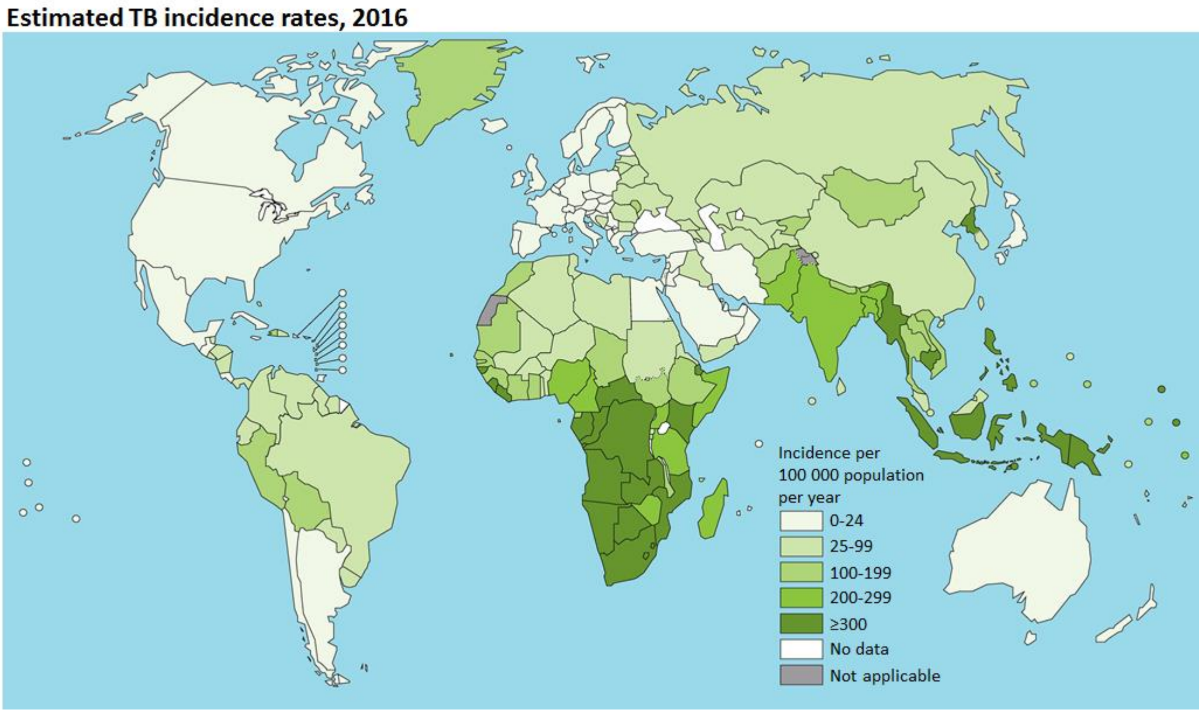

Figure 1.1: *Global overview of TB incidence rates in 2016. TB incidence rate was defined as the number of new cases of active TB disease in a given population during a year. Figure modified from "Global tuberculosis report 2017" [23].*

The WHO and the United Nations (UN) effort toward ending the TB epidemic has been articulated as defined goals, including a reduction of TB deaths by 35 % and a 20 % reduction of TB incidence by the year 2020. In addition, another focus is on affordable treatment, so that families do not suffer economically when battling the disease. By the year 2030, the objective is to reduce deaths and incidence of TB by 90 % and 80 %, respectively, compared to the numbers reported in 2015. Today, the progress towards ending TB is considered to be moving too slow [23] and therefore, the need for more research, capital and general effort is of great importance.

1.1.3 Initiation of tuberculosis infection and the assembly of granulomas

M.tb is a rod-shaped bacterium that is non-motile and aerobic; it can survive but not grow in anaerobic conditions. The bacteria are characterized by a thick, tough and waxy cell wall, primarily built up of mycolic acids. This cell wall makes the bacteria difficult to kill using antibiotics [30]. Human TB, primarily caused by *M.tb*, is naturally transmitted by air. The route of infection starts when an individual, suffering from an active TB infection, coughs and thereby releases bacteria from the lungs, suspended in small droplets of sputum, out into the air that subsequently become inhaled by another individual [31].

Studies performed using a rabbit model of TB have shown that fine droplets, containing 1-3 bacteria, are most prone toward establishing the infection [32]. This is because such small droplets will reach the alveolar spaces, the preferred site of infection. In contrast, larger droplets tend to get trapped on the mucosal surfaces along the airway, and are moved upwards by cilia and then swallowed [31]. If tubercle bacilli reach the alveolar space, one of two scenarios can occur. The alveolar macrophages, part of the innate immune system and first-line of defense in the lungs, phagocytose and kill off the bacteria and can thereby end the infection. This outcome will leave no trace of disease, and a tuberculin skin test will appear negative. In the other scenario, the bacteria survive and replicate within macrophages [31]. Two factors govern which of these two outcomes occurs: the number and phenotype of the inhaled tubercle bacilli and the bactericidal capacity of the alveolar macrophages [31]. The TB bacilli are not a uniform population, but vary in virulence and therefore in their capacity to initiate an infection. Similarly, the alveolar macrophages vary in their ability to kill the tubercle bacteria [31]. Sub-classes of alveolar macrophages that are rich in enzymes and microbicidal factors will more effectively destroy the tubercle bacilli in contrast to those alveolar macrophages that happen to be poor in both [31, 33].

There is a delicate balance between the ability of the bacteria to infect and the alveolar macrophages to kill. Therefore, in order to initiate an infection (at least according to prevailing theories), a highly virulent tubercle bacillus needs to be ingested by a “weak” alveolar macrophage, then survive and replicate, eventually rupturing the host cell and freeing the bacteria [31]. This leads to a local pro-inflammatory response, which causes the recruitment of monocytes from the blood stream to the site of infection, where they differentiate into dendritic cells (DCs) or macrophages [34], and subsequently take up bacteria via phagocytosis. The newly differentiated cells do not kill the ingested bacteria effectively, thus allowing intracellular replication once again [31]. At this stage, the bacteria grow exponentially and more monocytes and alveolar macrophages are recruited to the infection site. After a delay, infected DCs migrate to the local lymph nodes, where they activate the adaptive immune response by presenting *M.tb* specific antigens to naïve T-cells [35]. A hallmark of TB is the slow onset of adaptive immunity [35]. Experiments done in mice have shown a delayed onset of the T-cell response against TB, compared to other infections. In an acute, resolving infection, such as influenza, the T-cell response is activated after a few days and peaks about one week post-infection [36]. In the case of TB however, it takes over a week for the T-cell response to be activated, and several weeks before reaching full effect [37]. The accumulation and aggregation of various immune cells at the infection site leads to the formation of a lesion, referred to as the granuloma, a major hallmark of TB [31, 38]. The granuloma becomes tightly packed and organized as it progresses in size; key features of human granulomas are caseous necrosis and areas with hypoxic conditions [39]. Fig. 1.2 depicts an illustration of a typical human pulmonary granuloma.

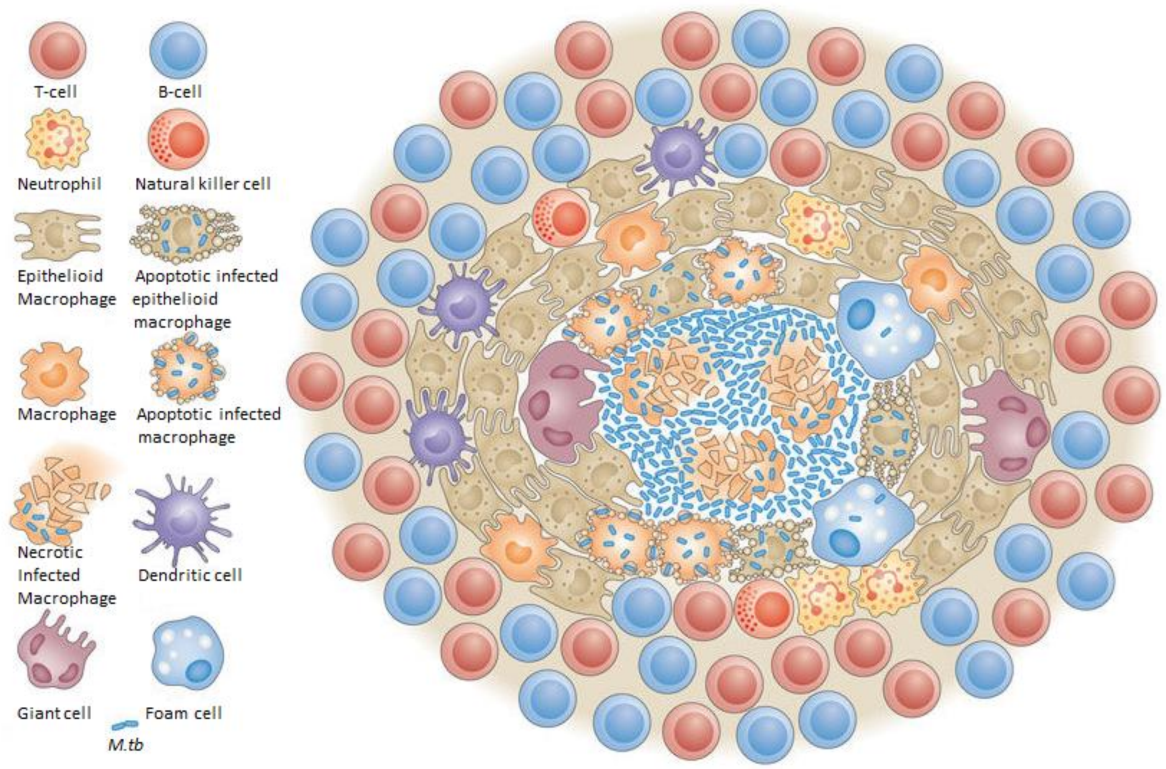

Figure 1.2: *Schematic illustration of a typical granuloma: Macrophages undergo maturation in response to the infection and differentiate into granuloma-specific cells, such as epithelioid macrophages that link adjacent cells, or foamy macrophages rich in lipid droplets. Macrophages can also fuse and become multi-nucleated giant cells. M.tb are at highest number in the necrotic core, inside*

and outside dead and dying macrophages. Neutrophils, natural killer cells, dendritic cells B- and T-cells occupy the granuloma in addition to fibroblasts that help build up the extracellular matrix and epithelial cells surrounding the whole structure (latter two cell types not shown). Figure modified from [39].

The classical view of granuloma formation as an exclusively host-protective response, which serves its function by containing the infection as a result of the attempt to eliminate the threat, has recently been challenged [39]. Studies performed in zebrafish embryos imply that the bacteria promote granuloma formation in order to proliferate, and seed new granulomas via infected macrophages escaping the structure [40-42], suggesting that the bacteria has evolved to take advantage of the granulomatous response.

1.1.4 Primary and secondary tuberculosis

Extensive research on the pathogenesis of human TB, focusing on pathology by autopsies of deceased individuals, came to an abrupt end in the 1950s when we entered the era of antibiotics. The research focus slowly shifted from pathology to molecular biology, immunology and genetics using new techniques and animal models. This advancement provided new and groundbreaking insights. The downside was that very little new knowledge was gained on the understanding of reactivation of latent infection and development of secondary TB, due to the difficulty of reproducing this form of the disease using an animal model [43]. Therefore, there is much controversy surrounding the pathogenesis of the different stages of TB. Presented below is a synopsis of the current thinking. Fig. 1.3 illustrates the general stages of TB, from transmission, to the development of active TB, and the risk in percent associated with entering the different stages.

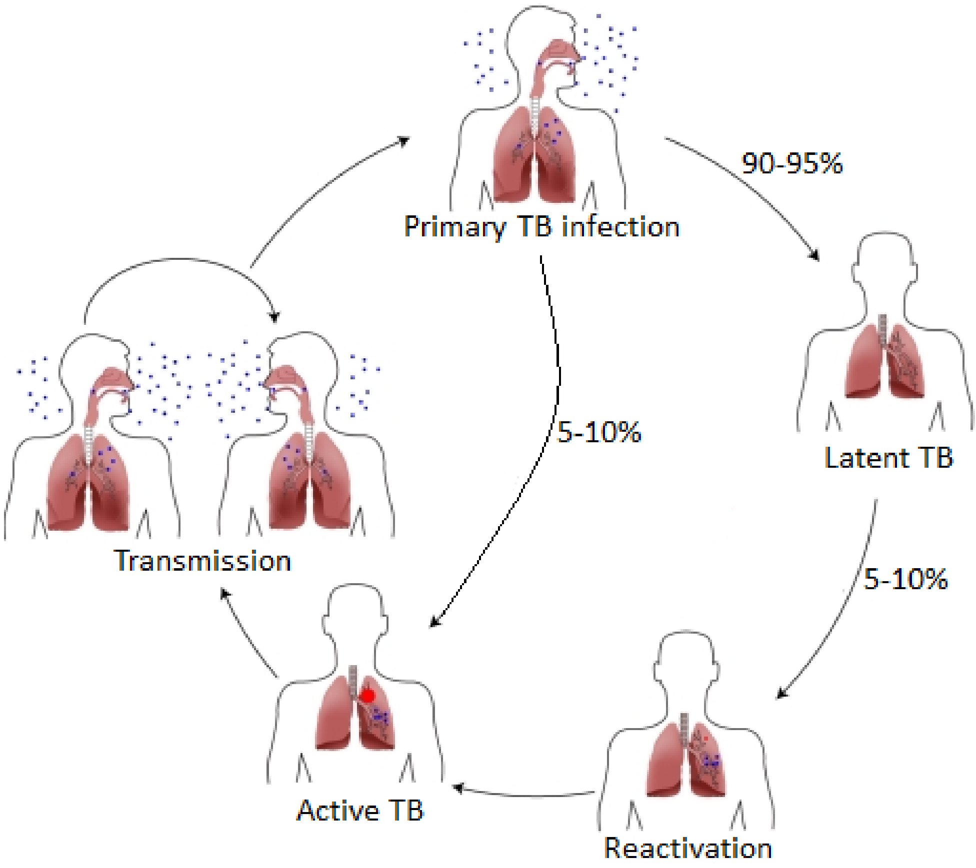

Figure 1.3: *The stages of TB infection and current consensus estimates of risk of developing active TB, either directly from a primary infection or through reactivation of a latent infection. Figure modified from [44].*

Primary TB, per definition first-time exposure and infection of *M.tb*, is established as a single granuloma, called a Ghon focus, situated sub-pleurally in the lower part of the upper lobes or upper part of the lower lobes of the lung [45, 46]. Usually the infection is arrested and enters a latent stage that can last for decades. Latency with respect to TB is a very elusive and somewhat vague concept, but the basic idea is that a group of bacteria reside within the granulomas and consists of either metabolically inactive (or low activity) bacteria, or active bacteria somehow kept in check by the immune system [25]. If the infection progresses into primary active TB, the disease usually manifests in the lungs as the granuloma grows in size, although hematogenous spread and subsequent extra-pulmonary TB sometimes occurs [31]. Progression of primary TB into active disease or latency is a constant battle between the tubercle bacilli, trying to multiply in numbers and disseminate, and the host immunity, trying to kill off the infection and contain it within granulomas. The lymph nodes can also become sites of infection; the combination of an enlarged lymph node and the primary granuloma is referred to as a Ghon complex [47]. The main hallmarks for primary active TB are the Ghon complex, granuloma formation, caseous necrosis, followed by arrest or progression of caseous granuloma into a cavity [47]. People with depressed or incompletely developed immunity are more prone to progress into primary active TB in comparison to immune-competent people [29, 31].

Secondary TB, defined as reactivation of latent infection, or secondary infection (reinfection), is responsible for ~80 % of all active TB cases, and almost all transmission of the infection [48]. The exact mechanisms behind reactivation are not known, but most likely the overall health of the patient in addition to local differences in oxygen, nutrients and pH between granulomas in the same lung and even within the same granuloma, play an important role in the activation of latent bacteria [49, 50]. Secondary TB usually manifests in the apices of the lungs [31], at some distance from the initial infection site, the Ghon focus. Secondary TB starts asymptomatically, with bacteria manipulating the alveolar macrophages they reside in and helping to transform them into foamy macrophages that are loaded with lipid droplets [51].

The foamy macrophages that are prominent in granulomas provide nutrition to the bacteria and serve as safe havens, and are therefore a crucial component for progression of disease [51, 52]. Next follows bronchial obstruction, which creates an isolated area and facilitates accumulation of host lipids and mycobacterial antigens without causing a strong immune response [43, 53]. This accumulation of antigens eventually leads to infiltration of lymphocytes, and the lesion grows and spreads via the bronchi, not the lymphatic system, as can be the case in primary TB. The fallout is usually regression of the lesion and subsequent healing. However, if the lesion progresses it can undergo necrosis that ends in caseous pneumonia. This can lead to tissue softening and cavity formation and eventually to the bacteria being coughed out. In secondary TB, granulomas are shown to form in response to pneumonia and cavity formation, instead of being the cause of them [43, 53].

1.1.5 The close relationship between *M. tuberculosis* and the macrophage

M.tb can survive and replicate extracellularly, but during the course of infection, it spends a major part of the life cycle inside macrophages. It is intriguing to consider the advantages and disadvantages for *M.tb* in this interaction. At the two extremes, the bacteria can replicate in macrophages, while at the other, these cells can kill the bacteria.

One advantage is that macrophages promote dissemination and spread of the infection across epithelial barriers [31]. In addition, studies show that *M.tb* gene expression is altered when inside macrophages. *M.tb* isolated from mouse macrophages display stronger virulence than bacteria cultured in cell-free media [54]. In order to take advantage of this specific niche, *M.tb* need to be taken up by the macrophage and adapt to the intracellular conditions, that are very different from the extracellular milieu. Uptake of the bacteria by the macrophage is done by phagocytosis, which can be defined as the uptake of particles with a diameter larger than 200-500 nm [55]. Phagocytosis is instigated by activation of various surface receptors through physical contact with corresponding ligands on the bacterial surface, which leads to trans-membrane signaling that in turns causes actin polymerization, a process that drives local extension of plasma membrane into pseudopod-like structures that engulf the target. The resulting phagosome undergoes so-called phagosome maturation, which includes fusion and fission events with endocytic organelles, leading to acidification and culminates in lysosome fusion, formation of the phagolysosome and degradation of the target [55].

M.tb has a wide assortment of mechanisms to promote phagocytosis by macrophages; among these, and of key importance, are bacterial components on the cell wall that directly bind macrophage surface receptors [56]. *M.tb* is also able to manipulate the normal phagosome maturation, and arrest the process before formation of the phagolysosome [57]. Several factors play a role in the arrest of phagosome maturation [58]. Various lipids in the bacterial cell wall, for instance lipoarabinomannan (LAM), are known to delay phagosome maturation [59]. The GTPase Rab5 and other Rabs on the phagosome surface are implicated in phagosome maturation and arrest, but the details are vague [60, 61]. Several other factors play a part in phagosome maturation and arrest as well, and it is therefore difficult to paint a clear picture of the situation. The outcome of the process is a topic of much debate, with findings ranging from no effect [62], to a bacteriostatic [63], or even bactericidal effect [64] if *M.tb* ends up in the lysosome. Regardless of this incomplete understanding of *M.tb* and its intracellular life, the fact is that the bacteria are extremely well adapted for survival and replication inside the macrophage.

1.1.6 Current drug regime and vaccine

TB is a difficult disease to treat, due to the bacterial robustness, adaptability and tendency to develop drug tolerance and resistance. In the 1950s and 60s, several new anti-TB drugs were discovered (Table 1.1) and put into clinical practice, and these discoveries led to a multiple-drug regimen to cure TB that required treatment for 18 months [65].

Table 1.1: *Main anti-TB drugs in clinical use and their targets with subsequent effect. Table modified from [65].*

Drug	Year introduced	Target	Effect
First-line drugs			
Isoniazid (Inh)	1952	Enoyl-[acyl-carrier-protein] reductase	Inhibits mycolic acid synthesis
Pyrazinamide (Pza)	1954	S1 component of 30S ribosomal subunit	Inhibits translation and trans-translation, acidifies cytoplasm
Ethambutol (Emb)	1961	Arabinosyl transferases	Inhibits arabinogalactan biosynthesis
Rifampicin (Rif)	1963	RNA polymerase, β-subunit	Inhibits transcription
Second-line drugs			
Para-amino salicylic acid (Pas)	1944	Dihydropteroate synthase	Inhibits folate biosynthesis
Streptomycin (Stm)	1944	S12 and 16S rRNA components of 30S ribosomal subunit	Inhibits protein synthesis
Cycloserine (Dcs)	1955	D-alanine racemase and ligase	Inhibits peptidoglycan synthesis
Kanamycin (Km)	1957	30S ribosomal subunit	Inhibits protein synthesis
Ethionamide (Eto)	1961	Enoyl-[acyl-carrier-protein] reductase	Inhibits mycolic acid synthesis
Capreomycin (Cm)	1963	Interbridge B2a between 30S and 50S ribosomal subunits	Inhibits protein synthesis
Amikacin (Amk)	1972	30S ribosomal subunit	Inhibits protein synthesis
Ofloxacin (Ofx)	1980	DNA gyrase and DNA topoisomerase	Inhibits DNA supercoiling

A joint effort between the Medical Research Council in the United Kingdom and United States Health Service (now CDC TB Trials Consortium), over several decades, followed this initial 18-month regimen and led to the development of today's 6-month "short-course" standard treatment against drug-susceptible TB [65]. The standard treatment consists of a four-drug therapy. The drugs are isoniazid (Inh), rifampicin (Rif), pyrazinamide (Pza) and ethambutol (Emb), where all four are given in daily doses for at least two months (intensive phase), followed by Inh and Rif only, for at least four months (continuation phase). With the rising prevalence of drug-resistant TB, this standard treatment is becoming increasingly inadequate [66, 67]. The WHO has implemented a control strategy for TB treatment, directly observed treatment short-course (DOTS), to aid in prevention of the development of drug-resistant TB. DOTS includes the administration of the standard treatment regimen under direct observation by trained health workers for at least the intensive phase of the treatment, in order to ensure patient compliance and lower the risk of developing drug resistance [66].

The only vaccine against TB in clinical practice today is BCG, described earlier. There is a consensus that is has some protective effect against TB in children [68], but the protection it offers adults is very much debated. Large field trials report protective effects ranging from 0-80 % in different countries. An ominous finding was the trend of having the lowest vaccine effect in the countries with the highest burden of TB [69].

1.1.7 Emergence of drug resistant tuberculosis

With time, and increasing exposure to antibiotics during treatment, pathogenic bacteria eventually acquire specific mutations in their genome, which confer drug resistance. This natural process limits the effective lifespan of antibiotics. Due to unnecessary or excessive use of drugs, failure of compliance with given drug-regimens, and the large-scale use of many antibiotics in the agricultural industry, the emergence of drug-resistant bacteria is a rapidly growing global concern [70]. This trend applies especially to *M.tb*. Multidrug resistant *M.tb* (MDR-TB), defined as resistance to Inh and Rif, the two most potent first-line drugs, was responsible for 490,000 cases of active-TB in 2016 [23]. Treatment of MDR-TB requires the use of more toxic drugs (with potentially severe adverse effects) in a lengthy drug-regime, with lower cure rates and higher mortality than for treatment of drug-susceptible TB [71, 72]. In addition, these treatments are more costly than those involving only first-line drugs [73]. MDR-TB has also evolved into the more serious form termed extensively drug resistant TB (XDR-TB), defined as being resistant to Inh, Rif, at least one drug in the fluoroquinolone group and also at least one of the second-line injectables: amikacin, capreomycin or kanamycin (Table 1.2) [23]. Needless to say, this form of TB is highly lethal and difficult to treat. To further worsen the situation, in 2009, a new form of drug resistant TB was observed in several countries, termed totally drug-resistant TB (TDR-TB), defined as being resistant to all first- and second-line drugs, both oral and injectable [74].

Table 1.2: *Anti-TB drugs categorized in groups according to efficacy against drug-susceptible or drug-resistant TB. Table modified from [65].*

Categorization; line, group & application	Drug name and route of administration
First-line drugs; Treatment for drug-susceptible TB	
Group 1.	Oral: isoniazid, rifampicin, pyrazinamide, ethambutol, rifapentine, rifabutin
Second-line drugs; Treatment of drug-resistant TB	
Group 2.	Injectable aminoglycosides: streptomycin, kanamycin, amikacin
	Injectable polypeptides: capreomycin, viomycin
Group 3.	Oral & injectable fluoroquinolones: ciprofloxacin, levofloxacin, moxifloxacin, ofloxacin, gatifloxacin
Group 4.	Oral: para-amino salicylic acid, cycloserine, terizidone, ethionamide, prothionamide, thioacetazone, linezolid
Third-line; unclear efficacy or undefined roles	
Group 5.	Clofazimine, amoxicillin plus clavulanate, imipenem plus cilastatin, clarithromycin

M.tb is a slow growing bacterium with a long generation time (usually dividing once every 24 hour), low mutation rate, no evidence of horizontal gene transfer amongst themselves or with other bacterial species, and no known natural reservoir except from the human host [75]. The emergence of genetic resistance in mycobacteria therefore occurs *de novo* as spontaneous mutations in genes directly or indirectly involved with specific antibiotics. For instance, a mutation could end in a conformational change in the translated protein, which might drastically decrease the binding affinity of the antibiotic targeting the protein in question, resulting in resistance. Aside from drug resistance, drug-tolerance is a problem associated with the treatment of TB. Drug-tolerant, persistent *M.tb* are genetically identical to drug susceptible bacteria, but they are somehow able to endure the antibiotic treatment and survive [76]; persistence and tolerance usually refer to the same phenomenon.

There are two possible, non-mutually exclusive, explanations for drug-tolerant, persistent *M.tb*. (1) The bacteria are protected by the relatively isolated granuloma they reside in, and by spending parts of their life cycle inside macrophages. Because of the difficulties for the drug to penetrate and accumulate within the granuloma, sub-therapeutic drug concentrations result, which facilitates survival. (2) A sub-population of bacteria can also acquire a phenotypic adaptation; for instance via up-regulation of efflux pumps that actively pump antibiotics out of the bacteria [77]. Studies suggest that the actual drug tolerance (bacterial persistence) observed is a combination of the two explanations outlined above [78].

1.2 The need for new and better drugs

1.2.1 New antimicrobial agents to fight tuberculosis

The treatment regime for drug-susceptible TB has been the same for the last four decades. Therefore, because of the problems outlined above, there is a desperate need for new drugs for improved TB therapy. The main goals of these new drugs are the shortening of treatment regimens, and increasing the therapeutic effect against drug-resistant TB. The global cure rate is only about 50 % for MDR-TB and only 30 % for XDR-TB [23]. However, there has been significant recent progress toward new drugs, due to the growing attention and extensive research done on over the last two decades. Now there are 17 anti-TB drugs in clinical trials, 10 new drugs and 7 repurposed ones (Fig. 1.4). Among the new drugs, three are in phase III clinical trials, bedaquiline, delamanid and pretomanid (formerly known as PA-824). Bedaquiline and delamanid are also in restricted clinical use against MDR-TB because of accelerated and conditional regulatory approval based on positive results in phase II clinical trials [23].

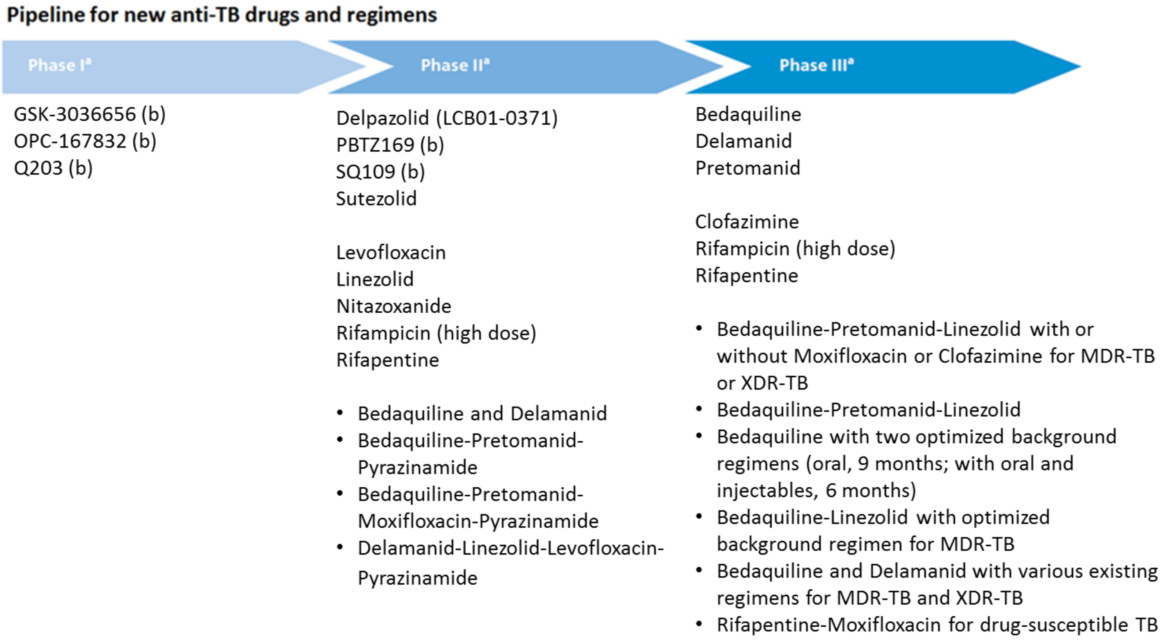

Figure 1.4: *Pipeline for new anti-TB drugs and regimens, divided into phase I, II and III. (a) Listed vertically from top to bottom; new drug, repurposed drug and lastly combined regimens. (b) Indicate drugs of a new chemical class. Figure modified from [23].*

1.2.2 Pretomanid and analogues

The road toward development of pretomanid and its analogues (Fig.1.5) started with cancer research. In 1979, a paper exploring the potential use of nitroimidazoles as radio-sensitizing agents in cancer treatment was published [79]. An analogue of the bicyclic compound reported in the cancer paper was later found to be active against *M.tb* both *in vitro* and *in vivo* (using mice), as were several other similar derivatives [80]. The lead compound was named CGI-17341 and was closer examined for activity against *M.tb* [81]. However, CGI-17341 was found to be mutagenic and further research on the compound and other analogues was halted, with the hope that chemical modifications could result in a new and safer compound [80]. Based on the structure of CGI-17341, Stover et al. synthesized a series of 3-substituded nitroimidazopyran (NAP) compounds [82]. Several of the NAPs were found to possess anti-tubercular activity without being mutagenic and, among them, a compound with sub-micromolar inhibitory effect against *M.tb* was found and named PA-824 [82]. The minimum inhibitory concentration (MIC) of PA-824 ranged from 0.015-0.25 µg/mL in drug-susceptible and drug-resistant *M.tb* strains, and this compound showed no cross-resistance with conventional anti-TB drugs. In addition, PA-824 displayed activity against non-replicating bacteria in hypoxic conditions, indicating a second effect that was different from killing replicating bacteria. The *in vivo* anti-tubercular efficacy of PA-824 was also demonstrated following oral administration to mice and guinea pigs infected with *M.tb,* as was its safety [82].

PA-824, from now on referred to as pretomanid, is a pro-drug that requires activation in *M.tb* by a cofactor-F_{420} dependent nitroreductase (Ddn) [83]. Pretomanid has a complex and not fully understood mechanism of action, and is effective in both aerobic and anaerobic conditions [84]. The original study on pretomanid found it to interfere with mycolic acid synthesis by inhibiting the conversion of the precursor hydroxymycolate into ketomycolate [82]. This mechanism provides an explanation for the activity against replicating bacteria, but not against non-replicating bacteria. It was later shown that pretomanid activation by Ddn converted the drug into three (inactive) primary metabolites, including the des-nitroimidazole derivative, and also cogenerated reactive nitrogen species such as nitric oxide (NO), which is known to have bactericidal capacity, especially against *M.tb* [85]. A recent study discovered an additional mode of action against both replicating and non-replicating bacteria, by comparing the metabolome of *M. smegmatis* cultures after exposure to pretomanid or other anti-TB drugs [86]. *M. smegmatis* is genetically similar to *M.tb*, and commonly used as a model for research on anti-TB drugs. The study observed a unique metabolome profile for bacteria treated with pretomanid and, in particular, increased levels of the toxic molecule methylglyoxal. This may be a consequence of pretomanid metabolism by a known homologue of Ddn in *M. smegmatis,* catalyzed by the cofactor F_{420}. The reductive form of F_{420} is involved in phosphate sugar synthesis and activation of this pathway leads to the accumulation of phosphate sugars, which in turn results in increased levels of toxic methylglyoxal [86].

The pretomanid analogues investigated in this thesis were made by our collaborator Dr. Andrew Thompson in Auckland, New Zealand, in an attempt to improve various drug-like properties, such as aqueous solubility, metabolic stability and anti-tubercular efficacy. We have investigated the *in vitro* and *in vivo* effects of four different analogues: 30485, 32625, 31354 and 32499. In this thesis, they are renamed for simplicity as drugs A, B, C and D, respectively. These four compounds have previously been tested *in vitro* and *in vivo* using the mouse *M.tb* model and all have shown improved efficacy compared to the parent compound, pretomanid [87-89]. Drug C (31354 or TBA-354) actually made it to human clinical trials phase I, but was discontinued due to mild signs of reversible neurotoxicity. A study in rats confirmed by mass spectrometric imaging that the drug crossed the blood-brain barrier [90]. In an attempt to improve free drug delivery in terms of toxicity and effectiveness, we proposed the investigation of NP-mediated delivery of these analogues to treat TB, in comparison to free formulation, using zebrafish embryos infected with *Mycobacterium marinum* (*M.m*) as a model system.

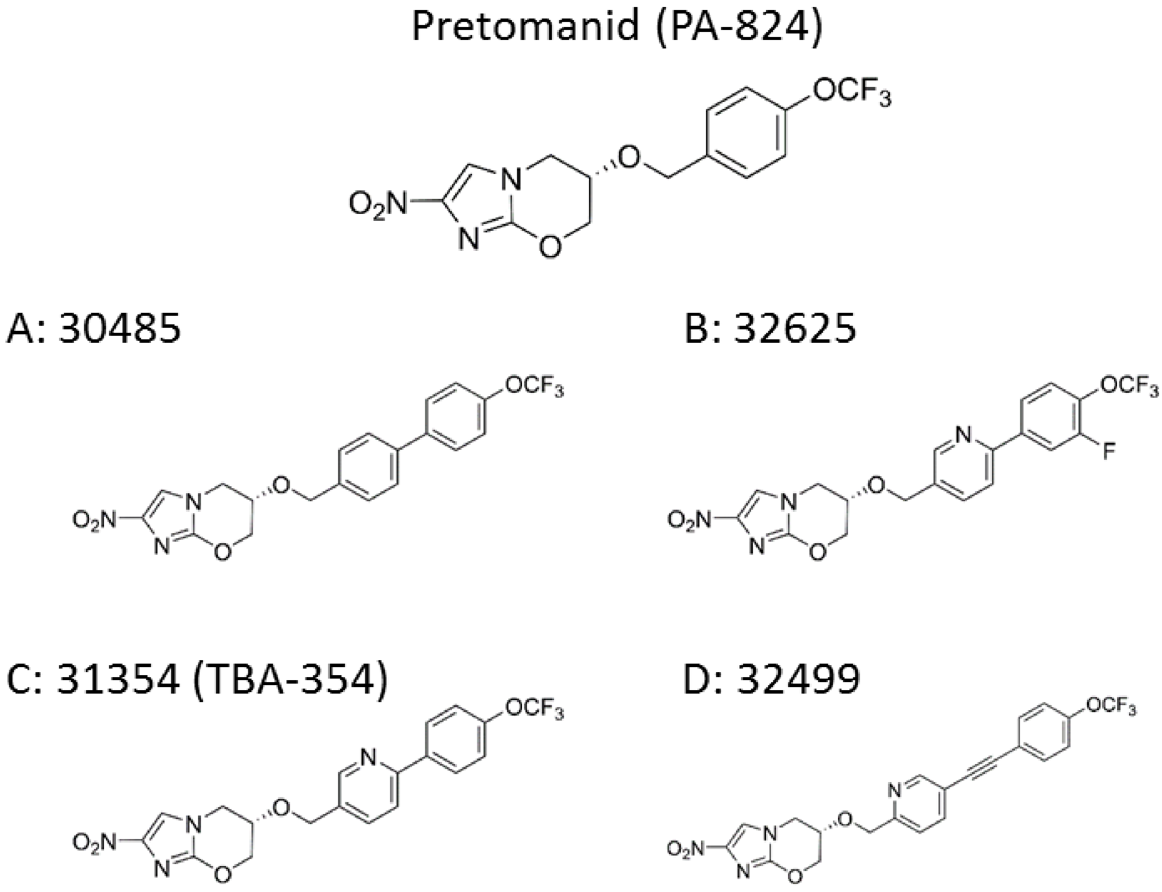

Figure 1.5: *Chemical structures of the parental drug pretomanid (formerly known as PA-824) and the four analogues described in this thesis. Each analogue is identified as a letter (A-D) and with a number. Drug C is additionally associated with a third name, TBA-354. Illustrations of chemical structures provided by Dr. Andrew Thompson.*

1.3 Nanoparticle mediated drug delivery

1.3.1 The concept of a novel approach

Conventional drug administration, e.g. via oral or intravenous routes, and subsequent systemic distribution is a well-established practice. The effect of the drug *in vivo* depends on the biopharmaceutical properties (e.g. solubility, stability and permeability), in addition to pharmacokinetic properties (e.g. half-life and clearance rate) [91]. Problems associated with conventional drug administration are systemic biodistribution and difficulties reaching the infection site (e.g. a highly structured granuloma), resulting in lower drug concentrations at the sites of infection and thereby a reduction in the therapeutic effect. Rapid clearance of drug from the body through liver or kidneys makes this problem even greater. Therefore, frequent drug dosing of relatively high concentrations, which often leads to adverse effects and/or patient non-compliance, is needed for satisfactory therapeutic effects [91, 92].

The idea of drug-carriers to treat different diseases by targeted delivery was first proposed by the great scientist and Nobel laureate Paul Ehrlich over a century ago. Because he was a medical doctor with immunology and bacteriology as fields of expertise, he envisioned something like antibodies to play the main role as target-seeking particles that he called “magic bullets” [93]. The nanoparticle (NP) field is relatively new and therefore some confusion exists regarding terminology. The definition used in this thesis is that NP range from 1-1000 nm in size diameter [93], and applies to all drug delivery systems within this size range (e.g. polymeric micelles). One of the great contributors and pioneers within the NP-field was Peter Paul Speiser. In the 1960s, his group worked on entrapment of drugs in non-toxic polymers in order to achieve sustained drug release [94], and developed the first polymer-based NP for drug and vaccine delivery [95]. Today, the NP-field has gained more interest, and although NP research has been directed mostly against cancer, other diseases have also been explored. Clinically approved NP-based therapeutics exist, such as doxorubicin (cancer medicine) and amphotericin B (against fungal and parasitic infections), both encapsulated in liposomes [96]. Because of the advantages and general interest in NP, many different types have been developed. Fig. 1.6 gives a schematic overview of some NP types.

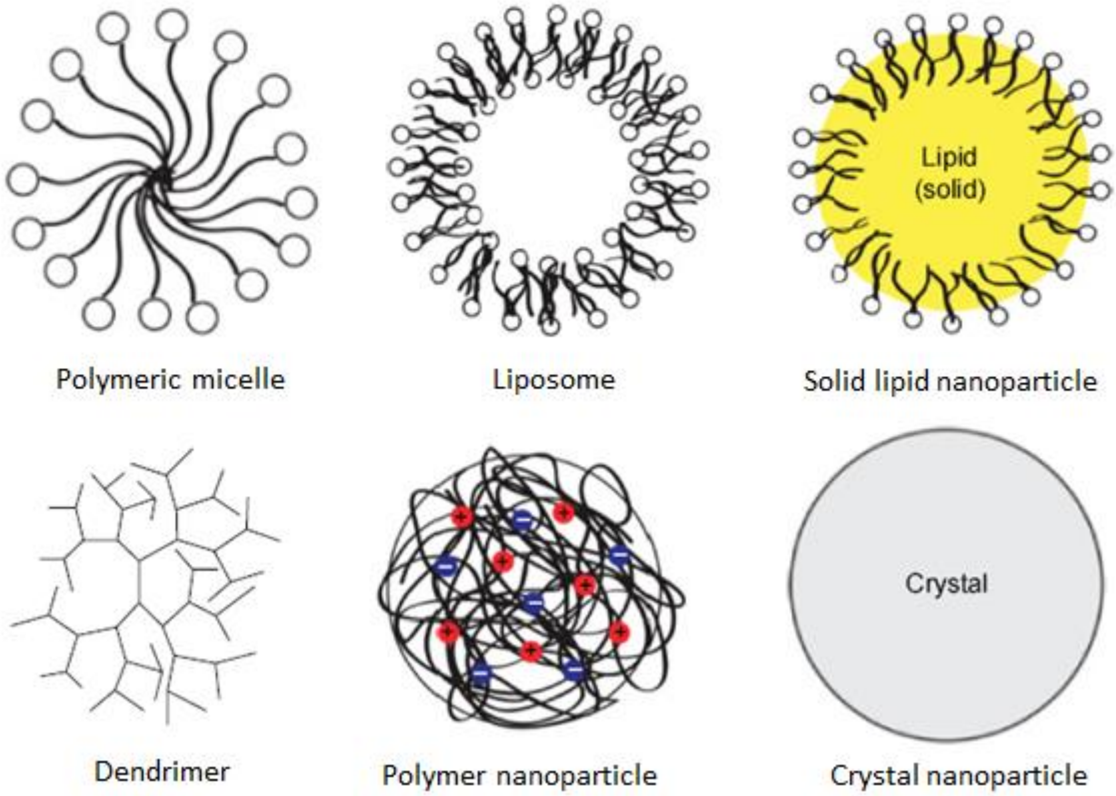

Figure 1.6: *Schematic presentation of general structures for a selection of NP types, including polymeric micelle NP and polymeric NP, which are both used in experiments described in this thesis. Figure modified from [97].*

The key arguments for NP formulation and delivery of drugs are: Controlled and sustained drug release, increased bioavailability, reduced toxicity due to fewer and smaller doses needed for therapeutic effects, and the potential for targeted delivery [98]. Targeted delivery can be defined as passive or active. Passive targeting involves accumulation of NP at the infection site without the aid of surface ligands for specific uptake, which is the case for active targeting [98].

Long-circulating NP are defined as NP that stay long in circulation by avoiding uptake by phagocytic cells due to their surface structure, e.g. by poly (ethylene glycol) brush on the surface (PEGylation) which creates a hydrated layer that lowers protein adsorption and consequently uptake by phagocytic cells [99]. These NP are found to passively accumulate to a higher degree at tumor sites compared to NP with a shorter circulation time [100]. This is most likely due to the enhanced permeability and retention (EPR) effect, discovered by Maeda and Matsumura in 1986 [101]. The EPR effect takes advantage of the fact that the vasculature adjacent to inflamed tissue loses integrity and become leaky, allowing drugs to diffuse out of the vasculature, accumulate in the tissue and display a long retention time. This effect is observed in cancer tumors [102]. Another form of passive targeting is short-circulating NP that are rapidly ingested by phagocytic cells in the bloodstream and subsequently migrate to the site of infection. This could be of interest when treating diseases caused by intracellular pathogens such as *M.tb* [103].

1.3.2 Tuberculosis and nanoparticles

Because of the inadequacies of conventional treatment of TB and the toxicities associated with it, the NP-based approach appears very attractive. Efforts have been made on NP-based approaches for treating different bacterial infections, including research on mycobacterial infections and the treatment of TB [103].

Apart from reducing toxicity, NP should also be considered because they naturally target and concentrate in macrophages, the niche of *M.tb* during infection [31]. The accumulation of proteins on the NP surface, referred to as a protein corona [104], facilitate uptake by phagocytes in the bloodstream, which represent potential host cells for *M.tb* [103]. NP-treatments against TB can exploit this feature for improved efficacy. *In vitro* experiments have shown that NP formulation of anti-TB drugs increases the intracellular drug concentration about 20-fold compared to the free formulation of the same drug in macrophages [105-107].

Cancer tumors and TB granulomas share many similarities, such as hypoxic microenvironments, fibrosis, angiogenesis and permeable surrounding vasculature [108], thereby suggesting that the EPR effect might work in favor for treatment of TB as well. The work by Oehlers et al. has introduced a new TB model, using zebrafish embryos infected with *M.m* via intraperitoneal injection in the trunk area [109]. Recent work from our group (Fenaroli et al., in revision, ACS Nano) has extended this model and shown that the injection site is in fact the neural tube (NT). Granulomas at this site are larger, become necrotic and form cavities that release bacteria to the outside world; they are, in general, more similar to human TB granulomas compared to the granulomas formed after intravenous injection of mycobacteria in the zebrafish embryo. In addition, the NT injection model has shown that NP and small molecules can accumulate in an EPR-like manner, such as observed in cancer.

These combined pathways give us two strategies for NP to accumulate in granulomas. (1) Short-circulating NP with direct uptake by macrophages and subsequent attraction to blood associated granulomas via chemotaxis [40]. (2) Long-circulating NP that avoid macrophages and accumulate by an EPR-like mechanism in neural tube granulomas (Fenaroli et al., in revision, ACS Nano).

The following two sub-chapters introduce the NP types used in this project, with special emphasis on their relevance concerning TB.

1.3.3 Polymeric micelle nanoparticles

Polymeric micelle NP (PM) are made of amphiphilic di-block co-polymers, which means that the polymer consists of a hydrophilic and a hydrophobic block. In water, above a certain concentration, defined as the critical micelle concentration (CMC), they will spontaneously self-assemble into core-shell structures [110]. The hydrophilic surface of the PM reduces protein adsorption and the formation of a protein corona of self-proteins, such as complement proteins and antibodies, which induces uptake via specific receptors on the surface of phagocytic cells [110]. First-generation PM, used in this project, are defined as PM with no core-crosslinking between polymers and/or covalent binding between drug and polymer [110]. The main advantage of first-generation PM is their capability for encapsulating hydrophobic drugs, thereby eliminating the need for excipients that often are associated with adverse side effects. Their main challenge, however, is poor stability *in vivo* due to dilution of the relative polymer concentration to below the CMC [110].

PM have been used to encapsulate anti-TB drugs, for example, PM encapsulation of the hydrophobic first-line drug Rif was reported in 2010 [111]. PM have later been shown to improve anti-TB drug delivery and effect against *M.tb* [112]. Less research has been performed using PM than polymeric NP in general, and this is also the case for TB research.

1.3.4 Polymeric nanoparticles

Polymeric NP (PNP) is considered an umbrella-term, sometimes referring to all types of NP made out of polymers [113]. In this thesis, the term specifically refers to particles with a solid porous matrix of interlaced polymer chains (Fig. 1.4), where the drug cargo can be dispersed within or adsorbed to the surface of the particle. The polymer used in this project to make the PNP is polylactic acid (PLA) combined with PEG. These PNP behave as long-circulating NP. Among the different types of PNP, poly (lactic-co-glycolic acid) NP, or simply PLGA-NP, are one of the most extensively studied and have shown beneficial effect against *M.tb* both *in vitro* and *in vivo*. Studies done in guinea pigs showed that three doses of the first-line drugs Inh, Rif and Pza, co-encapsulated in PLGA-NP, administered through the oral/aerosol route had the same effect against *M.tb* infection as 45 daily doses of the three drugs given orally in free formulation [114]. Similar results were also shown in mice [115]. Our group has performed studies with the same type of PNP in zebrafish embryos infected with *M.m*, and provided evidence of co-localization of PNP and bacteria within macrophages *in vivo* [116]. In the same study our group showed that uninfected macrophages that had taken up PNP could migrate from the bloodstream to the hindbrain ventricle, a chamber separated from the main circulatory system, when this was the site of bacterial injection and infection [116]. This attraction of macrophages to the site of infection is due to chemotaxis in response to chemokines released from dead and dying cells. *M.m* have been shown to promote recruitment of macrophages to the site of infection [40]. These observations illustrate the benefit of macrophage-targeted delivery of NP-based TB treatments.

1.4 Vertebrate and mammalian models of tuberculosis

1.4.1 Common mammalian model systems for tuberculosis

At a late stage during the development of new therapies and vaccines come clinical trials in humans, a time consuming and expensive enterprise. The use of a relevant animal model for testing before this stage is of great importance and an absolute requirement before new treatments and vaccines are to be tested in humans. Although *M.tb* is strictly a pathogen of humans [117], a good animal model can illuminate pathogen mechanisms and how it interacts with the host, and it can also enable efficient preclinical studies of new therapies and vaccines [118, 119]. In order to be a relevant model, the animal pathology should resemble the human pathology as closely as possible. Cost considerations and ethical concerns also play a major part. In the case of TB research, several animal models have been used. However, they vary in their ability to replicate different aspects of the human TB pathology, especially when it comes to latency and secondary TB [120]. This may reflect the fact that *M.tb* is a human-specific pathogen and no other natural animal reservoir exists that we know of [117, 121].

The most common model used for TB research is the **mouse**, a model that possesses several advantages: It is relatively cheap (at least compared to monkeys), mice respond to anti-TB drugs much like humans, it has a well-characterized genome, and several transgenic and knock-out strains are available [118, 122]. Still, in contrast to humans, the most commonly used mouse strains (C57BL/6 and BALB/c) fail to develop highly organized granulomas with caseous necrosis and local hypoxia [120]. However, in 1998, a mouse strain called C3HeB/FeJ was found to be highly susceptible to TB, without displaying other obvious signs of immunodeficiency, and to develop granulomas with a necrotic core. This strain is referred to as the “Kramnik” mouse model since it was first described in relation to TB infection by Igor Kramnik et al. [123]. The model is relatively new and is now gaining more acceptance and attention as a model for TB research [124, 125].

The **guinea pig** is another commonly used model that was used by Robert Koch himself when he discovered that *M.tb* was the causative agent of TB [15]. The guinea pig is highly susceptible to *M.tb* infection, it responds well to standard therapies, and displays a protective effect when vaccinated with BCG. However, the infection develops as a progressive tissue-destructive disease and does not display latent stage, as do 90 % of humans infected with *M.tb* [126].

The **rabbit**, like the guinea pig, also has a long history within the TB field. In 1898, Theobald Smith studied TB in rabbits infected with *M. bovis* or *M.tb*. Smith observed that the rabbits infected with *M. bovis* had a much higher mortality than those infected with *M.tb* [127]. In the 1920s, Lurie established the rabbit model for TB research, confirming these observations [128]. When using *M. bovis* or highly virulent *M.tb* strains, the model closely resembles human TB with regard to pathology, progression and immune response [129, 130].

The best model to study TB is the **cynomologus macaque,** a nonhuman primate. The model closely resembles all aspects human TB. However, due to obvious ethical and economic reasons, its use is limited [131, 132].

1.4.2 The zebrafish and its natural pathogen *Mycobacterium marinum*

The zebrafish (*Danio rerio*) is a small freshwater fish, native to the flood plains of the Ganges region in India [133]. In the early 1980s, George Streisinger, regarded as the father of the zebrafish model, developed a method for the production of homozygous diploid zebrafish [134]. Since then, it has become an important model for the study of embryonic development and various diseases [135]. There are several advantages with this model. Because of its small size, it is possible to keep large numbers at a low cost. The breeding of zebrafish can occur year round and generates big numbers of rapidly growing embryos, which are transparent in their early stages of development. Importantly, this animal model is relatively easy to manipulate genetically and, as a consequence, several transgenic strains are available [135]. The embryo is a rapidly developing organism and highly sensitive to exposure of toxic compounds and therefore a good indicator of drug toxicity [136]. The definition between zebrafish embryo and larvae stage varies in the literature. Usually the zebrafish is considered an embryo until it starts feeding by itself, which is considered day 5 post-fertilization. From then, the zebrafish is considered a larva until it is ready for reproduction, which usually occurs three months post-fertilization [137]. However, in this thesis, for simplicity, only the term embryo will be used when presenting data or discussing results.

M.m, a close relative of *M.tb* [138], is a natural pathogen and the causative agent of TB-like disease in ectotherms [139, 140], a group which includes all fish. These bacteria, by infecting macrophages, cause a systemic infection and induce granuloma formation in many ectothermic animals, making it a valuable tool for the study of TB [141]. In contrast to *M.tb*, which grows optimally at 37 °C, *M.m* has its temperature optimum at around 28-30 °C. Consequently, in humans with a body temperature of 37 °C, *M.m* can cause granulomas only in cooler superficial regions of the body (such as fingertips or elbows) rather than a systemic infection [142]. In addition, *M.m* grows relatively rapidly, with a generation time of 4-6 hours (h) versus >20 h for *M.tb* [143]. Research with *M.m* is attractive as *M.m* is considered only a biosafety level-2 (BSL-2) pathogen, in contrast to *M.tb*, which requires a BSL-3 facility [144].

The embryonic zebrafish model for TB was first established by Davis et al. in 2002 [42]. Thanks to the transparency of these embryos, it was possible to conveniently follow the progression and events that took place during the course of an infection *in vivo*, in real-time and with high resolution [42]. Zebrafish do not develop a fully effective adaptive immune system before 4-6 weeks post-fertilization [145], and therefore, prior to this period, the embryos rely exclusively on innate immunity, with macrophages and neutrophils in the frontline, to combat infections [146]. After intravenous injection of *M.m* in zebrafish embryos, granuloma-like structures of infected macrophages form, despite the lack of mature lymphocytes. These granulomas appear by histology to show some resemblance to granulomas from adult zebrafish and humans [42]. Nevertheless, I would like to emphasize that the granulomas that form in zebrafish embryos after injecting the bacteria into the blood are very small and relatively simple compared to millimeter size and highly stratified granulomas, which develop in humans.

The fact that embryos can form granuloma-like structures provided evidence that the innate immunity alone is sufficient to activate the granulomatous response. However, lymphocytes play a role in controlling the bacterial growth and burden at later stages in the infection [147]. These observations from the embryonic zebrafish model gave new insight about the pathogenesis of TB. Prior to this, it was long considered a dogma that the adaptive immune response was necessary for granuloma formation [148].

2 Aims of the study

This master's thesis had three main objectives:

i) My first objective was to establish and improve the zebrafish embryo model for TB as a screening system for rapid evaluation and selection of novel compounds aimed at TB therapy. Such a tool would allow a more efficient testing at the next level in mice, the classical preclinical model.

ii) More specifically, I intended to investigate the therapeutic potential of NP encapsulation of pretomanid analogues and to identify the most potent compounds.

iii) Finally, I aimed at the development of a model that would allow study of the TB granuloma dynamics in greater depth.

3 Materials and methods

3.1 Reagent list

Name	Supplier	Catalog number
96 % ethanol	Antibac AS, Asker, Norway	-
200 mesh hexagonal Cu grids	EMS, Hatfield, PA, USA	G200-Cu
300 mesh R1.2/1.3 Quantifoil grids	Quantifoil Micro Tools GmbH, Großlöbichau, Germany	-
Agarose, Low Melting Point	Promega, Madison, WI, USA	V2111
Anhydrotetracycline	Abcam, Cambridge, UK	Ab145350
Bovine Serum Albumin	Sigma-Aldrich, St. Louis, MO, USA	A4503-100g
Captisol®	Ligand Pharmaceuticals, San Diego, CA, USA	-
Catalase	Sigma-Aldrich, St. Louis, MO, USA	C9322
Chloroform	VWR, Radnor, PA, USA	22711.290
DAPI	Thermo Fisher Scientific, Waltham, MA, USA	D1306
D-Glucose	Merck & Co, Kenilworth, NJ, USA	1.08342.1000
Difco Middlebrook 7H9 broth	BD, Franklin Lakes, NJ, USA	271310
Difco Middlebrook 7H10 Agar	BD, Franklin Lakes, NJ, USA	262710
Dimethyl sulfoxide	Sigma-Aldrich, St. Louis, MO, USA	472301-1L
Doxycycline	Sigma-Aldrich, St. Louis, MO, USA	D-9891
Formvar	Agar Scientific, Essex, UK	R1201
Glycerol	Sigma-Aldrich, St. Louis, MO, USA	G7893-2L

Kanamycin	Sigma-Aldrich, St. Louis, MO, USA	70560-51-9
Liquid ethane	UiO, Oslo, Norway	-
Liquid nitrogen	UiO, Oslo, Norway	-
Mineral oil	Sigma-Aldrich, St. Louis, MO, USA	M3516-1L
N-Phenylthiourea	Sigma-Aldrich, St. Louis, MO, USA	P7629-10G
pGFPHYG	Addgene, Cambridge, MA, USA	30173
Phosphate buffered saline	UiO, Oslo, Norway	-
pmCherry::Myc/mKO	Cornell University, Ithaca, NY, USA	-
Poly(ethylene glycol)	Sigma-Aldrich, St. Louis, MO, USA	202398-250G
Polyvinyl pyrrolidone	EMD Biosciences, La Jolla, CA, USA	5295
Protease	Sigma-Aldrich, St. Louis, MO, USA	P8811-56
Rifampicin	Sigma-Aldrich, St. Louis, MO, USA	R3501-1G
SeaKem® LE Agarose	Lonza, Basel, Switzerland	50004
Tricaine-methanesulfonate	Argent Chemical Laboratories, Redmond, WA, USA	NDC051212-0001-3
Trizma base minimum	Sigma-Aldrich, St. Louis, MO, USA	038K5402
Tween 80	Merck & Co, Kenilworth, NJ, USA	8.22187.0500
Uranyl acetate	EMS, Hatfield, PA, USA	22400

3.2 Zebrafish husbandry

3.2.1 Maintenance and breeding

The zebrafish facility used by our group is located at the Norwegian University of Life Sciences (NMBU) in Oslo. Here the adult zebrafish were maintained and bred for embryo production. The fish were kept in a Benchtop Aquaria Rack System (Aquatic Habitats, FL, USA), with approximately three adult fish per liter of water. The water temperature was kept at 28 °C, and water quality, as specified in Table 3.1, was assured by mechanical filtration, bio-filtration and irradiation with UV light, in addition to a 10 % daily water turnover. Conductivity and pH were controlled at least three times per week plus weekly measurements of nitrite and nitrate levels. The light:dark cycle was 12:12 h year round, starting at 7 AM. Feeding occurred three times per day, once with dry-feed pellets and twice with brine shrimp.

Table 3.1: *Optimum water parameters for adult zebrafish maintenance. Modified from [137].*

Parameter	Optimum range
Alkalinity	50 - 100 mg/L $CaCO_3$
pH	6.8 – 7.5 (6.0 – 8.5 tolerated)
Temperature	26 – 28.5 °C
Hardness	50 - 100 mg/L $CaCO_3$
Un-ionized ammonia	< 0.02 mg/L
Nitrate	< 5 – 10 mg/L
Nitrite	< 0.1 mg/L
Dissolved oxygen	≥ 6.0 mg/L
Salinity/conductivity	300 – 1000 micro Siemens per cm (µS)

The zebrafish were bred at regular intervals, even when embryos were not needed for experiments. This was done in order to maintain the breeding cycle for the fish used [149]. Due to observations of increased embryo production and quality by extra feeding prior to being bred, an additional round of feeding were provided fish scheduled for breeding three days in advance. The evening prior to breeding, male and female fish (1:2 ratio for maximal embryo production [137]) were transferred into the breeding tank. Males and females remained separated overnight by a transparent and perforated plastic wall. The bottom of the tank were covered with glass marbles, which induced breeding by simulating a safe environment from predators in addition to protect the eggs from being eaten by the fish in the tank. During the night, the release and diffusion of pheromones in the water additionally induced breeding behavior and egg production. Next morning, when the day cycle started, the plastic wall was removed, allowing breeding to take place. After approximately 2 h, adult fish were transferred back to their respective tanks and embryos carefully collected, rinsed and kept in a dish filled with embryo water at 28 °C.

3.2.2 Enzymatic dechorionation of zebrafish embryos

The zebrafish embryos will naturally hatch from the protective chorion (egg) by themselves, the hatching period being 48-72 h post-fertilization [150]. This is however to be avoided when embryos are kept in large number in petri dishes as the chorion can act as a substrate for bacterial growth, thereby decreasing the survival of the developing embryos. The chorion was therefore removed by enzymatic digestion at 24 h post-fertilization. At this time point the embryos are sufficiently developed for living outside the protective chorion, their body axis have straightened, circulation and pigmentation have started in addition to early fin development [150].

Procedure

The embryos were observed through a stereomicroscope (Leica microsystems, Wetzlar, Germany) right before dechorionation. Dead and abnormal embryos were removed and euthanized by being placed in a water bath containing 190 µg/mL tricaine (an anesthetic) before transferring to a - 20 °C freezer. 40 mg of protease from *Streptomyces griseus* (Sigma-Aldrich, MO, USA) was weighed in a 10 cm petri dish using a Sartorius CPA 324S balance (Sartorius AG, Goettingen, Germany) and 20 mL embryo water was added to achieve a solution of 2 mg/mL (w/v) protease. The chorions were removed by incubation for 5 minutes (min) in the protease solution and zebrafish embryos were then washed twice with embryo water. Finally, dechorionated embryos were kept in embryo water supplemented with 42 µg/mL N-Phenylthiourea (PTU, Sigma-Aldrich, MO, USA) to block the development of pigmentation in the embryos. Before placing the zebrafish embryos into the 28 °C incubator, they were once again controlled under the stereomicroscope.

3.2.3 Ethical considerations

The zebrafish used in the following experiments were kept and treated in full compliance with local regulations at the University of Oslo, in addition to Norwegian and EU regulations. The number of zebrafish used in the different experiments was kept to a minimum for what was considered necessary in order to achieve reproducible data and results.

3.3 Synthesis of nanoparticles

Kerstin Johann, member of Matthias Barz group, at the Johannes Gutenberg-University Mainz, Germany, performed the synthesis of the polymeric micelle NP including their characterization by dynamic light scattering (DLS). Simon Van Herck, member of Bruno De Geest group, at Ghent University, Belgium, performed the synthesis of the PEG-PLA polymeric NP including their characterization by DLS. The two types of NP, with or without the novel-drug analogues of pretomanid, were then shipped to the University of Oslo for further testing in the embryonic zebrafish model by our group.

3.3.1 Polymeric micelle nanoparticle preparation

500 µL of a 100 mg/mL stock solution of the co-block polymer $PGlu(OBn)_{26}$-*b*-$PSar_{188}$-Ac in chloroform were added to a sterile 2 mL vial and the chloroform was allowed to evaporate overnight. The next day, 500 µL H_2O and 700 mg ceramic beads (SiLibeads ZY-S, 0.3-0.4 mm) were added to the vial and the polymer was allowed to swell for 4 h. Centrifugation was performed for 20 min at 3500 rpm with a dual asymmetric centrifuge (SpeedMixer DAC 150.1 CM, Hauschild & Co.KG). After centrifugation, the slightly turbid solution was separated from the beads with an Eppendorf Pipette and the vial was rinsed four times with 100 µL H_2O at a time.

For drug-loaded NP, 15 mg of the drug and 35 mg of the polymer were added to the vial and centrifugation was performed as described before. After centrifugation, a turbid solution was obtained. Size and size distribution of the obtained NP were determined by DLS both directly after the preparation and after filtration over GHP filters with a pore size of 200 nm. The NP solutions used for further experiments in zebrafish were not subjected to the filtration step.

3.3.2 PEG-PLA polymeric nanoparticle preparation

PEG-PLA NP were produced via a film method. In a small vial 5 mg of the polymer PEG-PLA alone (for empty NP) or together with 1 mg of drug C (31354) was dissolved in 1 mL acetonitrile and sonicated for 5-10 min to ensure full dissolution. The polymer-drug film was produced by slow evaporation of acetonitrile under reduced pressure while rotating in a water bath at 60 °C. Particle formation was induced by adding 200 µL preheated H_2O and sonication for approximately 30 min. Afterwards the polymer dispersion was frozen and freeze-dried. The size of the NP was measured before and after freeze-drying by DLS. No filtration step was included in the method; this to ensure the concentration of drug remained the same.

3.4 Characterization of nanoparticles

3.4.1 Dynamic Light Scattering

Physical characterization by DLS measurements were performed on a Zetasizer Nano ZS (Malvern Instruments) at an angle of 173° and a wavelength of 532 nm at 25 °C. Three measurements were performed per sample. Subsequent analysis of the data was done using Malvern Zetasizer Software version 7.11.

3.4.2 Transmission Electron Microscopy

To study the morphology and shape, estimating the size and verifying the stability of NP in aqueous suspension, we used Transmission Electron Microscopy (TEM) of negative stained NP. Due to the small sizes of the NP, which is less than 500 nm, these are difficult to observe accurately and with sufficient resolution by light microscopy. Electron microscopy uses electrons instead of light to visualize the sample. By using a focused electron beam, the sample is visualized as it interacts with and scatters electrons. Due to the significantly shorter wavelength of electrons compared to visible light it is possible to accurately image small details, down to the nanometer (nm) range.

Procedure

A small amount (3-4 µL) of NP in aqueous suspension were mounted on 200 mesh hexagonal copper grids (EMS, PA, USA) coated with a formvar film (Agar Scientific, Essex, UK). After 2 min, enough time for the NP to adsorb to it, the grids were floated on six drops of pure water, one after another, in order to wash away excess NP. Next, the samples were exposed to negative staining, by floating the grids sequentially on two drops of 1 % uranyl acetate solution (EMS, PA, USA) for 30 seconds. This provided contrast to the sample, and made visualization easier against the grid background [151]. Excess uranyl acetate was gently removed using lens paper. The grids were then air dried at room temperature before loading onto TEM sample holder and inserted into the microscope, a JEOL JEM 1400 120 kV TEM (JEOL, Tokyo, Japan). Digitally recordings of the samples were subsequently obtained with a TVIPS camera (TVIPS, Munich, Germany) and JEOL software.

3.4.3 Cryo-Transmission Electron Microscopy

Staining with uranyl acetate and air-drying of NP, subjects the sample to harsh treatment, which might alter the characteristics of the NP, such as shape. In order to verify that the shapes and sizes we observed by negative staining and TEM were accurate, NP were analyzed by Cryo-TEM. This method, developed by Dubochet and McDowall [152], is based on the concept of conserving life-like structures by extremely quick freezing of the sample to achieve the formation of non-crystalline ice, so-called vitrification of water.

Procedure

A tweezer holding a quantifoil grid (300 mesh R 1.2/1.3, Quantifoil Micro Tools GmbH, Großlöbichau, Germany) was attached to the plunge-freezing stage (Fig. 3.1). A metal beaker was placed in the center of a styrofoam box, which was then placed under the plunge-freezing stage. The styrofoam box were subsequently filled with liquid nitrogen (N_2), followed by addition of liquid ethane to the metal beaker. The temperature interval for the liquid phase of ethane is between - 82 °C and - 181 °C. The vitrification takes place below -140 °C and the solidification point of ethane is below - 182 °C.

A 3 µL drop of NP in aqueous suspension was applied on the quantifoil side of the grid. Using the pipette tip, the sample was evenly distributed across the grid, carefully avoiding touching the film. This was followed by blotting, using a filter paper to gently blot the quantifoil side of the grid for 1-3 seconds. Blotting was immediately followed by dropping the sample into liquid ethane. The sample was subsequently transferred, via liquid N_2, into a cryostage (GATAN, CA, USA) and kept at a stable temperature of about -190 °C. Finally, the cryostage was inserted into the microscope, a JEOL JEM 1400 120 kV TEM. Digitally recordings of the samples were subsequently obtained with a TVIPS camera and JEOL software.

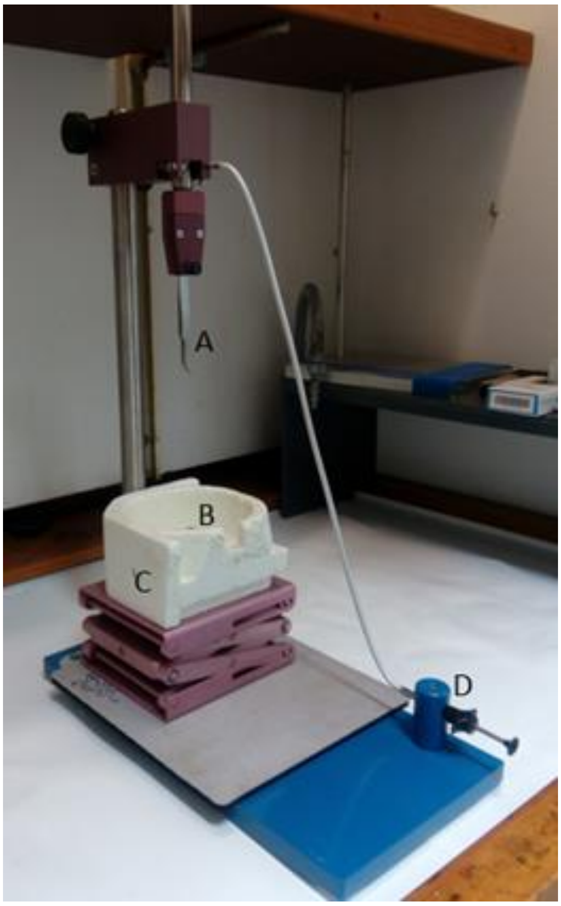

Figure 3.1: *Plunge-freezing set-up in the EM-lab at UiO. A: Tweezer, to hold the sample, attached to the stage. B: Beaker for liquid ethane inside the styrofoam box. C: Styrofoam box for liquid nitrogen. D: Lever for stage drop.*

3.5 *In vitro* studies

3.5.1 Culturing *M. marinum*

Three strains of *M.m* were used, wild type (Wt) *M.m*, dsRed-expressing *M.m* (transformed with the plasmid pMSP12::dsRed2, provided by Prof. Lalita Ramakrishnan) and GFP/mKO-expressing *M.m* (described below in chapter 3.5.2). The procedure used was adapted from Cosma, Swaim et al. and Gao and Manoranjan [144, 153].

Procedure

Bacteria were kept as frozen stocks at - 80 °C; the bacteria had an optical density, at 600 nm, (OD_{600}) between 0.8 and 1.0 before being frozen. Liquid cultures were prepared 6-7 days before use, to allow the bacteria to enter into the exponential growth phase (OD_{600} of 0.5 to 1.5). Liquid cultures were prepared under aseptic conditions in a sterile working hood. Liquid *M.m* culture medium was prepared using Difco Middlebrook 7H9 broth (Becton Dickinson, Franklin Lakes, NJ, USA) supplemented with glycerol (Sigma-Aldrich, MO, USA), ADC (comprising; bovine serum albumin, dextrose and catalase) and Tween 80 (Merck & Co, NJ, USA), see supplementary, chapter 8.1 for detailed recipe. The culture medium was sterilized by passing it through a 0.20 µm sterile filter (Sarstedt, Nümbrecht, Germany) using a 50-mL syringe into an autoclaved 100 mL glass bottle with a screw cap. Frozen bacterial stocks were thawed at room temperature and 20-30 µL were added to 20 mL of 7H9 liquid culture medium. Kanamycin (Sigma-Aldrich, MO, USA) was added to cultures of dsRed or GFP/mKO *M.m*, to a total concentration of 40 µg/mL to select for bacteria containing the plasmids, which both cases comprise a kanamycin resistance cassette. The bacterial cultures were incubated in a dark room, at 30 °C and placed on a slow shaker. After 6-7 days, the bacteria were, usually, in the exponential growth phase. To confirm this, OD_{600} was measured using a spectrophotometer (Eppendorf AG, Hamburg, Germany), with 7H9 broth functioning as a blank.

3.5.2 Construction of fluorescent reporter plasmids and transformation of *M. marinum*

The plasmid pGFP::Myc/mKO, containing constitutively expressed green fluorescent protein (GFP) and tetracycline (Tet) inducible monomeric Kusabira Orange (mKO), was generated by the former group member, Matthew Yoke Wui NG. The construct was produced by excising the sequence of mCherry and its promotor from the pmCherry::Myc/mKO plasmid (kindly provided by David G. Russell). GFP, under the mycobacterium specific promotor (MSP), was cloned from pGFPHYG2 (Addgene, MA, USA) and introduced into the plasmid to form pGFP::Myc/mKO. Plasmid maps with restriction sites of pmCherry::Myc/mKO and pGFPHYG2 are shown in the supplementary section, chapter 8.3. Subsequent transformation, or incorporation of the new construct into Wt *M.m*, was done by electroporation, as described below.

Procedure

Wt *M.m* was grown in 25 mL 7H9 liquid culture medium to an OD_{600} of ~0.8. The bacteria were collected by centrifugation at 3000x g for 5 min at 4 °C. The supernatant was then discarded and bacterial pellet re-suspended in 12.5 mL of ice-cold 10 % glycerol (Sigma-Aldrich, MO, USA) and kept on ice for the remaining steps. After a new centrifugation step, the bacterial pellet was re-suspended in 1 mL of ice-cold 10 % glycerol followed by centrifugation at 12,000x g for 5 min at 4 °C. The two last steps were repeated four times. Then the bacteria were re-suspended in five volumes of the bacterial pellet, around 500 µL. 100 µL of bacterial suspension were added to a pre-chilled 0.2 cm gap cuvette, kept on ice and gently mixed with an equal volume of ice-cold 10 % glycerol. 1 µL of plasmid DNA (1-500 ng) was added to the cuvette and mixed by trituration, followed by 5 min of incubation on ice. Electroporation was done using a Bio Rad Gene Pulser ™ with following settings; 2.5 kV and resistance at 800 ohms, for more than 10 msec. Immediately after electroporation, 900 µL of 7H9 liquid culture medium were added to the bacteria and the bacterial suspension was incubated overnight at 30 °C for recovery. Next, the bacteria were collected by centrifugation at 12,000x g for 5 min, and re-suspended in liquid culture medium before being plated on 7H10 agar plates, containing kanamycin for selection of transformed colonies. The plates were sealed in plastic bags to avoid evaporation and incubated at 30 °C for around two weeks. The resulting bacterial colonies were inspected using a Leica M205 FA stereomicroscope. By thorough inspection in the GFP channel, the brightest colonies were selected using a sterile pipette tip and re-cultured in 10 mL of liquid culture medium. Aliquots of bacterial cultures were frozen in 10 % glycerol at – 80 °C for later use.

To further test if the transformation with the reporter plasmid was successful, the selected colonies of transformed bacteria were exposed to doxycycline (Dox, Sigma-Aldrich, MO, USA), a Tet derivative. Bacteria were grown to the exponential phase and left untreated or treated with 1 µg/mL or 50 µg/mL for 24 h. Expression of GFP and mKO in the bacteria was checked using the GFP and DSR channels of the fluorescence stereomicroscope, respectively.

3.5.3 *In vitro* dose-response of novel-drugs against *M. marinum*

The novel antibiotics described in this thesis had so far not been tested against *M.m*, and it was therefore important to first establish in principle the activity of these compounds against *M.m* using an *in vitro* assay. Due to extensive work already done by our New Zealand collaborator Dr. Andrew Thompson and colleagues [87-89], the minimum inhibitory concentrations (MIC) against *M.tb* were already established for all four compounds tested. We therefore decided to perform a relatively simple dose-response assay based on OD_{600} measurements to determine the activity of the compounds against *M.m*, before moving onto *in vivo* experiments using the zebrafish embryo model.

<u>Procedure</u>

5 mg drug were weighed in an Eppendorf tube using a Sartorius CPA 324S balance, and dimethyl sulfoxide (DMSO, Sigma-Aldrich, MO, USA) was added to achieve a drug concentration of 10 mM. The solution was then sonicated for 2 min followed by brief vortexing to completely solubilize the drug. From this, a stock solution of 1 mM was made by diluting the drug stock solution in 7H9 liquid culture medium. Another round of sonication and brief vortex followed to re-solubilize the drug. Next, a serial dilution was prepared in 7H9 liquid culture medium ranging from 16 µM to 0.25 µM. The experiments were performed using flat bottom glass flasks with screw caps (Bergmanlabora AB, Danderyd, Sweden), in a total volume of 5 mL in each flask.

Wt *M.m* cultures were prepared 6-7 days before initiation of the experiment and allowed to grow until they reached the exponential growth phase and OD_{600} adjusted to 1.0 using 7H9 medium. Next, 20 µL bacterial suspension was added to each drug concentration sample, including untreated (no-drug) growth control. The samples were incubated in a dark room, at

30 °C under gentle shaking. The experiments were ended 5-6 days post-exposure to drug, the time point when untreated control group had reached the exponential growth phase. Bacterial growth was determined by measuring the OD_{600} using the spectrophotometer. At the highest concentrations tested, the drugs themselves showed absorbance at 600 nm, as determined in a separate experiment, using only 7H9 liquid culture medium and drug titrations, without bacteria. Background absorbance due to the drug themselves was therefore subtracted within each concentration group. Finally, the average absorbance of the untreated control was defined as 100 %, and all other groups were converted to a percentage of the control thereafter from the raw data before further analyzes were done.

3.6 *In vivo* studies in the zebrafish embryo model for fish-tuberculosis

3.6.1 Preparing *M. marinum* for microinjection

Bacteria were grown to the exponential growth phase as described in chapter 3.5.1. Bacterial suspension was then transferred into two Eppendorf tubes, and the bacteria were collected by centrifugation at 6000x g for 5 min using a tabletop centrifuge. After centrifugation, the supernatant was carefully removed without disrupting the bacterial pellet, the bacteria were re-suspended in 1 % Tween 80 in PBS and passed five times through a 27-gauge needle (BD Drogheda, Lagavooren, Ireland) in order to break up aggregates which may lead to the clogging of the needle during microinjection. Tween 80 is a surfactant which prevents re-aggregation of bacteria and therefore aiding the production of a stable single cell suspension. Due to loss of bacteria by this process, the OD_{600} was measured again and adjusted to 1.0 with Tween 80 in PBS, which corresponds to ~5.65 x 10^7 *M.m*/mL.

3.6.2 Preparing free-drug for microinjection using different solvents

DMSO plus PVP or Tween 80

The drugs were weighed and dissolved in DMSO to make a free drug stock-solution of 7.5 mg/mL. The stock solution was sonicated for 2 min to make sure the free drug was completely dissolved. After sonication, the stock solution was diluted by addition of either a 2 % solution of Polyvinyl pyrrolidone (PVP) or Tween 80 in PBS to make a final solution of

2.25 or 4.5 mg/mL drug in 30 % or 60 % DMSO respectively. The final solution was sonicated for 2 min right before being used in microinjections.

PEG400 plus DMSO

The drugs were weighed and dissolved directly to injectable concentrations, using an 80 % Poly-ethylene glycol 400 (PEG400; Sigma-Aldrich, MO, USA) and 20 % DMSO mixture (4:1 ratio). Drug solutions were sonicated for 2 min right before being used in microinjections.

Captisol

The drugs were weighed and dissolved directly to injectable concentrations in a 40 % (w/v) Captisol solution (Ligand Pharmaceuticals, CA, USA). The drug samples were sealed with parafilm, covered with aluminum foil and placed on a tumbling apparatus at 4 °C for 72 h to solubilize the drugs.

3.6.3 Preparing drug-encapsulated nanoparticles for microinjection

All NP samples were stored at 4 °C before use.

Polymeric micelle NP, PGlu-b-PSar and MPEO-b-PCL, were received from our collaborators in aqueous suspension, with determined polymer and drug concentration ready for injection. The samples were briefly sonicated prior to injection in order to break up possible aggregates. The therapeutic dose was set by adjusting the injection volume.

PEG-PLA NP, empty or loaded with drug C, were received from our collaborators in a freeze-dried state. NP were weighed and subsequently dissolved by 2 % PVP in PBS. Drug-loaded NP had a total concentration of 30 mg/mL, of which 20 % drug, when injected. Empty NP were dissolved to the same polymer concentration as the drug-loaded sample. The samples were briefly sonicated prior to injection and therapeutic dose was set by adjusting the injection volume.

3.6.4 Microinjection of zebrafish embryos

Microinjections of zebrafish embryos were performed on agarose injection plates, as an injection platform. To produce injection plates, 8 grams of LE agarose (Lonza, Basel, Switzerland) were mixed with 400 mL of distilled water in a 1 L glass bottle (final concentration 2 % w/v). The mixture was microwaved to dissolve the agarose and to achieve a clear solution with no bubbles, which then was poured into the lids of petri dishes (~24 plates with 400 mL solution). Finally, the lids were closed and set to solidify at room temperature, before being sealed in plastic and stored at 4 °C.

The microinjection protocol was adapted from Cosma et al. 2006 [144]. At 2 days post-fertilization, the zebrafish embryos were sufficiently developed to be injected with either bacteria, free or NP drug compounds. The injection sites used in this thesis are illustrated in Fig. 3.2.

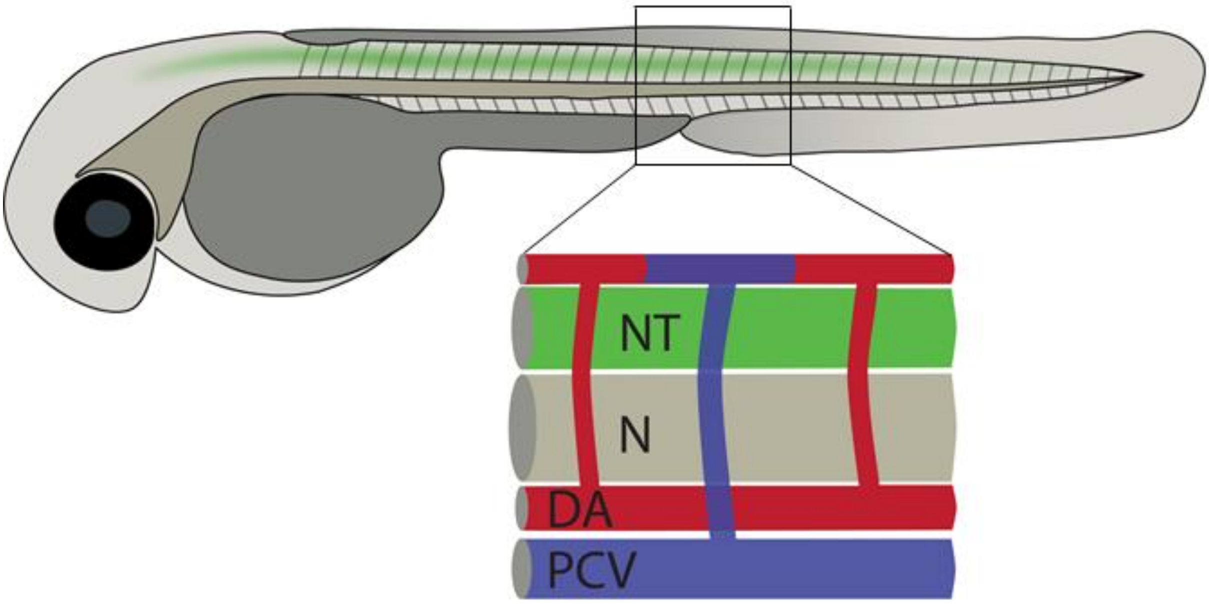

Figure 3.2: *Schematic illustration of a zebrafish embryo. The black square points out the area of injection and illustration below show the two injection sites, the posterior cardinal vein (PCV) and the neural tube (NT). Also shown are the dorsal aorta (DA) and the notochord (N). Illustration created by Agnese Kocere, member of Griffiths group.*

In the drug treatment experiments, the zebrafish embryos were infected with *M.m* at day two post-fertilization and received treatment, free drug and NP formulation, the following day. The majority of experiments used the posterior cardinal vein as intravenous injection site. The procedure for injecting drugs, NP, and bacteria were the same for both blood and neural tube injections.

Injection needles were produced using borosilicate capillaries, with an outer diameter of 1.0 mm, an inner diameter of 0.78 mm and a length of 100 mm (Harvard Apparatus, MA, USA). The borosilicate capillaries were pulled into needles using a Flaming/Brown P-97 micropipette-puller (Sutter, CA, USA) with the following settings: delay 110, heat 610, pull 40, velocity 50 and pressure 500.

The injection needles were loaded with either 2-5 µL bacteria, free drug or NP solution using a micro-loader pipette tip. The injection needle was then mounted on a micromanipulator (Narishige, Tokyo, Japan) that enabled to move the needle in all three dimensional planes. The needle was attached to a pressure controller (Femtojet; Eppendorf AG, Hamburg, Germany), connected to a tank of nitrogen gas. The pressure controller was used to regulate the constant background pressure, the injection pressure and the time interval of the injection. This setup ensured an accurate and consistent injection volume throughout the injection procedure. Fine jewelers forceps (Dumont No. 5) were used to break open the needle tip and adjust the diameter of the opening.

The injection volume was set by adjusting the injection pressure, time interval pressure, as well as the size of the needle opening. The injection volume was estimated by injecting drops of the solution of interest into mineral oil (Sigma-Aldrich, MO, USA). The diameter of the droplet was measured in arbitrary units at 60x magnification using a scale printed on the inside of the oculars. Previous work done by a former group member, Carina Vibe [154], had established the correlation of drop diameter in arbitrary units to actual volume of the drop using a 1 mm Stage Micrometer (Thorlabs, NJ, USA), see Fig. 3.3 and table 3.2.

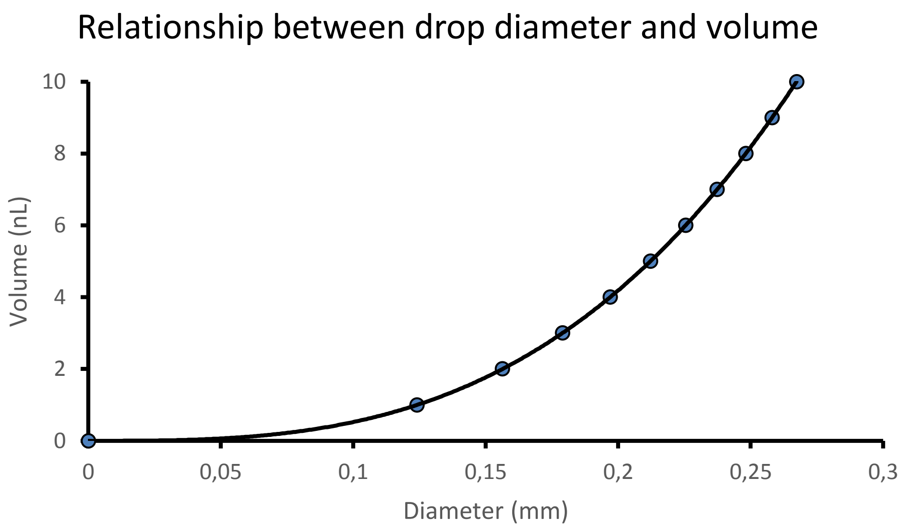

Figure 3.3: *The relationship between drop size in mm and the volume of the drop in nL. Figure modified from [154].*

Table 3.2: *The table shows the relationship between the drop size in arbitrary units at 60x and the corresponding volume in nL. The relevant volume interval for injection of zebrafish embryos without causing damage (1-10 nL) is shown. Table modified from [154].*

Drop size (arbitrary units, 60x)	**Volume (nL)**
0.74	1
0.94	2
1.07	3
1.18	4
1.27	5
1.35	6
1.42	7
1.49	8
1.55	9
1.60	10

Before injection, zebrafish embryos were anesthetized, 10-20 at a time, with 190 µg/mL tricaine in embryo water. The anesthetized embryos were then placed onto the injection plate, up to five at the same time, and excess fluid was carefully removed using a plastic pipette. The embryos were then rapidly injected in the posterior cardinal vein (or neural tube), and subsequently transferred into a dish containing fresh embryo water for recovery. Approximately 2-3 h post-injection, the zebrafish embryos were controlled, dead embryos removed, and severely damaged embryos were euthanized.

3.6.5 Toxicity and efficiency studies of pretomanid analogues in the zebrafish embryo model for tuberculosis

Three different experiments were based on survival: DMSO toxicity, drug toxicity and infection with Wt *M.m* followed by treatment.

For the DMSO and drug toxicity experiments, the solutions to be tested were injected 2 days post-fertilization. For the treatment experiments, bacteria were injected 2 days post-fertilization and the treatments were administered the following day. Approximately 2-3 h post-injection, dead and severely damaged embryos were removed and excluded from the experiment. The different groups were kept in separate 10 cm petri dishes filled with embryo water supplemented with PTU (42 µg/mL). Every two days the embryos were transferred to a new and clean petri dish with fresh embryo water. Once daily, at the same time, the groups were controlled using a Leica M205 FA stereomicroscope and dead and live embryos were counted. Dead embryos were removed, the criteria for death being complete absence of a visible heartbeat. The toxicity experiments, involving DMSO and drug, were terminated 12 days post-fertilization while, treatment experiments were terminated when the majority of infected embryos not receiving treatment were considered dead. An injection volume of 5 nL Wt *M.m* (OD_{600}= 1.0), corresponding to ~250 colony forming units (CFU), will normally result, if bacteria is injected into the bloodstream, in an infection that kill the zebrafish embryos within 5-8 days.

3.6.6 Quantification of bacterial burden by fluorescence pixel count

The fluorescence pixel count (FPC) protocol was adapted from the work of Fenaroli et al. 2014 [116].

Zebrafish embryos were infected with dsRed *M.m* via the posterior cardinal vein, treated with free drugs and drug-loaded NP as described in 3.6.5. The dsRed *M.m* are generally less virulent than the Wt strain and therefore kill the embryos at a later time point. Imaging and subsequent analysis of bacterial burden was therefore conducted at day 5 post-infection to allow the infection enough time to progress before the onset of infection-related mortality in untreated embryos. Images were obtained using a Leica M205 FA stereomicroscope and the imaging software LAS AF (Leica microsystems, Wetzlar, Germany). All images were obtained at 30x magnification using the exact same settings as specified in Table 3.3. After imaging, the embryos were placed back to their respective groups and survival was recorded over the following days.

Table 3.3: *LAS AF imaging settings used for FPC experiments including exposure time and gain used for the different light channels.*

Channel	Transmitted	Green (GFP)	Red (DSR)
Exposure	16 ms	277 ms	277 ms
Gain	1	6.4	6.0

Subsequent analysis of the bacterial fluorescence was done using the imaging software ImageJ. The average fluorescence value obtained from the uninfected control group were defined as the background fluorescence; this value was subtracted from the total fluorescence of all images analyzed. By subtracting the background fluorescence, the subsequent fluorescence value reflected the bacterial burden only. Next, the average value of the infected control group (not receiving treatment) was defined as 100 % and all fluorescence values were converted to percentage relative to this group.

3.6.7 Qualitative analysis of nanoparticle localization in zebrafish embryos

Localization of NP in the zebrafish *in vivo* was conducted using fluorescent dye loaded MPEO-b-PCL NP, provided by our collaborator Jiri Trousil from the Academy of Sciences, Czech Republic. Experiments for testing the therapeutic efficacy of Rif-loaded MPEO-b-PCL was done as described in 3.6.5.

Localization of $MPEO_{112}$-b-PCL_{33} NP labelled with tetramethylrhodamine in the zebrafish *in vivo*:

Stereomicroscopy: At 2 days post fertilization tg(-fli1a:EGFP) zebrafish embryos expressing GFP in the endothelial cells of the vasculature [155], were injected in the posterior cardinal vein with MPEO-b-PCL NP labelled with tetramethylrhodamine (1 mg/mL, PBS) at a dose app. 5 ng per embryo. 2 h post-injection, the embryos were imaged using a Leica M205 FA stereomicroscope and the imaging software LAS AF.

Confocal microscopy: Zebrafish embryos previously injected with red fluorescent NP and observed using a stereomicroscope were further analyzed with a confocal microscope. For this, anesthetized embryos were mounted on a glass bottom dish (MatTek, MA, USA) in low melting point agarose. Images were obtained using an Olympus FluoView 1000- Confocal Laser Scanning microscope- BX61WI (Upright), and subsequently analyzed and processed using Imaris Image Analysis Software (Bitplane, Belfast, UK).

3.6.8 Tetracycline-controlled transcriptional activation in transformed *M. marinum* using the zebrafish model

The GFP/mKO *M.m* constitutively express GFP and upon exposure to a tetracycline induces the expression of the red fluorescent protein mKO via Tet-On expression [156]. Using the GFP/mKO *M.m* strain in the zebrafish embryo TB model we aimed to establish a novel system to discriminate between live, metabolically active bacteria from dead or metabolically inactive bacteria *in vivo*. In contrast to live metabolically active bacteria, dead or metabolically inactive bacteria are not able to induce mKO expression in response to tetracycline’s such as Dox or anhydrotetracycline (ATc). Thus, the latter bacteria only show GFP fluorescence, whereas live bacteria express both GFP and mKO. In order to induce mKO expression in this complex *in vivo* model, the inducer (Dox or ATc) has to cross two barriers. First, the inducer has to enter the embryo and reach *M.m* infected macrophages and second, the inducer has to reach intracellular bacteria to activate expression of mKO. In the literature, there are several examples of tetracycline-inducible gene expression systems in transgene zebrafish [157-159] and in mycobacteria, such as *M.tb* [160, 161]. However, this specific set-up, where the Tet-On system was used for transcriptional activation in mycobacteria in live zebrafish embryos has not yet been described.

Inducer tolerability (bath immersion)

The two Tet-derivatives inducers tested in this project were Dox and ATc. Dox had a tendency to precipitate in embryo water at relatively low concentrations, due to the salt content of the water. We therefore decided to dissolve both inducers in dH_2O supplemented with PTU, and in addition, ATc in embryo water with PTU. During the tolerability experiments embryos were kept in 12-well plates at 2-3 embryos per well. First, we tested whether embryos survived being in dH_2O supplemented with PTU. Next, we tested different concentrations of Dox and ATc. The experiments lasted 72 h, with embryos checked every 24 h for possible deaths.

Infection with GFP/mKO *M.m* and induction of mKO expression

The microinjection procedure was performed as described in chapter 3.6.4. Embryos were infected via the posterior cardinal vein or the neural tube. Infected embryos were kept in petri dishes filled with embryo water supplemented with PTU.

Inducer exposure by immersion: At day 4 or 5 post-infection embryos were transferred to 12-well plates (2-3 embryos per well) containing Dox or ATc at different concentrations, dissolved in dH_2O or embryo water. The plates were covered in aluminum foil, due to light sensitivity of the inducers, and kept in the zebrafish incubator for 24 h, followed by screening using a stereomicroscope and subsequent confocal microscopy for analysis.

Inducer exposure by injection: At day 4 or 5 post-infection embryos were injected with ATc (500 µg/mL) dissolved in PBS via the posterior cardinal vein and kept in the zebrafish incubator for 24 h. This procedure was then followed by screening using a stereomicroscope and subsequent confocal microscopy for analysis.

Confocal microscopy and image analysis

24 h after inducer (Dox or ATc) exposure, at day 5 or 6 post-infection, the embryos were imaged using a confocal microscope. The embryos were anesthetized by immersion in a tricaine bath and mounted on a glass bottom dish in low melting point agarose. Images were obtained using an Olympus FluoView 1000- Confocal Laser Scanning microscope- BX61WI (upright), and subsequently analyzed and processed using the imaging software ImageJ. Table 3.4 provide technical information about objectives used.

Table 3.4: *Technical information about objectives used during confocal microscopy.*

Magnification	Type	Numerical aperture	Working distance (mm)	Immersion
20x	LumpPlanFI	0.5	3.3	Water
40x	LumpPlanFI	0.8	3.3	Water
60x	LumpPlanFI	0.9	2	Water

3.7 *In vivo* studies in the mouse model for tuberculosis

The experiments were conducted by Yitian Xu in the group of Prof. David Russell, at Cornell University College of Veterinary Medicine, New York, USA.

Mice infection and treatment experiment

C57BL/6 Wt mice, reared at the local animal facility at the Cornell University College of Veterinary Medicine, were anesthetized with isoflurane and subsequently infected intranasally with 25 µL of Erdman (Wt) *M.tb* inoculum, via both nares [162]. The bacterial inoculum contained approximately 10^3 CFU suspended in PBS plus 0.5 % Tween 80. The mice were then randomly divided into five groups: infection input control, untreated, empty NP, drug-loaded NP and free drug, with 5 mice each. At day 24 post-infection, the infection input control group was sacrificed for CFU and histology analysis. The test groups received treatment (drug B) via retro-orbital injection at day 24, 28, 32 and 36 post-infection. The NP used were polymeric micelles (batch KS136) suspended in aqueous solution with known polymer and drug concentration and free drug was solubilized and injected using PEG400. Mice in the NP-drug B group was injected with 100 µL, drug concentration 18 mg/mL, at each treatment. Mice in the free-drug B group was injected with a matching dose, 120 µL of 15 mg/mL drug dissolved in PEG400, at each treatment. The mice were sacrificed at day 40 post-infection followed by CFU and histology analysis.

NP localization experiment

Three C57BL/6 Wt mice were infected with Erdman (smyc'::mCherry) *M.tb* as described above. Four weeks post-infection, 100 µL of 50 mg/mL polymeric micelle NP labelled with 4 % Alexa Fluor 647 (AF647) (batch KS137) were administered through retro-orbital injection. 24 h later mice were sacrificed and lungs were dissected and fixed in 4 % paraformaldehyde in PBS overnight. Using a razor blade, lung tissue was cut into 1 mm thick slices. Next, the slices were blocked and permeabilized in PBS supplemented with 3 % BSA and 0.1 % Triton X-100 buffer, in the dark for 1 h at room temperature. After blocking, the samples were incubated for 2 h in the dark at room temperature with DAPI (1:500) and AF647 conjugated Phalloidin (1:50). This was followed by three washing steps using PBS before samples were mounted on a glass slide with mounting medium (Vectorshield). Images were obtained using a Leica SP5 confocal microscope and subsequently analyzed by Volocity software (PerkinElmer, MA, USA).

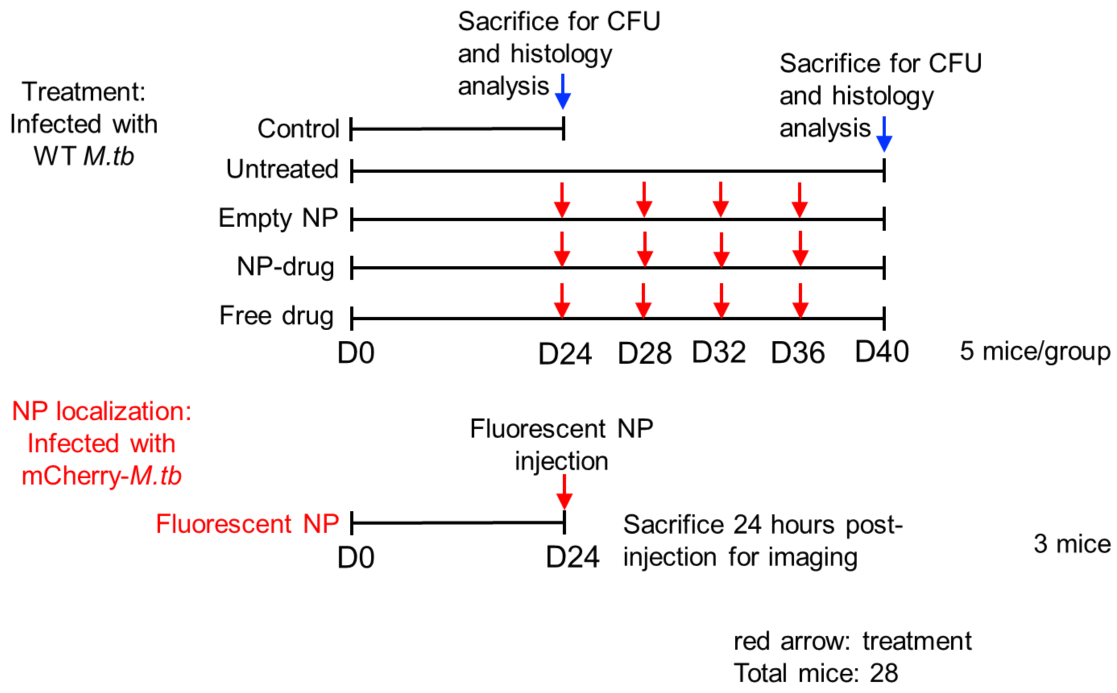

Figure 3.4: *Experimental scheme of the mice experiments performed at Cornell University.*

3.8 Statistics

All statistical analyses were performed using GraphPad Prism 7 software (GraphPad Software, CA, USA). After confirming overall significance of the data set, post hoc multiple comparisons tests between groups of interest were performed. Specific tests chosen for the different experiments are specified below, as well as in figures presenting the results.

- Data sets analyzed by column table: Column statistics using D'Agostino & Pearson normality test to check for Gaussian (normal) distribution of the data.
    - In the case of normal distribution, data were analyzed by one-way ANOVA, followed by Dunnett's multiple comparisons test.
    - If not normally distributed, data were analyzed by Kruskal-Wallis test, followed by Dunn's multiple comparisons test.
- Data sets analyzed by survival table: Based on the Kaplan-Meier estimate using the Log-rank (Mantel-Cox) test for overall significance and pairwise comparison of groups.

Significance level is indicated as $^{*}p < 0.05$, $^{**}p < 0.01$, $^{***}p < 0.001$ and $^{****}p < 0.0001$.

4 Results

The work in this thesis is based on the availability of analogues of the parental anti-TB drug pretomanid, provided to us by Dr. Andrew Thompson (Auckland Cancer Research Center, University of Auckland, New Zealand). The selected compounds were encapsulated in polymeric micelle NP, prepared from the amphiphilic block copolymer PGlu(OBn)-block-PSar, by the group of Matthias Barz (Institute for Organic chemistry, Johannes Gutenberg-University Mainz, Germany). The group of a second NP specialist, Bruno De Geest (Department of Pharmaceutics, Ghent University, Belgium) provided us with a different drug-loaded NP, poly (ethylene glycol) - polylactic acid (PEG-PLA) NP.

4.1 Nanoparticle characterization

4.1.1 Characterization of polymeric micelle nanoparticles

Before shipment to our lab in Oslo and following *in vivo* testing using the zebrafish embryo model, the sizes of the polymeric micelles (PM) were determined by dynamic light scattering (DLS). The z-average, which is the averaged particle diameter, is given in nanometers (nm).

Due to aggregates of non-encapsulated drug, the drug-loaded samples were too polydisperse for a reliable DLS measurement. Therefore, an aliquot of all samples were filtered using a 200 nm filter and measured again as a comparison. Table 4.1 presents the results from DLS. Unfiltered samples were sent to our group in Oslo. The reasoning behind using the unfiltered samples for *in vivo* testing is simply the fact that we knew the drug concentration, and therefore could control the injected drug dose. This was not possible with the filtered samples, as the drug concentration was unknown due to loss of particles and drug during the filtration process. Currently, work is being done optimizing the preparation of drug loaded PM.

Table 4.1: *Size characterization of PM by DLS, performed by Kerstin Johann (University Mainz). Unfiltered samples at the top (used in following experiments), and 200 nm filtered samples below. All drug-loaded samples contained 30 % drug relative to the total concentration.*

Batch name	**NP type**	**Total c/ [mg/mL]**	**Z-average/ nm**	**PDI**	**PDI width/ nm**
KS112B	PM + B	25	626 ± 106	0.53 ± 0.06	457 ± 100
KS117	PM empty	25	108 ± 2	0.15 ± 0.03	42 ± 3
KS124	PM + C	20	394 ± 32	0.46 ± 0.06	267 ± 16
KS125	PM + D	20	340 ± 21	0.54 ± 0.05	250 ± 18
KS132A	PM empty	50	111 ± 3	0.18 ± 0.03	47 ± 5
KS132B	PM + B	50	616 ± 25	0.42 ± 0.09	398 ± 55
KS149	PM + B	25	407 ± 44	0.52 ± 0.11	294 ± 64
KS150	PM + C	25	388 ± 18	0.37 ± 0.05	237 ± 27
KS151	PM + D	25	297 ± 5	0.28 ± 0.02	158 ± 9
KS152	PM empty	25	111 ± 0	0.12 ± 0.06	37 ± 10
200 nm filtered samples					
KS112B	PM + B	25	109 ± 1	0.16 ± 0.03	43 ± 4
KS117	PM empty	25	101 ± 2	0.10 ± 0.03	32 ± 4
KS124	PM + C	20	90 ± 1	0.11 ± 0.05	28 ± 7
KS125	PM + D	20	99 ± 1	0.13 ± 0.04	35 ± 5
KS132A	PM empty	50	98 ± 1	0.08 ± 0.02	28 ± 3
KS132B	PM + B	50	90 ± 1	0.20 ± 0.02	40 ± 1
KS149	PM + B	25	117 ± 2	0.13 ± 0.02	42 ± 3
KS150	PM + C	25	118 ± 4	0.15 ± 0.02	46 ± 2
KS151	PM + D	25	122 ± 2	0.13 ± 0.02	45 ± 4
KS152	PM empty	25	103 ± 2	0.08 ± 0.01	28 ± 2

We received the PM in aqueous suspension, where they are stable for about a year according to the experience of the Barz’s group. To verify the stability of the PM and for, additionally, perform a secondary independent determination of the physical size of the particles, we used transmission electron microscopy (TEM) to obtain images of a selection of samples. The samples imaged were batch OSB.3, KS112B and KS117, see supplementary, chapter 8.2, for details on the specific batches. Fig. 4.1 show selected representative images (negative staining TEM and cryo-TEM) from the samples examined by electron microscopy.

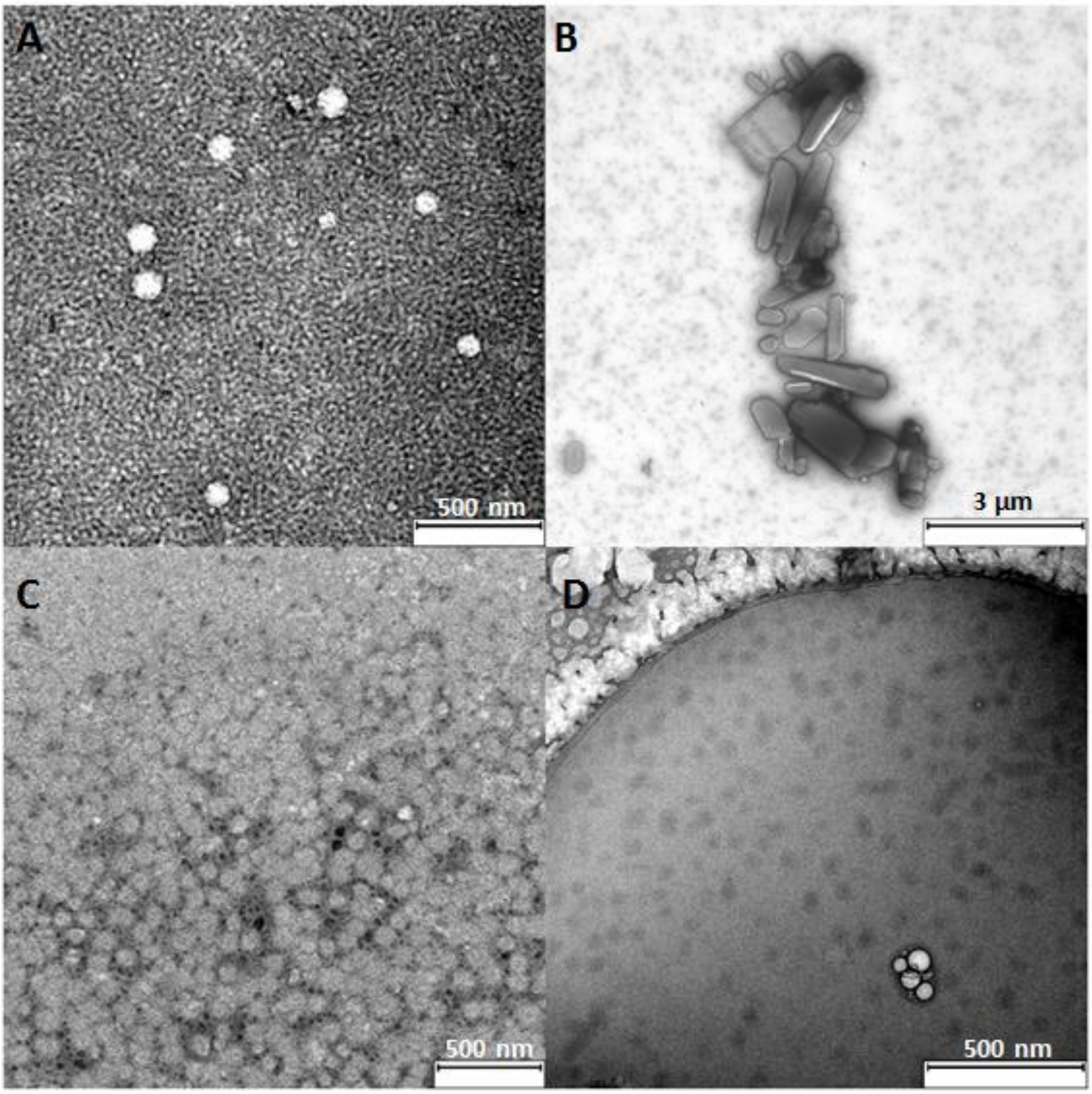

Figure 4.1: *Transmission electron microscopy images of polymeric micelles, with or without drug B. (A) Empty PM, treated with uranyl acetate prior to imaging. Image obtained at 12,000x. (B) Crystallized drug aggregate from old PM sample. Sample treated with uranyl acetate prior to imaging. (C) Drug B loaded PM, treated with uranyl acetate prior to imaging. Image obtained at 10,000x, in an area with high particle concentration. (D) Cryo-TEM image of drug B loaded PM. Image obtained at 15,000x. Boiling ethane due to beam damage is visible in the top part of the image.*

We observed, by TEM imaging, that the size of empty PM (KS117) correlated well with the z-average of empty PM obtained from DLS. The average diameter of the eight empty PM, Fig. 4.1(A), was found to be 96 nm using ImageJ. In addition, the empty PM were all spherical in shape.

The PM in the drug-loaded sample (KS112B) were somewhat more irregular in shape and size when examined, after negative staining, using TEM. As illustrated, Fig. 4.1(C), spherical and long tubular shapes were present. We hypothesized that the harsh treatment with uranyl acetate and subsequent air-drying possibly distorted the PM. Therefore, we applied cryo-TEM to better preserve the native structure of the particles. The same pattern was observed in cryo-TEM, as illustrated, Fig. 4.1(D), indicating that drug-encapsulation altered to some degree the particle shape and size. It was interesting to see that the z-average of filtered drug-loaded samples correlated relatively well with the sizes of PM observed in the TEM images. This is based on diameter measurements of randomly selected particles from image (C) and (D), plus other images not shown here.

Fig. 4.1(B) shows crystallized free drug aggregates. The sample was taken from a relatively old batch (OSB.3), about 1 year old when imaging took place. Although many drug-loaded PM were intact, considerably more drug aggregates were present compared to the newer samples imaged later. This observation illustrated two key factors concerning the *in vivo* experiments, with respect to PM and the hydrophobic compounds. (1) The PM are relatively stable over long periods in aqueous suspension, as long as the polymer concentration exceeds the CMC. (2) Outside the PM, the hydrophobic drug aggregates into a few large complexes, making microinjection of free drug difficult, as well as reducing bioavailability.

4.1.2 Characterization of PEG-PLA polymeric nanoparticles

Before shipment to our lab in Oslo and following *in vivo* testing using the zebrafish embryo model, the sizes of the PEG-PLA NP were determined by DLS. Table 4.2 presents the data from DLS, of the PEG-PLA NP used for one treatment study (bacterial burden by fluorescence pixel count) in this thesis. We have not examined these NP by electron microscopy yet, therefore the size estimate is only based upon DLS measurements.

Table 4.2: *Size characterization of PEG-PLA NP by DLS, performed by Simon Van Herck (Ghent University). Measurement of drug-loaded and empty NP at the top, and freeze-dried empty NP below. We received drug-loaded and empty NP in a freeze-dried state.*

Sample	Z-average/ nm	Volume mean/ nm	PDI
Before freeze-drying			
PEG-PLA	116	134	0.80
PEG-PLA-31354(C)	410	817	0.26
After freeze-drying			
PEG-PLA	86.4	47.7	0.51

4.2 *In vitro* studies

4.2.1 Dose-response against *M. marinum* using pretomanid analogues

Before testing the therapeutic effect of the pretomanid analogues encapsulated in NP, or as free formulation in the zebrafish model of TB, we tested their effects against *M.m in vitro*. Table 4.3 presents the relative solubility and inhibitory effect against *M.tb* of pretomanid and the selected analogues examined in this thesis.

Table 4.3: *Overview of compounds examined in this thesis in addition to pretomanid, the parental drug. Minimum inhibitory concentration (MIC) and CLogP values reported in [87-89].*

Drug	**CLogP**	**MIC *M.tb* (µM)**
Pretomanid	2.70	0.50 ± 0.30
30485 (A)	4.36	0.035 ± 0.015
32625 (B)	2.99	0.025 ± 0.005
31354 (C)	3.01	0.05 ± 0.01
32499 (D)	3.77	0.02 ± 0

We first analyzed the effect against *M.m* by a dose-response titration of drugs A and B. Later, when we received drugs C and D, we tested these compounds at the two concentrations that in the previous assay were found to significantly inhibit the growth of *M.m*, and compared them to drug B. Figs. 4.2 and 4.3 presents the results obtained from the *in vitro* dose-response assays.

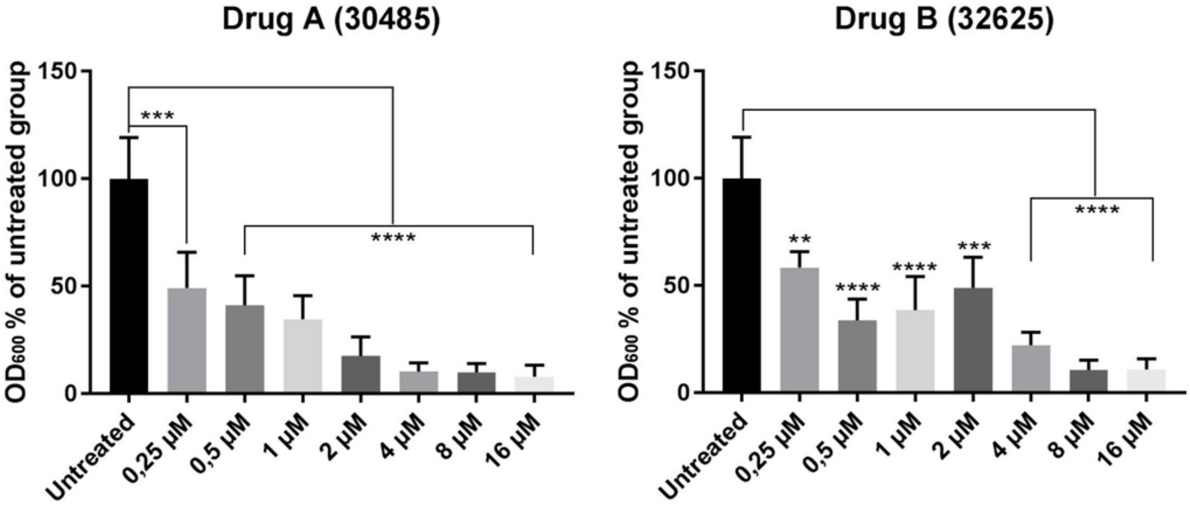

Figure 4.2: *Dose-response assay; titration of drugs A and B against wild type M.m. Bacterial growth was analyzed by measuring the OD_{600} when the untreated control group was in the exponential growth phase (5-6 days post-treatment). Average absorbance value of untreated control defined as 100 %, all other groups converted to a percentage thereafter. Data show the mean ± SD of three independent experiments analyzed by one-way ANOVA, followed by Dunnett's multiple comparisons test.*

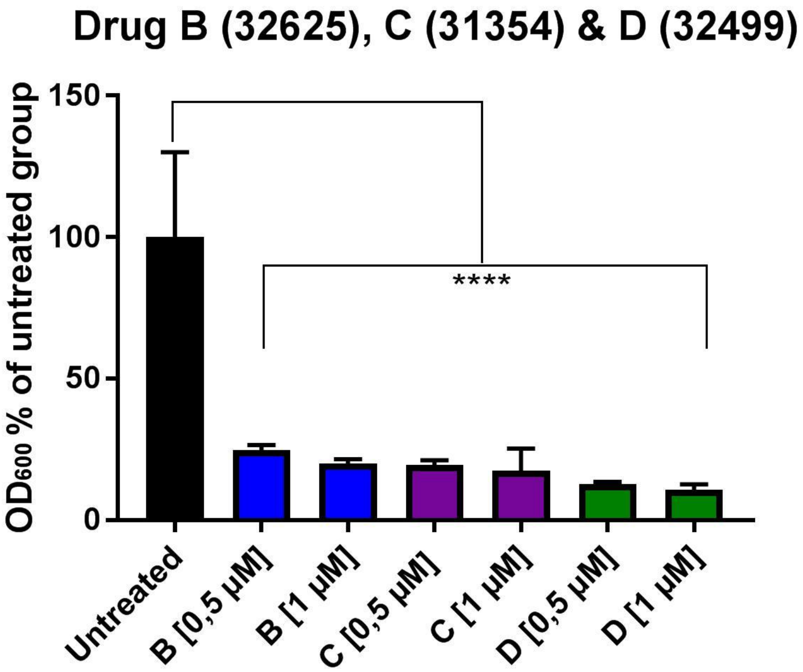

Figure 4.3: *Efficacy comparison between drug B, C and D. Bacterial growth was analyzed by measuring the OD_{600} 5 days post-treatment. Average absorbance value of untreated control defined as 100 %, all other groups converted to a percentage thereafter. Data show the mean ± SD of three independent experiments analyzed by one-way ANOVA, followed by Dunnett's multiple comparisons test.*

From the first series of experiments, examining drugs A and B, it was clear that A was more potent in inhibiting *M.m* growth than B. However, neither of the compounds displayed the sub-micro molar MIC (defined as >90 % inhibition of bacterial growth) as previously seen against *M.tb,* see Table. 4.3. When drugs C and D were tested at two concentrations, where drug B had inhibited >50 % of bacterial growth, the same tendency was observed. None of the drugs were able to match the inhibitory effect seen against *M.tb*. Regardless, all the drugs displayed inhibitory effect against *M.m* at relatively low concentrations, this observation had to be closer examined *in vivo* using the zebrafish embryo.

4.3 *In vivo* studies

For all experiments, performed using polymeric micelles (PM), supplementary section, Table 8.1 provides information regarding batch names, drug and polymer concentration.

4.3.1 Toxicity study: Nanoparticle formulation versus free drug

In vitro toxicity, using Raw 264.7 macrophage-like cell line [163], was investigated prior to toxicity screening in zebrafish. However, due to their hydrophobic character, the free drugs precipitated when added to cell medium from a DMSO drug stock solution. As a result, drug crystals were visible on top of the cells, which prevented their internalization. This was not the case when drugs were encapsulated in the NP formulation. The cytotoxicity had already been tested by our collaborators using VERO cells (monkey) in a 72 h tetrazolium dye assay [164], and found them to be relatively nontoxic. The half-maximal inhibitory concentration for the drugs (A-D) was found to be higher than 128 µM [87-89]. We observed no toxicity against Raw 264.7 cells at this concentration when drug B was in NP formulation (data not shown). Because of the problems in dissolving the free drug, instead of further investigating *in vitro* cytotoxicity, we decided to screen directly *in vivo*, using the zebrafish.

Prior to testing the toxicity of the drugs, we had to analyze the tolerability of the drug carrier DMSO in the embryos, which was essential to dissolve the hydrophobic compounds. The original plan was to use the Casper zebrafish strain, with a double mutation that prevents pigmentation and keeps the embryo transparent without the need of the clearing reagent PTU [165]. However, it soon became evident that the Casper strain was significantly less robust against DMSO injections than the wild type (data not shown). We therefore continued using only Wt embryos. We experienced difficulties injecting a relevant dose of free drug without the aid of solutions comprising much DMSO. Therefore, we had to establish an upper limit of how much DMSO could be in a solution before it killed the embryos. Multiple DMSO concentrations were tested and, from these experiments, we concluded that a ≤10 nL injection with a solution containing 60 % DMSO was the upper limit for avoiding killing of the embryos or inducing severe signs of toxicity (data not shown).

The main goal of the drug toxicity experiment was to establish an acceptable drug dose for the following experiments, in addition to determining if the NP encapsulation reduced mortality relative to the free drug. The experiment was performed using the polymeric micelle samples, collected from the NP batches named OSA and OSB. Fig. 4.4 presents the results of the toxicity experiment.

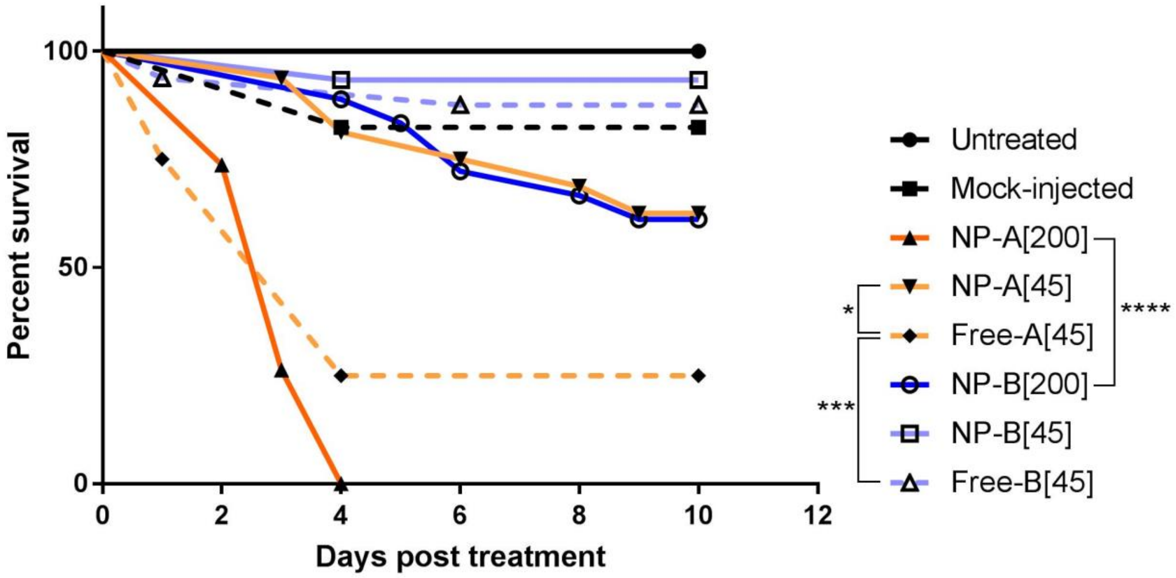

Figure 4.4: *In vivo toxicity assay, survival graph. Drug B, NP encapsulated or free formulation, injected via the posterior cardinal vein 2 days post-fertilization. Free drugs dissolved in PBS with 60 % DMSO and < 1 % PVP, mock-injected group injected with 10 nL of this solvent as a vehicle control. Dose= [mg/kg]. Data analyzed by Log-rank (Mantel-Cox) test and show the cumulative mortality of one experiment, n (embryos per group) = 12-19.*

Embryos treated with drug B had lower mortality than embryos treated with drug A. This was the case for both free and NP encapsulated drugs at both concentrations. Thereby, this identified drug B as the most promising of the two compounds for closer *in vivo* examination, although drug A appeared more potent *in vitro*.

Even though there was no statistical difference between drug B in NP or free form, NP encapsulation of drug A significantly reduced the mortality compared to the same concentration of the free drug. This demonstrated the beneficial effect of reduced toxicity that is generally associated with NP.

4.3.2 Treatment study: Nanoparticle formulation versus free drug

After the toxicities of drug A and B were determined, we concluded that drug B was the most promising one for further testing. The next natural step was to examine the therapeutic effect of drug B encapsulated in polymeric micelles, referred to as NP-B, and compare it to the free formulation of the same drug.

In the first series of treatment experiments, we tested three doses of NP-B and two matching doses of the free drug. The NP samples used (drug-loaded and empty) were taken from batch KS112B and KS117. Due to the drug concentration of the NP sample, the highest dose we could test was 75 mg/kg, assuming the average weight of a zebrafish embryo to be ~1 mg and the maximum tolerable injection volume 10 nL [116]. Due to the hydrophobicity of the drug, precipitation and clogging of the needle during injections was a problem, limiting the therapeutic dose of free drug to 45 and 22.5 mg/kg, depending on the amount of DMSO used for dissolving the drug. 60 % DMSO was needed for 45 mg/kg free drug injection while 30 % DMSO was sufficient for 22.5 mg/kg free drug injection.

Figs. 4.5 and 4.6 present the cumulative mortalities of zebrafish embryos infected with Wt *M.m* at day two post-fertilization and given treatment the following day. Both infection and treatment were initiated by injections via the posterior cardinal vein. The presented data consist of five independent experiments, all under the same conditions, merged. Table 4.4 shows the total number of embryos in each group after merging the experiments. Free- and NP-drug groups are shown in two separate graphs to avoid crowding and improve visualization, the control groups are shown in both graphs. Except for the conditions indicated by asterisks in Fig. 4.6, no significant differences were detected between treatment groups and infected control group.

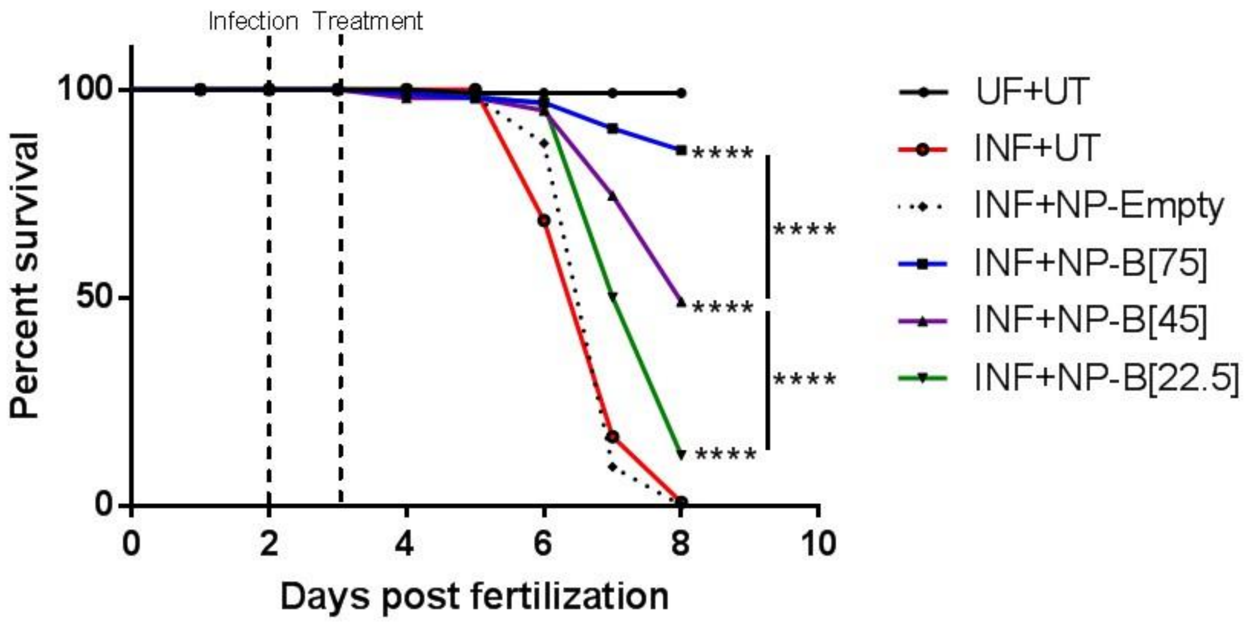

Figure 4.5: *Cumulative mortality of M.m infected zebrafish embryos treated with NP encapsulating drug B. Day of infection and day of treatment is indicated by vertical dotted lines. Dose= [mg/kg]. Data analyzed by Log-rank (Mantel-Cox) test and show the cumulative mortality of five independent experiments merged.*

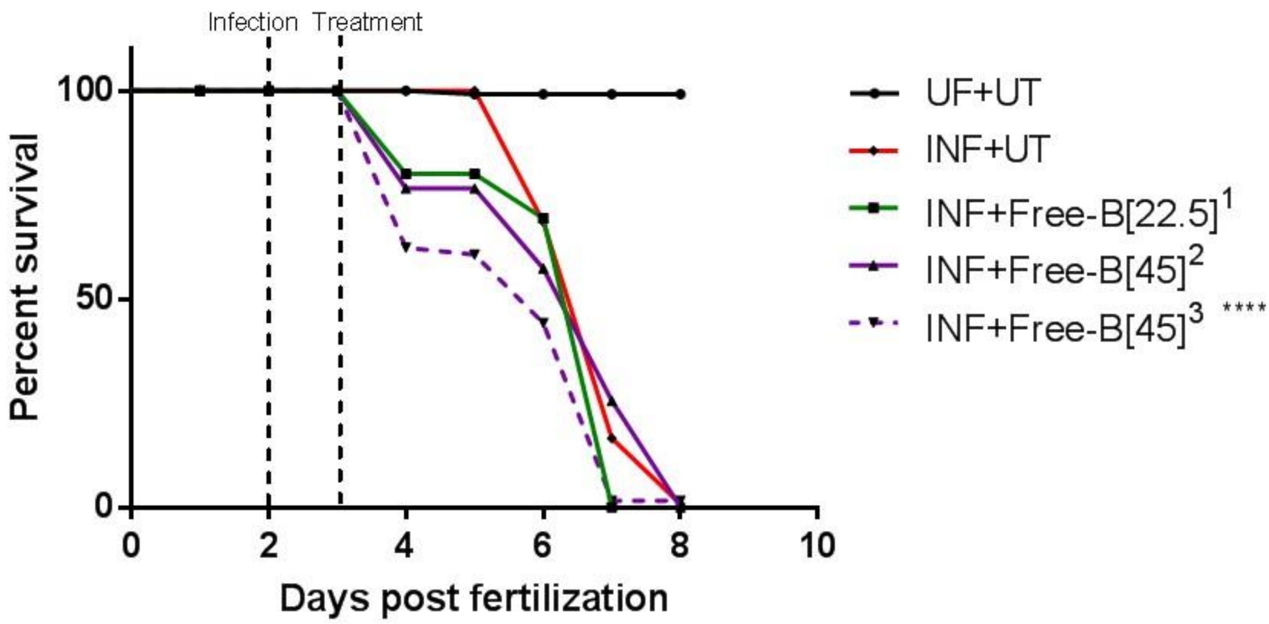

Figure 4.6: *Cumulative mortality of M.m infected zebrafish embryos treated with free drug B dissolved in three different solutions: (1) 30 % DMSO+Tw80< 1 % or (2) 60 % DMSO+Tw80< 1 % or (3) 60 % DMSO+PVP< 1 %. Day of infection and day of treatment is indicated by vertical dotted lines. Dose= [mg/kg]. Data analyzed by Log-rank (Mantel-Cox) test and show the cumulative mortality of five independent experiments merged.*

Table 4.4: *Total number of embryos, in each group, of the five independent experiments merged.*

Group	Total number of embryos
UF+UT	120
INF+UT	96
INF+NP-Empty	54
INF+NP[75]	96
INF+NP[45]	98
INF+NP[22.5]	58
INF+Free[22.5][1]	19
INF+Free[45][2]	16
INF+Free[45][3]	61

It was evident that encapsulation of drug B in polymeric micelles has a significant therapeutic effect against *M.m* infection in zebrafish embryos. Additionally, the efficacy is dose-dependent. The free formulation of drug B had no therapeutic effect, on the contrary, embryos treated with free drug B tended to die before the infection progressed. However, only one free drug group showed a significant (negative) difference compared to the infected control group. Embryos in the toxicity experiment did not display the high mortality observed 24 h post-treatment as seen in the free drug groups here. We hypothesized that the stressful effect of two injections of high volumes (for a zebrafish embryo) in combination to what is injected (bacteria, drug, etc.) is responsible for this sudden mortality observed. Another possible reason is that the free drug aggregates into larger complexes the moment it is injected and these aggregates physically block the circulation, or damage the heart. One explanation does not exclude the other.

In the second series of treatment studies, we tested a mixture of PEG400 and DMSO (4:1 ratio) or the commercial compound captisol (40 % w/v in water) to see if these were better at solubilizing drug B in its free form. The solubility of drug B drastically increased using PEG400-DMSO; captisol however did not completely dissolve the drug at the concentrations needed. We therefore decided to inject 2 nL of drug B (30 mg/mL) in PEG400-DMSO solution, resulting in a therapeutic dose of 60 mg/kg in an embryo at this low injection volume. The NP samples used (drug-loaded and empty) were taken from batch KS149 and KS152. Vehicle control experiments were performed in infected and uninfected embryos, no therapeutic or adverse effects observed (data not shown). Fig. 4.7 present the data of three experiments, all under the same conditions, merged.

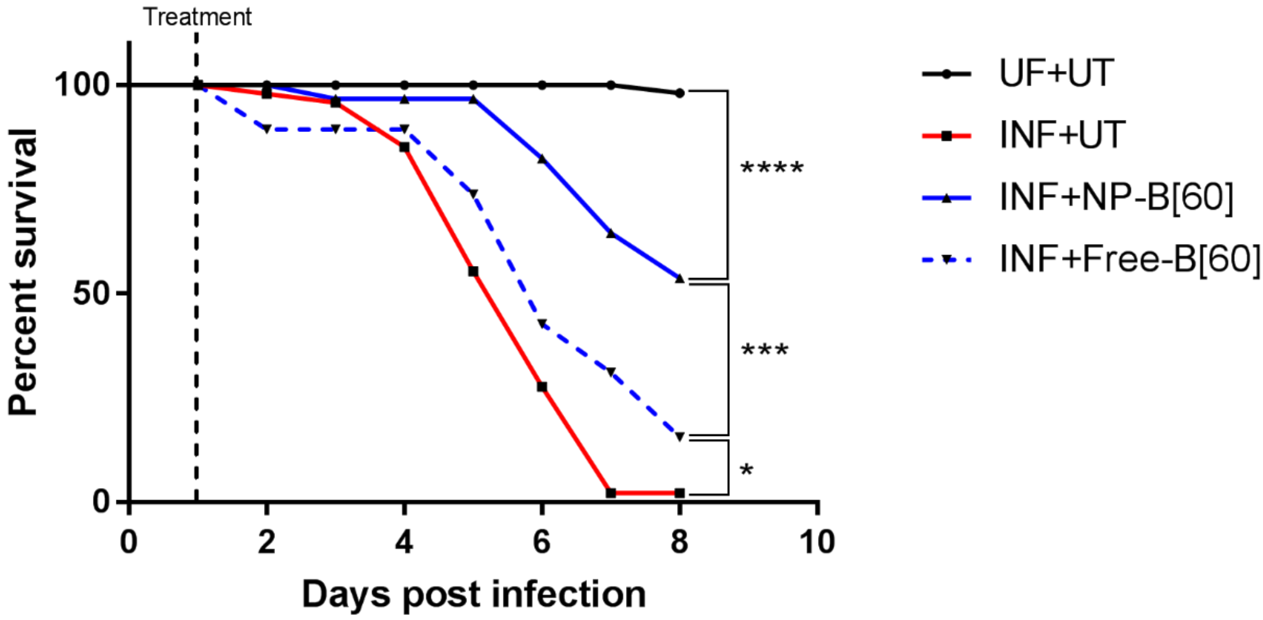

Figure 4.7: *Cumulative mortality of M.m infected zebrafish embryos treated with free drug B, dissolved by PEG400 and DMSO (4:1), or NP encapsulated drug B. Day of treatment is indicated by vertical dotted line. Dose= [mg/kg]. The experiment ended at day 8 post-infection. At this time point, almost all the embryos in the infected control group were dead. Data analyzed by Log-rank (Mantel-Cox) test and show the cumulative mortality of three independent experiments merged, n (embryos per group) =26-52.*

This time we observed a therapeutic effect from the free drug, but the NP formulation was still significantly better, thereby showing, at least for drug B, the beneficial effect from NP encapsulation of hydrophobic compounds. Embryos injected with PEG400-DMSO mixtures showed an increased mortality at 24 h albeit lower than that observed in our first treatment experiments with drug B.

4.3.3 Treatment study: Survival and quantification of bacterial burden

By recording the cumulative mortality and analyzing the bacterial burden using fluorescence, we could examine the therapeutic effect of the different drugs using two different approaches in the same experiment.

The fluorescence pixel count (FPC) method quantifies the total fluorescence associated with the red fluorescent protein expressed by the dsRed *M.m* used for infections [116]. These experiments were performed before starting to dissolve the free drug using PEG400. Due to the absence of a therapeutic effect of the free drug formulation at the time, and the difficulties in administering it, we decided that only the lowest dose, 22.5 mg/kg, was to be tested. In the first experiment conducted, we analyzed the doses used in the initial treatment studies. We used the same NP batches as well, namely KS112B and KS117, for treatment samples. Figs. 4.8 and 4.9 presents cumulative mortality and bacterial burden analysis via FPC of zebrafish embryos infected with red fluorescent *M.m*.

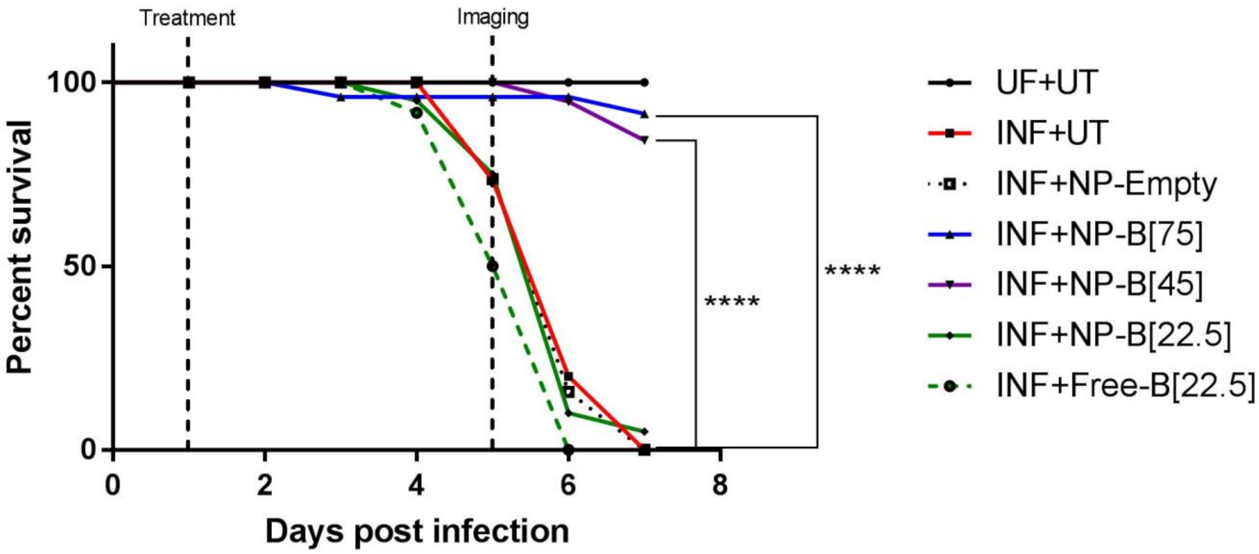

Figure 4.8: *Cumulative mortality of zebrafish embryos infected with dsRed M.m and treated with different doses of drug B encapsulated in polymeric micelles in addition to one dose of drug B in free formulation. Day of treatment and day of imaging is indicated by vertical dotted lines. Dose= [mg/kg]. The experiment ended at day 7 post-infection. At this time point, all embryos in the infected control group were dead. Data analyzed by Log-rank (Mantel-Cox) test and show the cumulative mortality of one experiment, n (embryos per group) =12-25.*

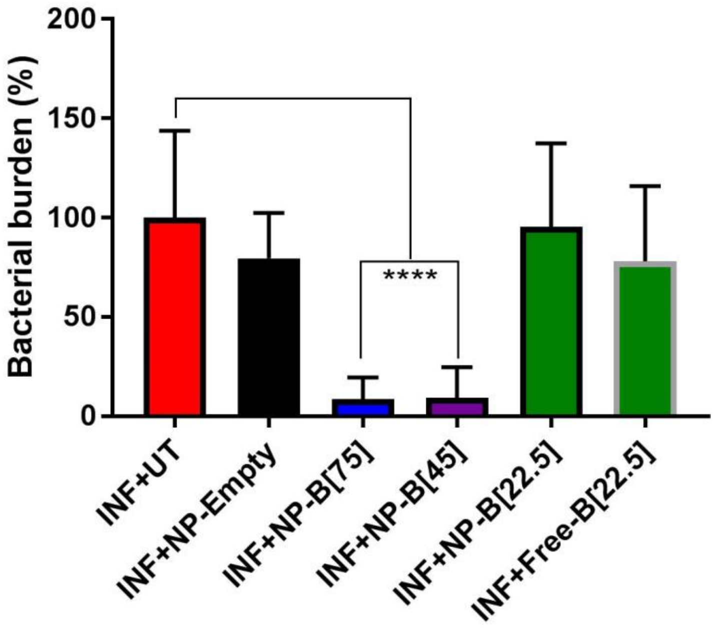

Figure 4.9: *The bacterial burden in dsRed M.m infected zebrafish embryos treated with different doses of drug B encapsulated in polymeric micelles, and one dose in free formulation, at day 5 post-infection. The bacterial burden is displayed as percentage relative to infected control group. Data analyzed by Kruskal-Wallis test, followed by Dunn's multiple comparisons test and represent the mean ± SD of one experiment, n (embryos per group) =8-21.*

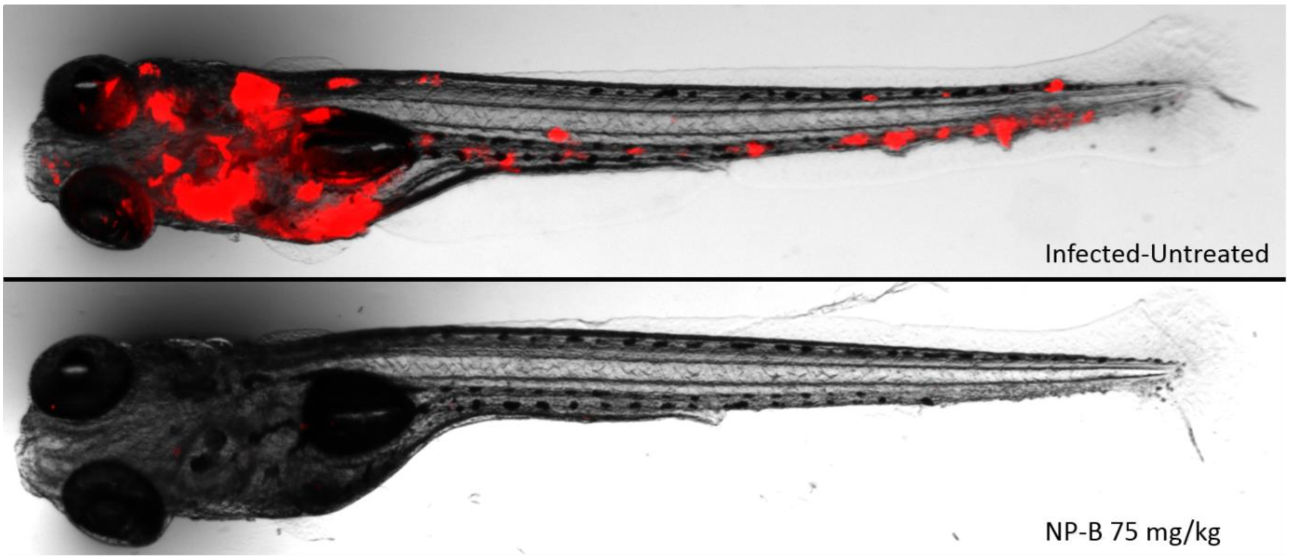

Figure 4.10: *Representative images of the FPC experiment, obtained 5 days post-infection using a stereomicroscope. At the top, an embryo from the infected control group heavily infected (red color). At the bottom, an embryo infected and given drug B in polymeric micelle formulation (75 mg/kg) the following day, displaying almost no visible signs of infection. Image obtained at 30x magnification.*

The results from the cumulative mortality correlated well with the bacterial burden analysis and with the previous treatment study, except for the NP 22.5 mg/kg group, which showed little effect. It is important to note that 4 out of 12 embryos in the free drug group were dead (due to infection) before imaging took place and were therefore excluded from the imaging part, thereby introducing a bias.

At the time of the first FPC study, we received two new compounds for screening, namely drug C and D from Dr. Andrew Thompson (University of Auckland, New Zealand). A sample of both drugs were sent to University Mainz for encapsulation in polymeric micelles by Kerstin Johann while drug C was sent to the lab of Bruno De Geest for encapsulation in another type of NP. Therefore, in the second series of FPC experiments we tested drugs B, C and D in NP formulation at a single concentration together. Due to the measured drug concentration of the new NP samples, the highest dose we could test was 60 mg/kg. In the first series of experiments, we used the NP produced in Barz's lab (batches KS124, KS125, KS132A and KS132B). Figs. 4.11 and 4.12 present the cumulative mortality of the zebrafish embryos and the bacterial burden at 5 days post-infection respectively. The presented data consist of four independent experiments, with the same conditions, merged. Table 4.5 presents initial infection (CFU), therapeutic doses and total number of embryos in each group plus numbers of embryos imaged.

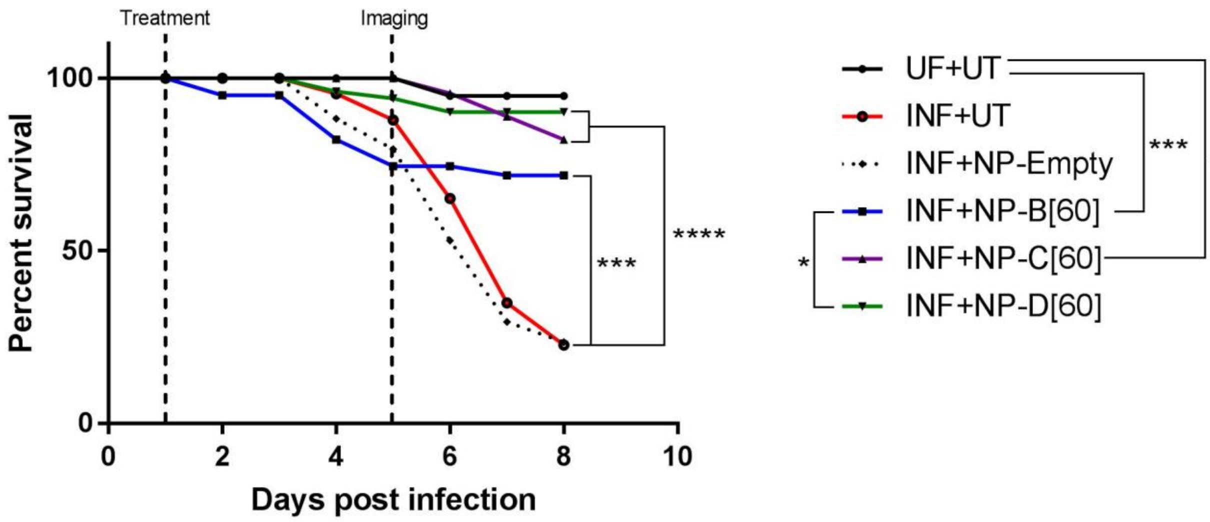

Figure 4.11: *Cumulative mortality of zebrafish embryos infected with dsRed M.m and treated with drugs B, C or D, encapsulated in polymeric micelles. Day of treatment and day of imaging is indicated by vertical dotted lines. The experiment ended at day 8 post-infection. At this time point, about 80 % of the embryos in the infected control group were dead. Data analyzed by Log-rank (Mantel-Cox) test and show the cumulative mortality of four independent experiments merged, n (embryos per group) =34-66.*

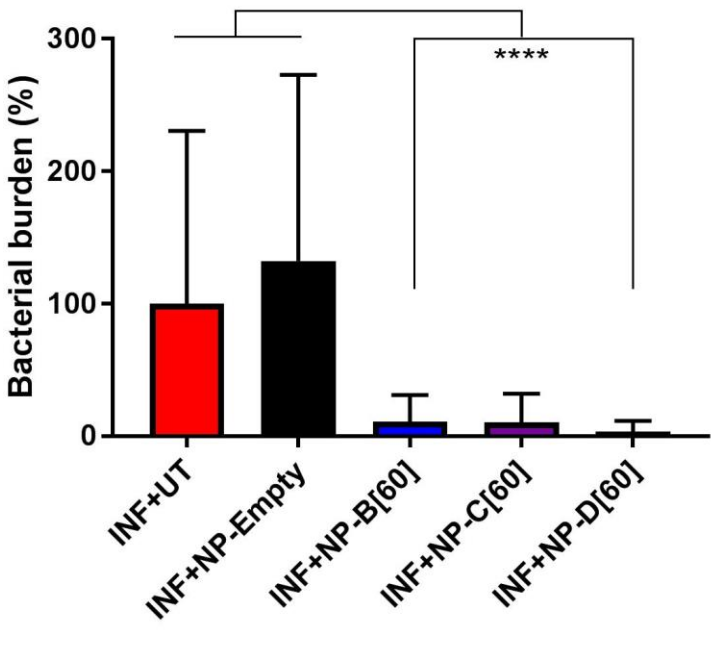

Figure 4.12: *The bacterial burden in dsRed M.m infected zebrafish embryos treated with drugs B, C or D, encapsulated in polymeric micelles at day 5 post-infection. Bacterial burden displayed as percentage relative to infected control group. Data analyzed by Kruskal-Wallis test, followed by Dunn's multiple comparisons test and show the mean ± SD of four independent experiments merged, n (embryos per group) =28-61.*

__Table 4.5:__ Group and batch names of the various samples in addition to infection dose, therapeutic dose and total number of embryos infected and included in the experiment, and the total number of embryos imaged for each group.

Group	Initial infection, dsRed Mm	Therapeutic dose	N=ZF-embryos Total/Imaged
UF+UT	-	-	57/54
INF+UT	5 nL, OD_{600}= ~1.0 (250 CFU)	-	66/61
INF+NP-B (KS132B)	5 nL, OD_{600}= ~1.0 (250 CFU)	50 mg/mL drug + polymer (30 % drug), 4 nL= **60 mg/kg**	38/29
INF+NP-C (KS124)	5 nL, OD_{600}= ~1.0 (250 CFU)	20 mg/mL drug + polymer (30 % drug), 10 nL= **60 mg/kg**	45/39
INF+NP-D (KS125)	5 nL, OD_{600}= ~1.0 (250 CFU)	20 mg/mL drug + polymer (30 % drug), 10 nL= **60 mg/kg**	50/48
INF+NP-Empty (KS132A)	5 nL, OD_{600}= ~1.0 (250 CFU)	50 mg/mL polymer only, 10 nl	34/28

The two new compounds, drug C and D, had a significant therapeutic effect against the *M.m* infection. Bacterial burden reflected the cumulative mortality nicely, for all three drugs tested. In addition, drug D emerged as the most promising drug candidate, not being significantly different from the uninfected control group. This was in agreement with results that had been reported earlier [87-89].

Our collaborator Bruno De Geest at Ghent University in Belgium, sent us poly (ethylene glycol)-polylactic acid (PEG-PLA) NP encapsulating drug C. Therefore, in the third FPC experiment we wanted to examine the therapeutic effect of this new NP. We tested the same drug dose, 60 mg/kg, as the previous FPC experiment. Figs. 4.13 and 4.14 presents cumulative mortality and bacterial burden analysis, respectively.

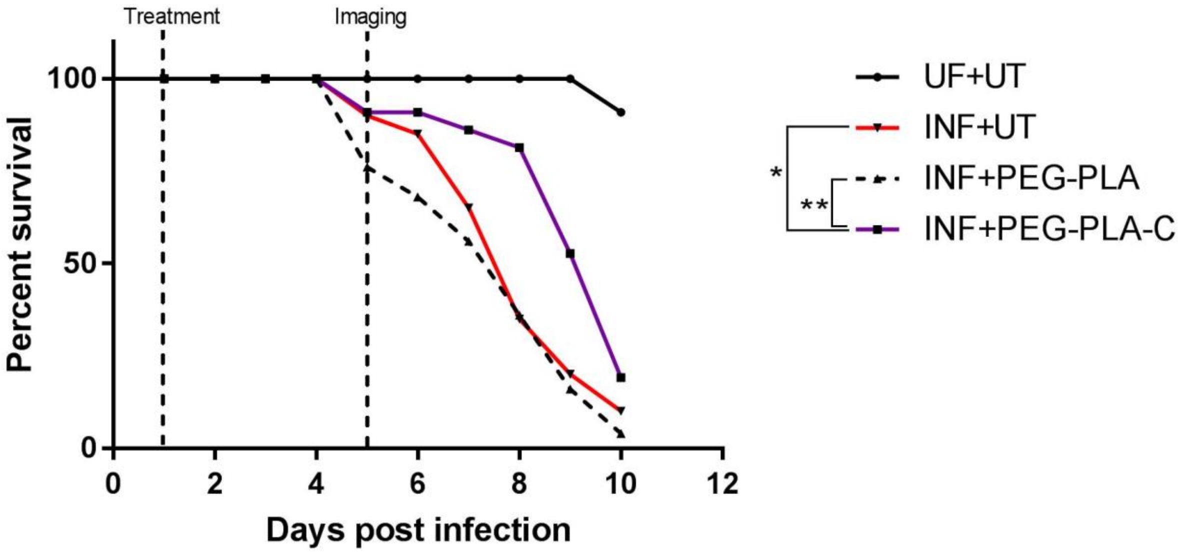

Figure 4.13: *Cumulative mortality of zebrafish embryos infected with dsRed M.m and treated with 60 mg/kg of drug C encapsulated in PEG-PLA NP. Day of treatment and day of imaging is indicated by vertical dotted lines. The experiment ended at day 10 post-infection. At this time point, almost all embryos in the infected control group were dead. Data analyzed by Log-rank (Mantel-Cox) test and show the cumulative mortality of one experiment, n (embryos per group) =20-25.*

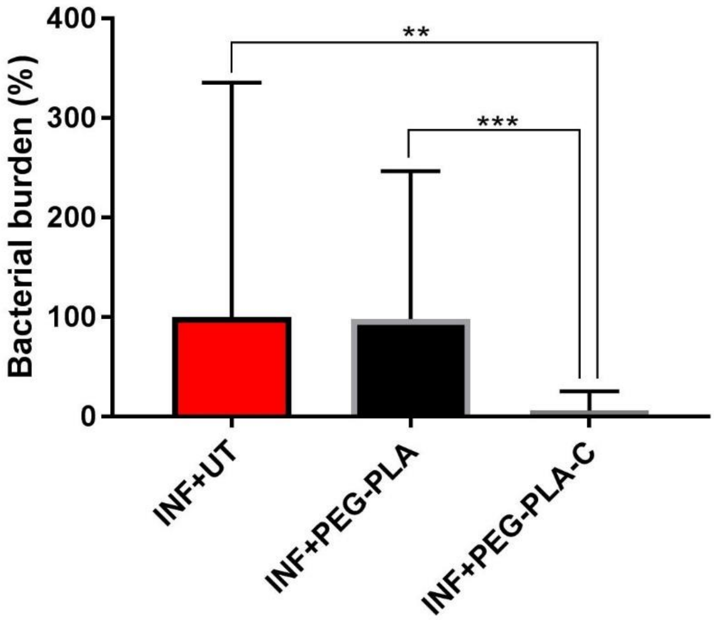

Figure 4.14: *The bacterial burden in dsRed M.m infected zebrafish embryos treated with 60 mg/kg drug C encapsulated in PEG-PLA NP at day 5 post-infection. Bacterial burden displayed as percentage relative to infected control group. Data analyzed by Kruskal-Wallis test, followed by Dunn's multiple comparisons test and show the mean ± SD of one experiment, n (embryos per group) =20-25.*

Due to a weak infection and slow mortality rate within the infected control group, we had to record the overall survival until day 10 post-infection (12 days post-fertilization). Regardless, in this experiment, the same pattern was observed as with the polymeric micelles. We could detect, in infected embryos treated with drug-NP, a significant increase in survival and reduction in bacterial burden compared to infected control embryos and embryos treated with empty NP.

4.3.4 Rifampicin loaded MPEO-b-PCL nanoparticles: Treatment and nanoparticle localization studies

Another collaborator with our group, Jiri Trousil at the Institute of Macromolecular Chemistry (Academy of Sciences, Czech Republic), sent us rifampicin (Rif) loaded MPEO-b-PCL (polymeric micelles) NP for testing in the zebrafish embryo model of TB. *In vitro* studies had showed rapid macrophage uptake and improved efficacy against mycobacterium infection when Rif was encapsulated in these NP compared to free Rif [166]. We therefore wanted to test the therapeutic effect of the NP and examine if they accumulated within macrophages *in vivo*. Potentially, these NP could also be used to encapsulate the pretomanid analogues. The results are presented separately below as treatment study (survival) and NP localization studies. Fig. 4.15 presents the treatment study, Figs. 4.16 and 4.17 presents NP localization studies.

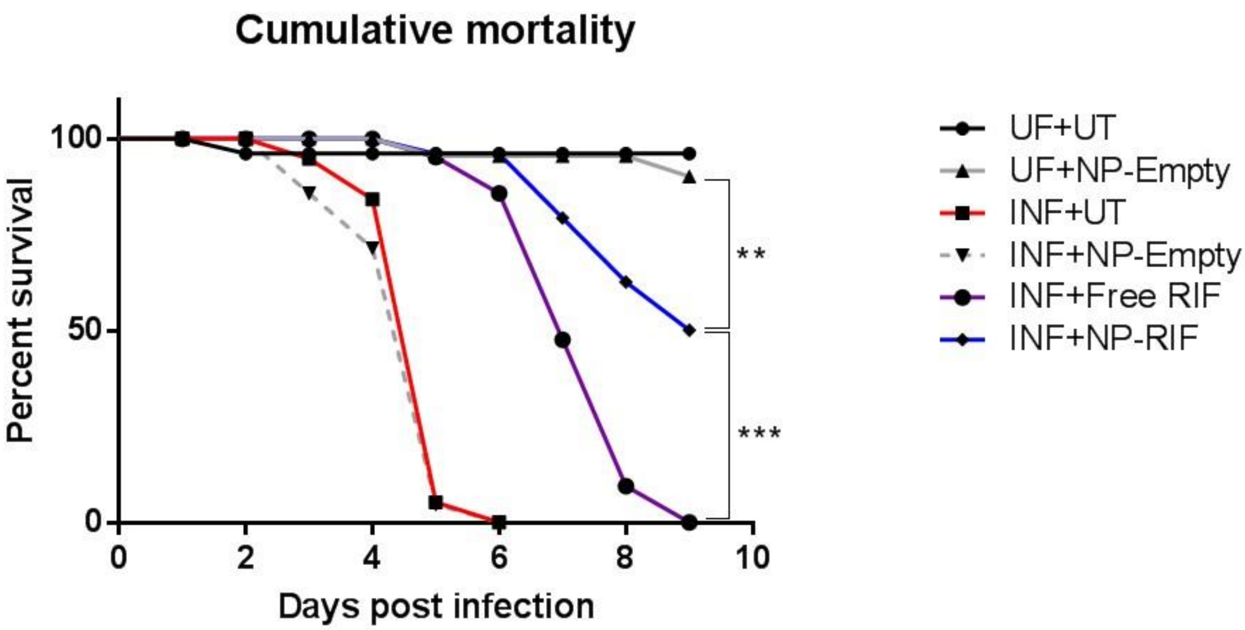

Figure 4.15: *Cumulative mortality of Wt M.m infected zebrafish embryos treated with 10 mg/kg rifampicin, in free form or NP formulation. Infection and treatment were administered through injection into the bloodstream. Concentration of polymer in empty-NP is equal to that in NP-RIF. Data analyzed by Log-rank (Mantel-Cox) test and show the cumulative mortality of one experiment, n (embryos per group) =19-24.*

Treatment study: Rif in the free form had a protective effect against the *M.m* infection, delaying the mortality by about 3 days. However, when Rif was encapsulated in NP, 50 % of the embryos were alive at day 9 post-infection, a significant improvement compared to free Rif. Nevertheless, both groups receiving Rif had a significantly higher mortality than the uninfected control groups. NP by themselves had no therapeutic or toxic effect on uninfected or infected embryos.

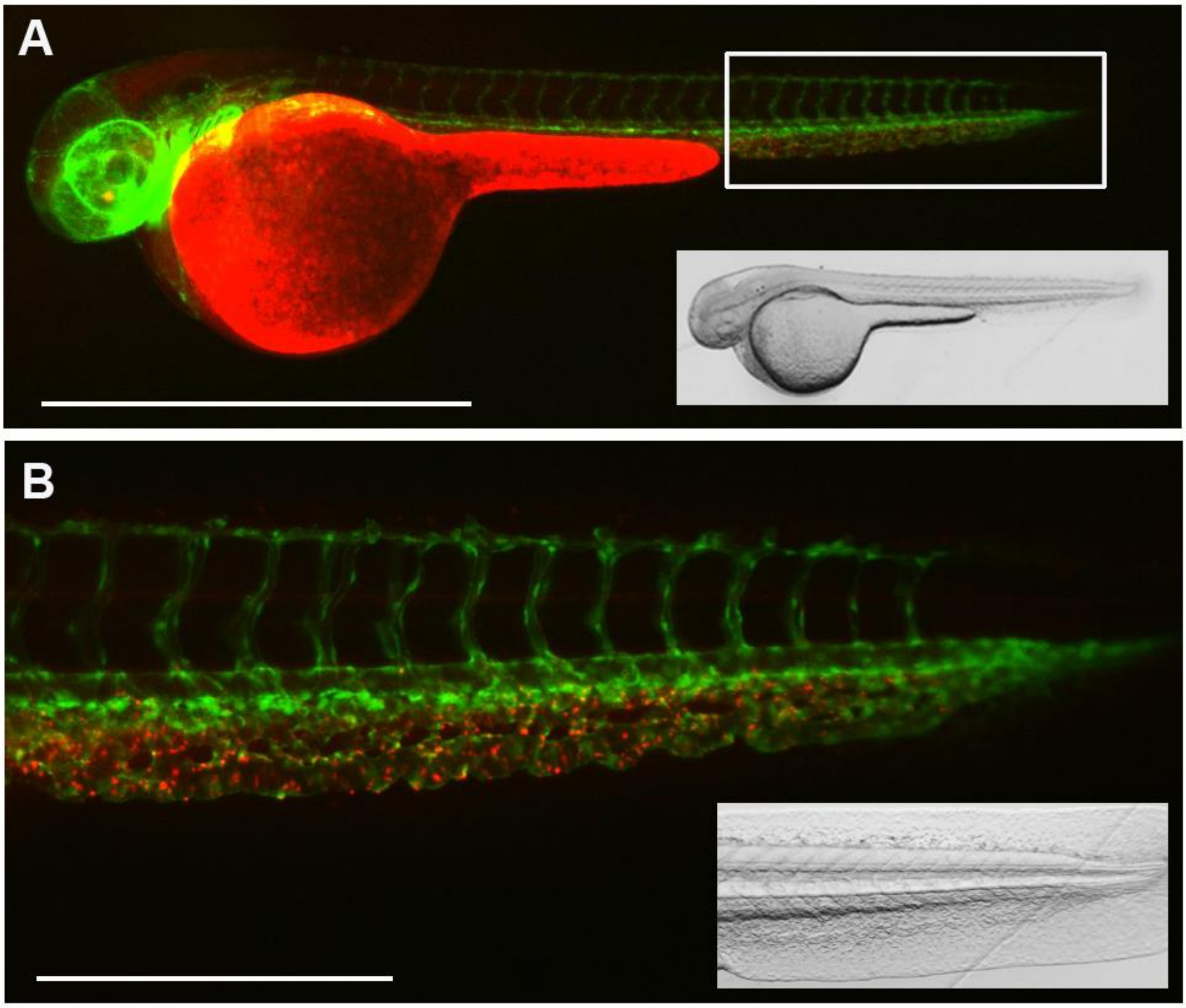

Figure 4.16: *Stereomicroscopy of tg(-fli1a:EGFP) zebrafish embryos (green endothelia) injected with red fluorescent NP. Images obtained at 30x and 120x magnification, 2 h post-injection. (A) Fluorescent image of the whole embryo. Green- blood vessels, red- NP in addition to strong auto-fluorescence from the yolk sack. Bottom right is the correspondent transmission image of the whole embryo. Scale bar 1 mm. (B) Enlargement of the white rectangle in (A) showing the fluorescent image of the tail area. The NP, in red, clearly co-localize with endothelial cells and the majority is no longer circulating in the blood stream. Bottom right is the correspondent transmission image of the tail region. Scale bar: 300 μm.*

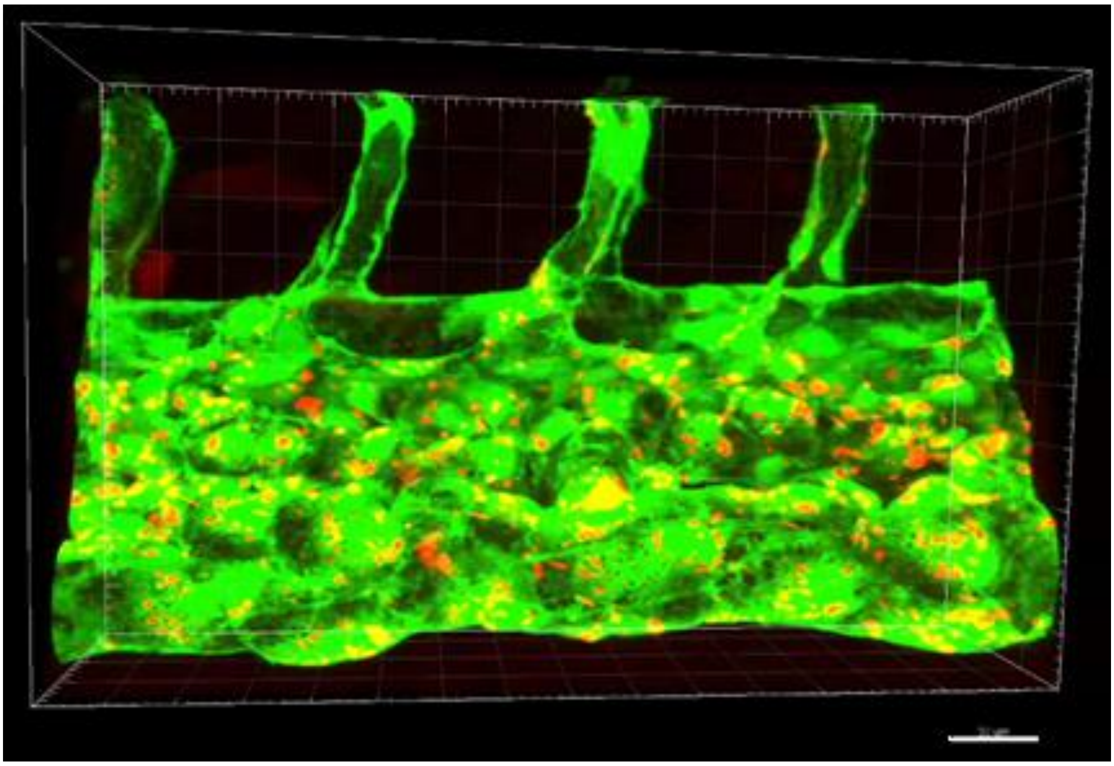

Figure 4.17: *Confocal microscopy of tg(-fli1a:EGFP) zebrafish embryos (green endothelia) injected with the red fluorescent NP. Images obtained using the 60x water immersion lens and subsequently analyzed and processed using Imaris Image Analysis Software. The image is a snapshot of a 3D reconstruction of the tail area of the embryo, green- blood vessels, red- NP. Red NP co-localize with the green endothelial cells making up the blood vasculature. Scale bar: 30 µm.*

NP localization study: The majority of the red fluorescent NP co-localized with endothelial cells, not macrophages, at 2 h post-injection into the bloodstream (Fig. 4.16). By confocal microscopy, it became evident that the majority of NP were taken up by the endothelial cells (Fig. 4.17 for 3D presentation).

4.3.5 Mice treatment and nanoparticle localization studies

Based on the results obtained from the zebrafish embryo model, which showed a significant therapeutic effect of the NP encapsulated drugs (B, C and D), we decided to do an experiment using the mouse model with our collaborators in David G. Russell group at the department of Microbiology and Immunology at Cornell University College of Veterinary Medicine, USA. The compound tested in mice was drug B (the most extensively examined drug in our group at the time). Polymeric micelles, loaded with drug or fluorescent dye or left empty, were used. Kerstin Johann at Johannes Gutenberg-University Mainz made the NP, and Yitian Xu at Cornell University performed the experiments in mice. The NP samples used were from batch

KS135-KS137. The results from the treatment study is presented in Fig. 4.18 while Fig. 4.19 presents the NP localization results.

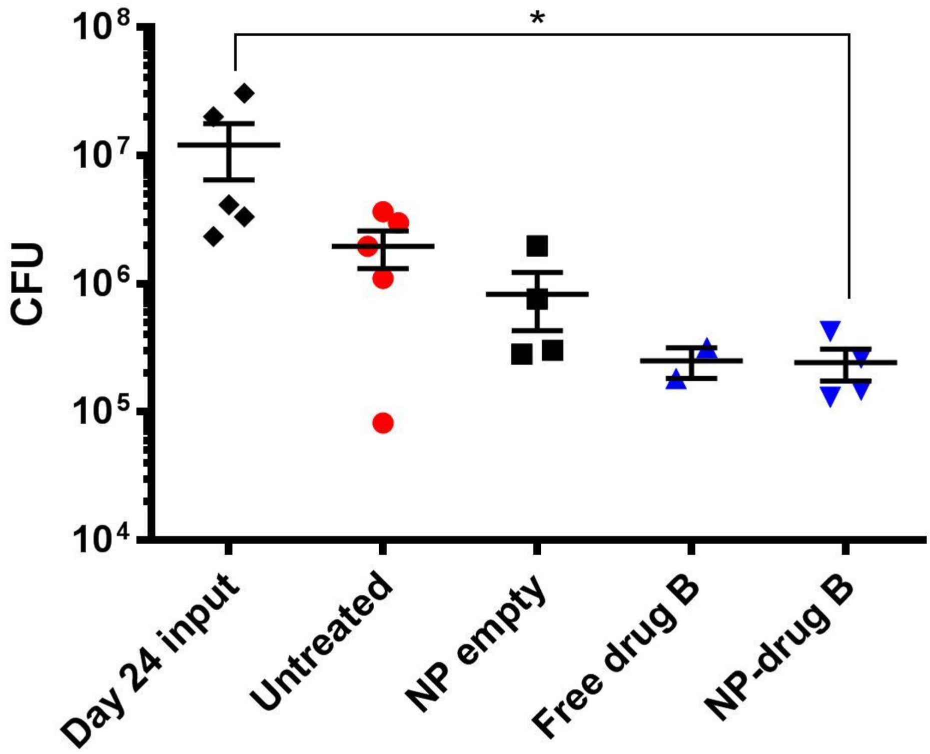

Figure 4.18: *CFU analysis, of tissue obtained from the lung of M.tb infected mice, at day 40 post-infection. Data analyzed by Kruskal-Wallis test, followed by Dunn's multiple comparisons test and show the mean ± SEM of one experiment, n (mice per group) =2-5.*

The test groups received the appropriate treatment at day 24, 28, 32 and 36 post-infection, assuming an average weight of 20 grams per mouse, then one injection dose equals ~90 mg/kg drug. There were five mice in each group at the start of the experiment. However, three mice died in the free drug group after the second injection, likely due to complications directly associated with injecting the viscous PEG400 drug solution. Two mice were excluded in the NP groups, one in each, due to no bacterial growth when plated for CFU analysis. Kruskal-Wallis test, followed by Dunn's multiple comparisons test, detected a significant difference between the NP-drug group and the infection input group. However, we would need more data to say anything conclusive, and must therefore repeat this experiment. Nevertheless, the trend of CFU reduction in both groups receiving drug B, in combination with the observation of difficulties administering the free drug in a safe fashion is a strong argument for further testing.

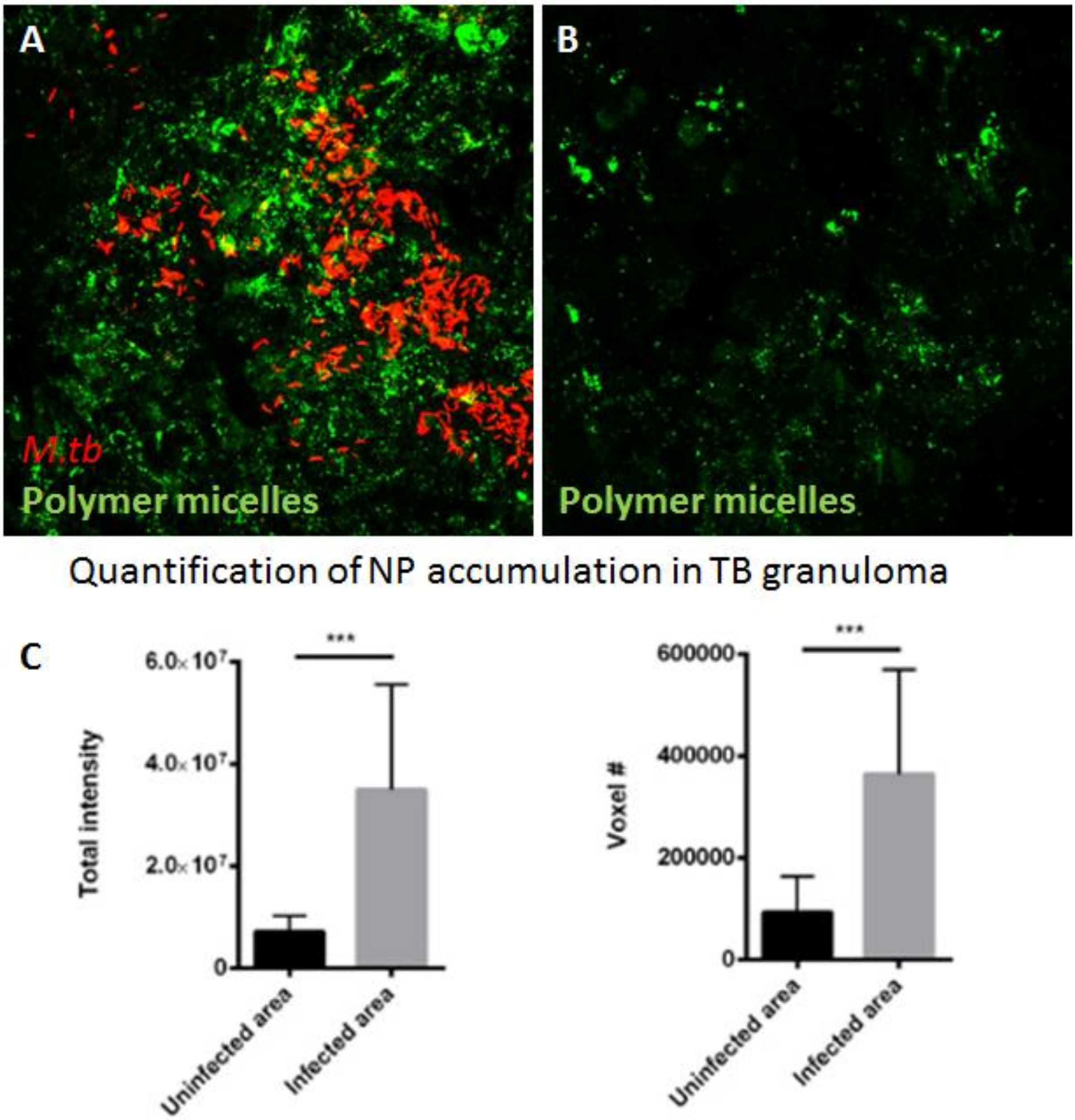

Figure 4.19: *Accumulation of polymeric micelles in granulomas within the lung of M.tb infected mice. (A) Area of the lung heavily infected with M.tb and high accumulation of PM. (B) Non-infected area of the lung, less PM accumulation relative to (A). (C) Quantification of PM accumulation in image (A) and (B), presented as total fluorescence intensity and voxels, which is defined as an arbitrary unit of graphic information that defines a point in three-dimensional space.*

From the localization studies, it was evident that the PM accumulated to a significantly higher degree at infected lung areas compared to non-infected areas. This observation, in combination with the CFU reduction trend in drug groups from the treatment experiment further strengthens the argument for NP encapsulation of hydrophobic drugs.

4.3.6 Tetracycline-controlled transcriptional activation in transformed *M. marinum* using the zebrafish model

The last objective for this thesis was to establish a new model for studying the dynamic character of the granuloma within a zebrafish embryo infected with *M.m*. The construction of the plasmid containing GFP/mKO and subsequent transformation of wild type *M.m* are described in materials and methods section.

The transformed *M.m* constitutively express GFP (green) while mKO (red) is only expressed upon induction by a tetracycline. This construct allows us to observe the fitness of *M.m* during infection as only bacteria capable to actively transcribe the protein will become fluorescent in the red channel. In order to test this new construct, we infected zebrafish embryos with GFP/mKO bacteria and let the infection progress over a few days, allowing for granuloma formation, before inducing mKO expression. Only metabolically active bacteria were able to express the mKO protein, thereby separating themselves from metabolically inactive or dead bacteria that still can appear green in color due to remaining GFP.

Two different inducers were tested, Dox and ATc. In addition, we tried two different approaches for administering the inducer, water bath immersion and intravenous injection. The model is still in the early stages of development and needs to be optimized with regard to inducer concentration and minimum time required for sufficient mKO expression. Fig. 4.20 presents the *in vitro* results. Fig. 4.21 presents the *in vivo* mKO-induction via the inducer-immersion technique. Figs. 4.22 and 4.23 presents the *in vivo* mKO-induction via the inducer-microinjection technique.

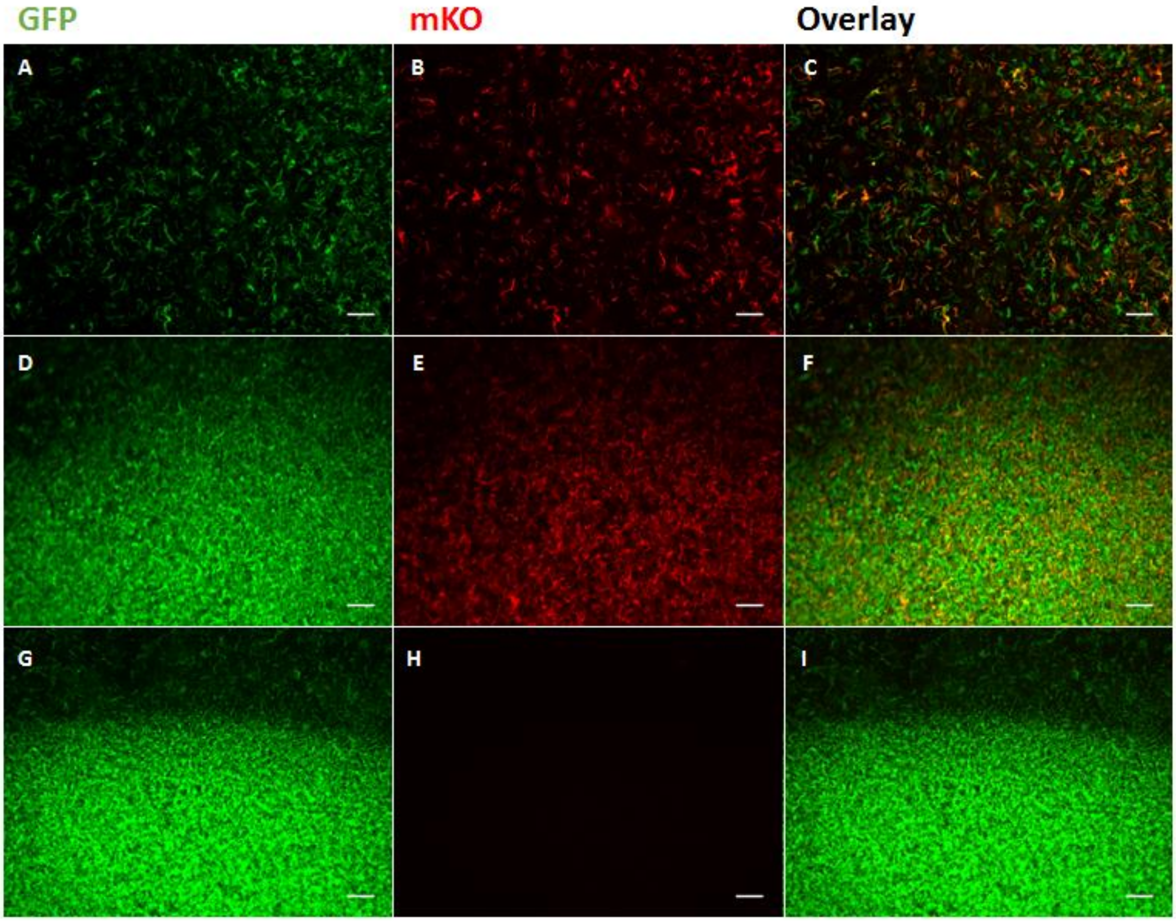

Figure 4.20: *Stereomicroscopy of GFP/mKO M.m 24 h post Dox exposure. Left column- GFP, middle column- mKO, right column- overlay. A-C: bacteria exposed to 1 µg/mL of Dox. D-F: bacteria exposed to 50 µg/mL Dox. G-I: Negative control, no Dox exposure. Scale bar: 100 µm.*

Tetracycline is a class of antibiotics that are broadly bacteriostatic; their mode of action is to bind the bacterial ribosome and inhibit protein synthesis [167]. Doxycycline inhibits the growth of *M.m*, and the minimum inhibitory concentration after five days of exposure has been reported to be 4 µg/mL [168]. Our *in vitro* results showed Dox induced activation of mKO expression at both high (50 µg/mL) and low (1 µg/mL) concentrations when incubation period was 24 h. In the negative control (no Dox added), GFP was expressed as normal and no mKO expression was detected. This was sufficient evidence to allow us to move to the *in vivo* experiments.

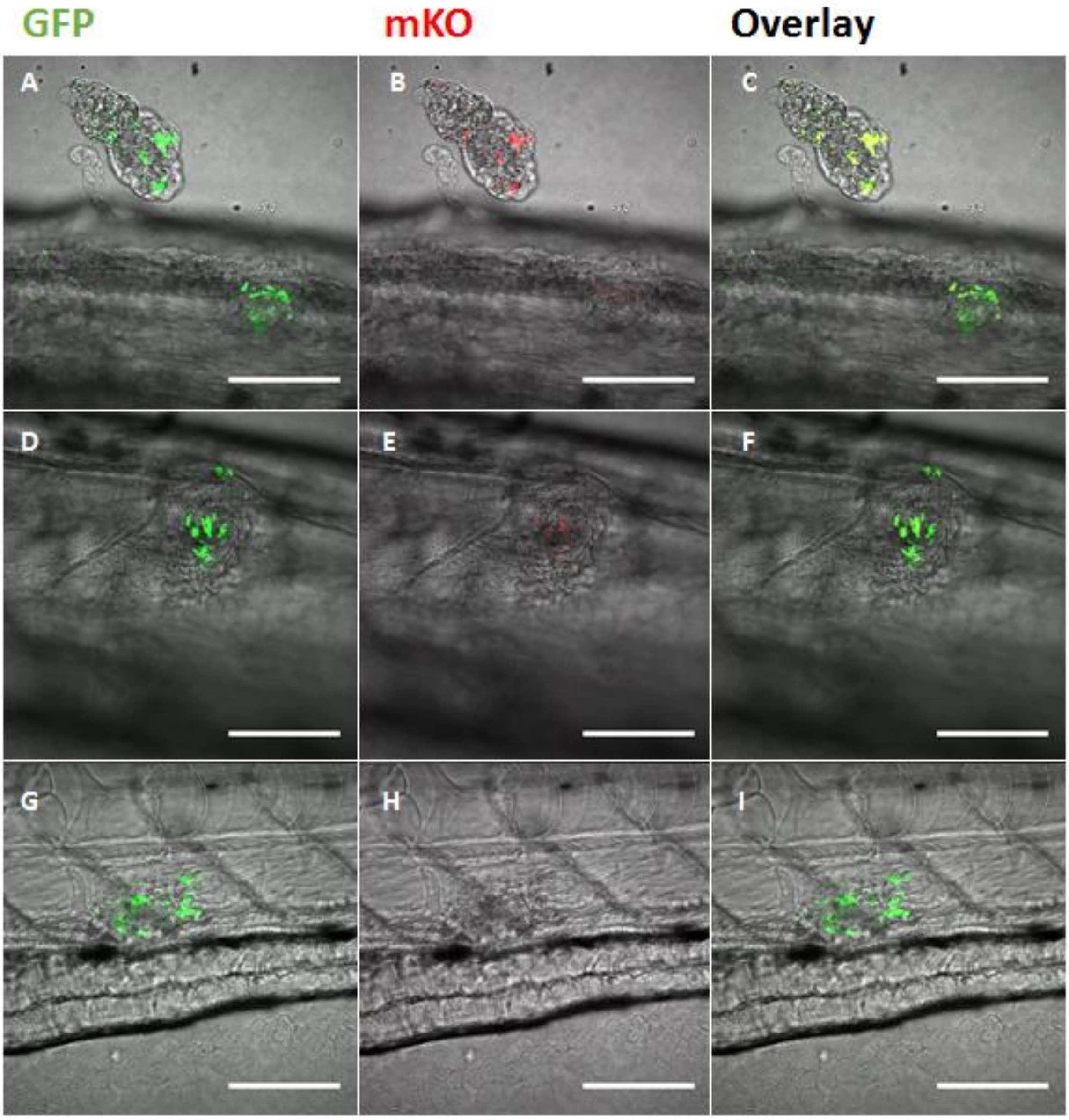

Figure 4.21: *Confocal microscopy of zebrafish embryos infected with GFP/mKO M.m via the posterior cardinal vein at day 2 post-fertilization, followed by mKO induction through 24 h immersion in a Dox (50 µg/mL) or ATc (10 µg/mL) water bath, initiated at day 4 post-infection. Images obtained right after the 24 h induction period, using the 40x water immersion lens. Left column- GFP (excitation at 488 nm), middle column- mKO (excitation at 543 nm), right column- overlay. A-C: Dox exposed embryo, with granuloma that protruded out of the tail region and detached during preparation. D-E: ATc exposed embryo, with granulomas found in the tail region. G-I: Negative control, no exposure to either Dox or ATc. Granulomas were in the tail region. Scale bar: 100 µm.*

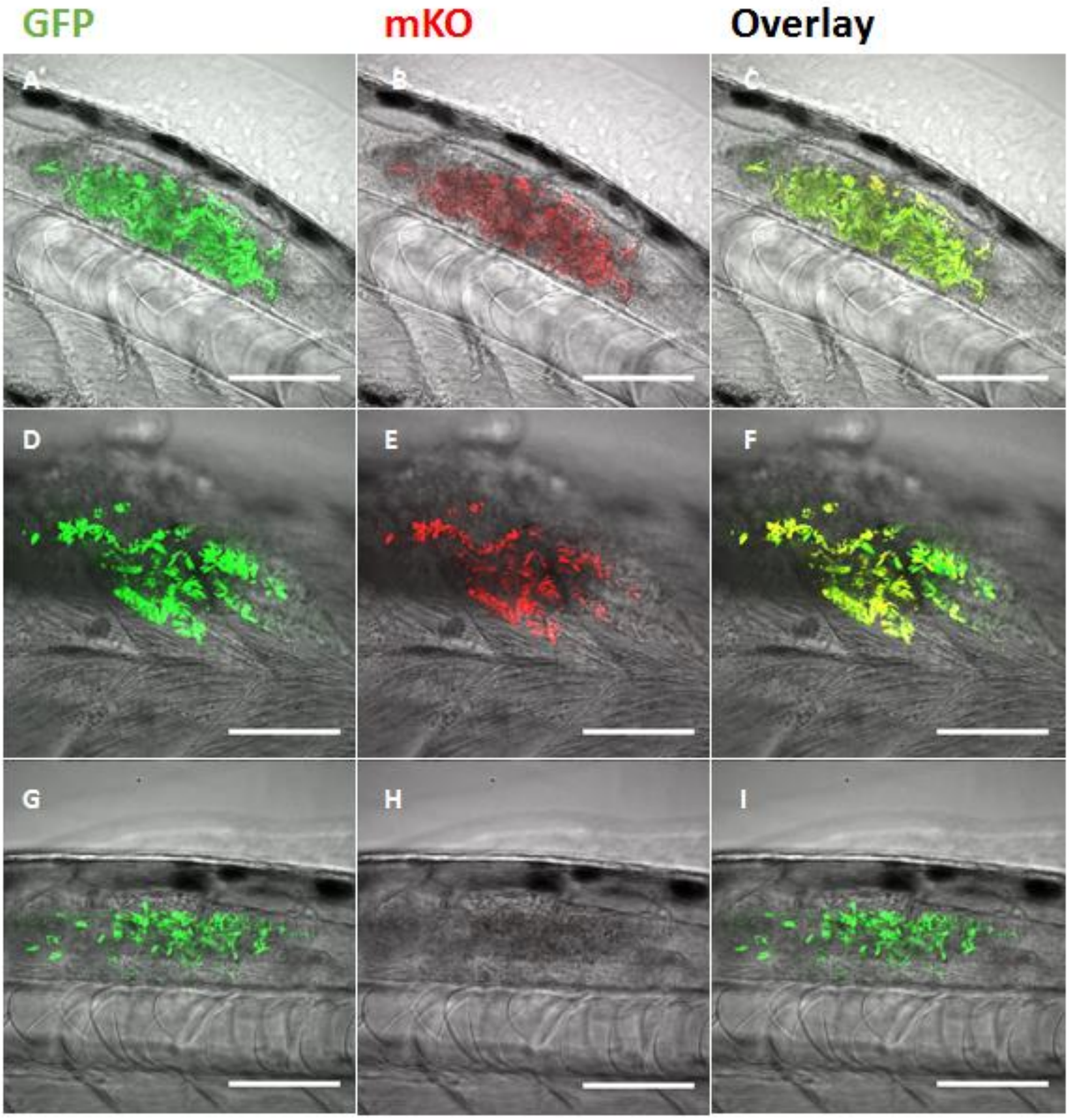

Figure 4.22: *Confocal microscopy of zebrafish embryos infected with GFP/mKO M.m via the neural tube at day 2 post-fertilization, followed by mKO induction through injecting ~5 nL ATc dissolved in PBS (500 µg/mL) into the posterior cardinal vein at day 4 post-infection. Images obtained 24 h post ATc exposure, using the 40x water immersion lens. Left column- GFP (excitation at 488 nm), middle column- mKO (excitation at 543 nm), right column- overlay. A-C: Granulomas located in the neural tube. D-F: Granulomas located in the neural tube with some dissemination to surrounding tissue. G-I: Negative control, not injected with ATc, showing granulomas in the tail region. Scale bar: 100 µm.*

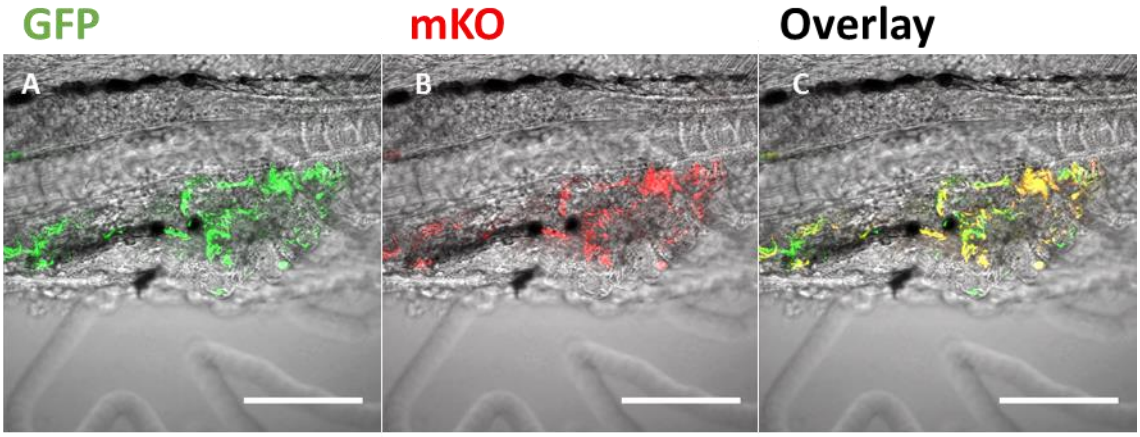

Figure 4.23: *Confocal microscopy of zebrafish embryos infected with GFP/mKO M.m via the posterior cardinal vein at day 2 post-fertilization, followed by mKO induction through injecting ~5 nL ATc dissolved in PBS (500 µg/mL) into the posterior cardinal vein at day 5 post-infection. Images obtained 24 h post ATc exposure, using the 40x water immersion lens. Left column- GFP (excitation at 488 nm), middle column- mKO (excitation at 543 nm), right column- overlay. A-C: Granulomas located in the tail region. Scale bar: 100 µm.*

The initial plan was to induce mKO expression *in vivo* through water bath immersion with the inducer dissolved in embryo water. Unfortunately, unlike ATc, Dox interacted with the salt present in the solution and precipitated, especially at higher concentrations. The solution was to use distilled water instead of embryo water for dissolving Dox with the clearing agent PTU added anyways. A tolerability screen with embryos in distilled water with PTU was conducted over 72 h, and the embryos all survived without any visible signs of toxicity. Next followed a tolerability screen against the inducers, Dox or ATc, dissolved in a water solution. With respect to survival and toxicity, we established that an incubation period of 24 h of 50 µg/mL Dox or 10 µg/mL ATc was acceptable.

In the first series of *in vivo* experiments, we observed that induction by immersion worked to some extent, as illustrated in Fig. 4.21. However, at the inducer concentrations tested, the red signal coming from mKO expression was very weak, only present close to the outer rim of the zebrafish embryo and not deep into the tissue. We concluded that immersion, as a way of inducing protein expression of GFP/mKO *M.m* was insufficient. We therefore decided to inject the inducer in the bloodstream at a concentration far higher than that used in the water bath. ATc is broadly used as an inducer for Tet-On protein expression in bacteria, having the advantage over Dox of being less bactericidal, possibly by having a different mechanism of action than ribosome binding [169]. ATc was therefore selected to be the inducer when injecting higher concentrations directly into the bloodstream of an infected embryo.

In the second series of *in vivo* experiments, it became clear that injecting the inducer was much more effective than the immersion technique, as illustrated in Figs. 4.23 and 4.24. The downside of this approach is that the individual injections of 7 day old embryos, are time consuming and technically difficult. With this technique however, the inducer reached the site of infection and penetrated both neural tube (Fig. 4.22) and bloodstream granulomas (Fig. 4.23). This was confirmed when confocal imaging was applied and red (mKO) signal was present in all slices of the z-stacks obtained. In an attempt to quantify the area of red signal compared to green, a trend of higher ratios of red-to-green was observed in bloodstream granulomas compared to neural tube granulomas. However, this observation requires more examination with an optimized protocol to say anything conclusive about the analysis and its implications. The quantification analysis (data not shown) was conducted by setting a threshold for the each respective signal, thereby excluding the background noise, and convert image to binary information followed by particle analysis using ImageJ.

In the late stages of the work described in this thesis, Julien Resseguier performed cryostat-sections (30 µm) of zebrafish embryos (previously infected with GFP/mKO *M.m*, followed by ATc exposure) fixed in 4 % paraformaldehyde in PBS and subsequently imaged using an Andor Dragonfly spinning disk confocal microscope (Andor Technology, Belfast, UK). Fig. 4.24 illustrates a posterior cardinal vein-infected embryo and Fig. 4.25 illustrates a neural tube-infected embryo.

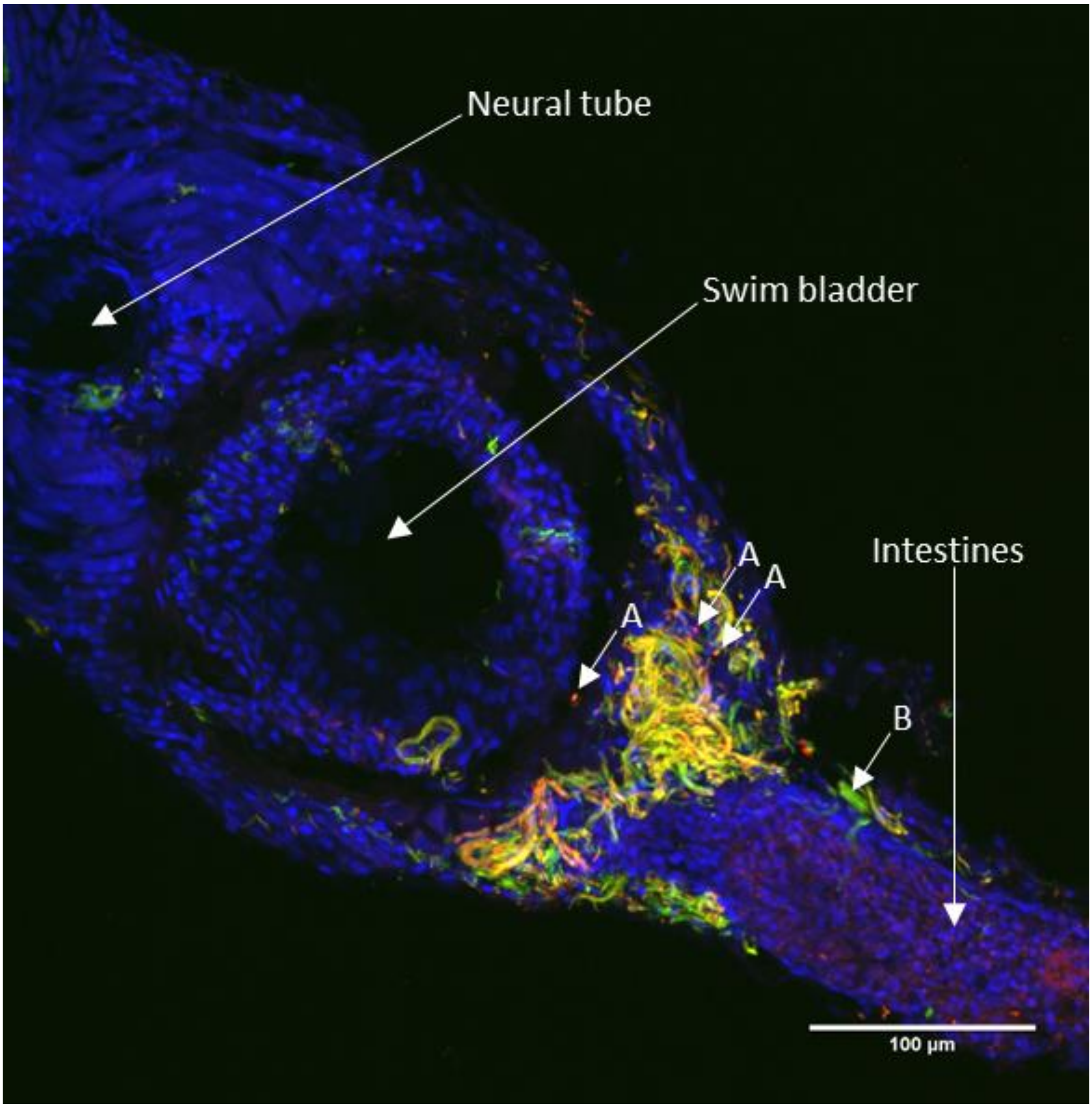

Figure 4.24: *Illustrative image (20X lens) of a transversal section of a zebrafish embryo, which was intravenously infected with GFP/mKO M.m, and subsequently mKO-induced with an ATc (~5 nL, 500 µg/mL) injection into the posterior cardinal vein at 5 days-post infection. DAPI stained cells are shown in blue while M.m are visualized in green (GFP), red (mKO) or yellow (GFP, mKO co-localization). (A)Bacteria that appear to express mKO coupled with faint expression of GFP. (B) Bacteria only expressing GFP, indicating area of low metabolic activity.*

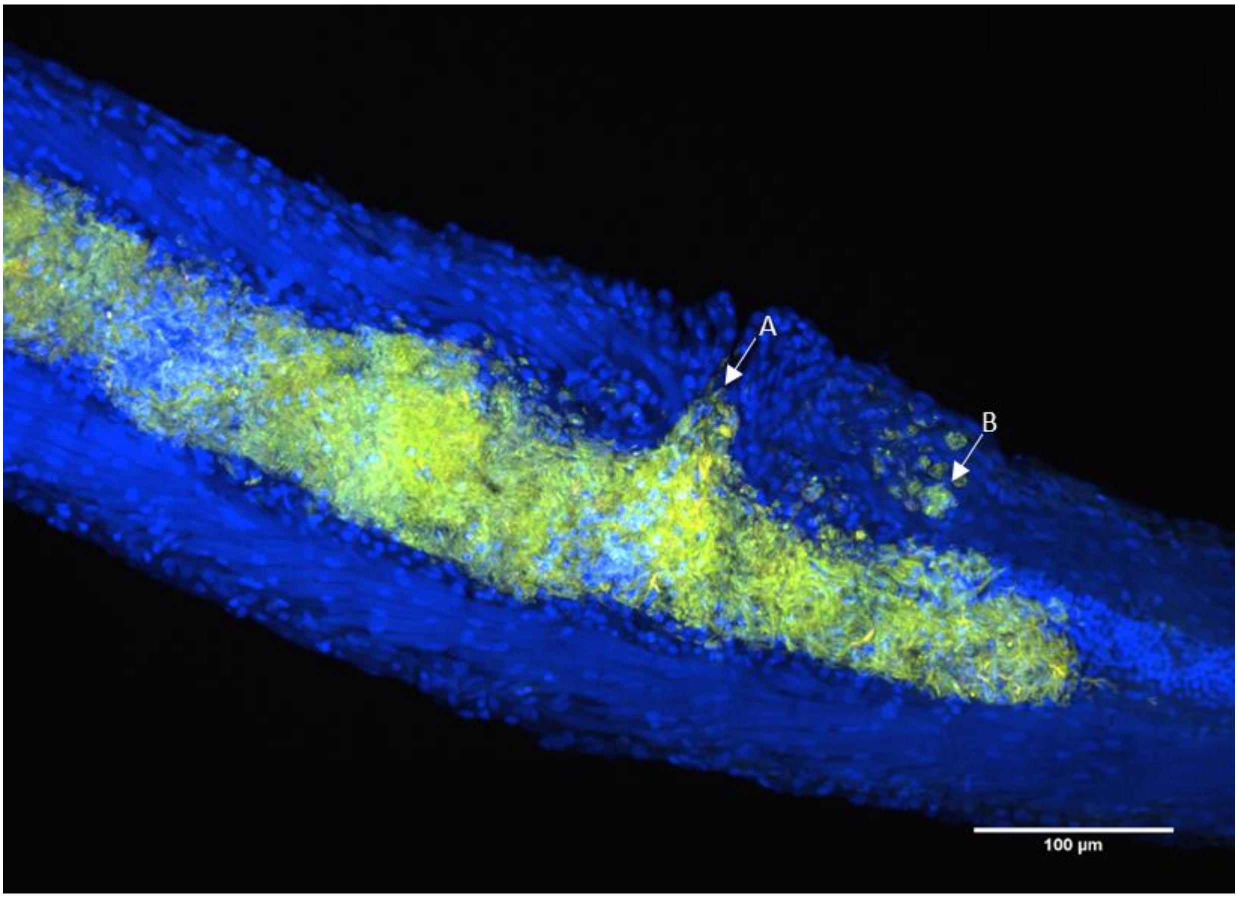

Figure 4.25: *Illustrative image (20X lens) of coronal section of a zebrafish embryo, which was infected via the neural tube with GFP/mKO M.m, and subsequently mKO-induced with an ATc (~5 nL, 500 µg/mL) injection into the posterior cardinal vein at 4 days-post infection. DAPI stained cells are shown in blue and M.m is visualized in green (GFP), red (mKO) or yellow (GFP, mKO co-localization). (A) Bacteria in the process of protruding out of the embryo, which will eventually lead to cavity formation. (B) Area of infection were the bacteria appear to be in a low metabolically state compared to the bacteria seen elsewhere (weak mKO expression).*

5 Discussion

5.1 So many nanoparticles, so few approved

The global nanomedicine market was valued at over 130 billion US dollars in 2016, with an estimated annual growth rate of 14 % through 2022 [170]. At the end of 2017, over 200,000 scientific papers had been published on the subject [96], and the vast majority of the efforts in the field had been in cancer research. These numbers reflect the extensive research in nanomedicine, and the potential benefit it offers compared to conventional medicine. The effort is paying off as multiple studies have shown reduced toxicity and increased therapeutic effect from NP formulation of various drugs in animal models during preclinical studies, including for treatment of TB [171]. However, the road from bench to bedside for NP-based drugs is long and complicated. Venditto et al. have evocatively summarized this problem in the title of a 2013 review: “Cancer Nanomedicines: So many papers and so few drugs!” [172]. Since the FDA approved the first treatment based on nanomedicine in 1992, there are only around 50 approved nanomedicine based formulations, and even fewer NP-based formulations approved for clinical use in humans today [96]. Polymeric micelles, the type of NP most extensively used in this thesis, only appears in two clinically approved treatments. One is against cancer, named Genexol-PM®, approved in South Korea and under evaluation in the US [173]. The other is Estrasorb, a topical emulsion against hot flushes associated with menopause [174].

This illustrates the fact that despite all the research done, the transition into clinical approval remains challenging. Especially evident is the gap between academia, that initially develop new NP formulations, and the commercial interests, that need to scale up production and maintain reproducible and stable products [175]. Our group argues that the road from bench to bedside could be significantly improved by introducing an intermediate screening stage between *in vitro* characterizations and testing in the mouse preclinical models. As explained in more detail below, this intermediate stage is the zebrafish.

5.2 The zebrafish as an intermediate model

For all new drugs and treatments, the preclinical evaluation stage is a requirement before progression into human clinical trials. Preclinical evaluation includes data on the drug itself in addition to animal studies with data on toxicity and efficacy. So far, there are no specific regulations for either preclinical or clinical testing of NP-based drugs and treatments. The same regulations apply as for conventional drug testing [175]. The normal approach for preclinical testing starts with a thorough examination of the chemistry and manufacturing process of the drug in question. This involves analysis of composition, stability and physiochemical characterization. Additional parameters for NP formulations are size, homogeneity, surface characterization, morphology and drug loading [176]. When all these parameters are determined to be satisfactory, the next step is *in vitro* and *in vivo* testing and characterization. The aim of *in vitro* cell testing is to investigate the therapeutic efficacy, cellular uptake, drug release, toxicity, etc. These factors are investigated in order to establish some reference points for following the subsequent *in vivo* studies in an animal model. Only when each step goes well human clinical trials can be initiated.

The most commonly used model system is the mouse, which is also the case for anti-TB therapeutic research [118, 122]. The leap from *in vitro* to *in vivo* testing in mouse is big. A significant problem with the mouse model is its opacity. It is difficult to image cellular details at high resolution in a non-invasive manner. Additionally, there is a general trend for minimizing the use of mammals for biomedical research due ethical and financial considerations. This is especially relevant for nanomedicine, where multiple NP formulations need to be examined alone and in combination with the drug they encapsulate.

We therefore argue for the introduction of the embryonic zebrafish model to serve as an intermediate screening model that will create a foundation for reducing the subsequent numbers of mice required at the preclinical stage of drug testing. This intent would be in compliance with the 3Rs principle, that is recommended from an ethical perspective; replacement, reduction and refinement [177]. The zebrafish has proven its relevance in several medical research fields, resulting in numerous publications [135]. In a recent review, the potential of implementing the zebrafish as a screening tool for evaluating nanomaterials for efficacy and toxicity prior to rodent testing was specifically discussed [178], resonating perfectly with our vision. Our group is, to my knowledge, the only one specifically investigating NP formulations of conventional and experimental anti-TB drugs using the embryonic zebrafish model for fish-TB. Additionally, we apply sophisticated microscopy techniques to study the fate of NP *in vivo,* thereby providing a unique platform to investigate nano-sized drug carriers. Through collaboration with other groups, which specialize in different fields such as novel-drug synthesis, NP development and TB research in mice, we are now in the early stages of making our vision an established practice.

5.3 Nanoparticle mediated therapy against tuberculosis

Although the term nanomedicine was for many years heavily associated with, and almost synonymous with anti-cancer drug delivery, it is now recognized as a broader term. Still, there are far fewer publications on NP against TB relative to cancer. Nevertheless, the quality of the research done on TB has been impressive, as described in a review by Griffiths et al. [171]. A big advantage of NP-based treatment of TB compared to cancer is the macrophage. The bacteria causing TB use the macrophage as a host [31], thereby making macrophage uptake of NP a benefit instead of a hindrance, which is the case for cancer, where the macrophages remove the NP from circulation [104]. Despite this theoretical advantage for TB, no NP-based treatments have resulted in clinical trials to date [96, 179]. Additionally, the term nanomedicine is not discussed in the WHO global TB report 2017 [23]. This is in stark contrast to the promising, and occasionally even striking results from NP-based treatments against TB that have been reported in different animal models such as mice [115], guinea pigs [114] and zebrafish [116].

5.4 Two different strategies for treating tuberculosis with nanoparticles

There are two main mechanisms for targeted delivery of NP to TB granulomas, both are considered passive, but use different approaches. In short, these mechanisms can be summarized as: 1) short-circulating NP being taken up by macrophages, that migrate to the site of infection by chemotaxis in response to various chemical signals [40]. 2) long-circulating NP avoiding macrophage uptake stay in circulation longer and, over time passively accumulate at the site of infection, due to a higher degree of permeability in the vasculature surrounding the granuloma, a phenomenon called the enhanced permeability and retention (EPR) effect [101].

Our group started exploring the macrophage uptake strategy in zebrafish, infecting and administering NP via the bloodstream, following the pioneering work of Ramakrishnan group [42]. The results showed rapid NP uptake by infected and non-infected macrophages, in addition to an impressive therapeutic effect of drug in NP formulations [116]. Recently, we have established a new strategy for TB, where the EPR effect is investigated as a targeting approach. In a paper recently submitted by our group and currently under review, the EPR-like strategy for NP targeting of the granuloma was investigated. For these experiments, the site of bacterial infection is in the neural tube (NT) and NP, which are subsequently injected into the blood circulation, accumulate significantly in the NT granuloma. Whereas in the blood granulomas, that are small and dynamic, NT granulomas are much larger, more stable and have a number of features that much more resemble human TB granulomas. Among these, NT granulomas exhibit new growing vessels in response to local hypoxia and undergo cavity formation leading to the release of bacteria to the outer medium (Fenaroli et al., in revision, ACS Nano). This is highly reminiscent of the mechanism by which *M.tb* is released from necrotic cavities in humans via the airways. The work described in this thesis started before we became aware of the neural tube infection model. Therefore, in the majority of the experiments we conducted, as summarized below, both infection and treatment are administered via the blood circulation.

5.5 Toxicity and therapy

Four analogues of pretomanid were tested in this thesis; 30485 (A), 32625 (B), 31354 (C) and 32499 (D) respectively. As already mentioned, I refer to these drugs as A-D for simplicity. All have been tested in polymeric micelle formulation. Additionally, C was also tested in a PEG-PLA formulation.

We initially started studying drugs A and B, while drugs C and D were sent from New Zealand to our lab a few months later. Our New Zealand collaborators had already carried out *in vitro* testing against *M.tb*. We therefore started the analysis by testing their efficacy against *M.m in vitro*. Drug A was more potent than B in inhibiting *M.m* growth *in vitro* during the dose-response assay. However, both drugs displayed significantly lower inhibitory effects against *M.m* than had been reported earlier against *M.tb* by our collaborators [87-89]. When we later received drugs C and D and tested their *in vitro* effects against *M.m*, a similar trend was observed; *M.m* was more resistant to the drugs than what had been reported for *M.tb*. This trend was also evident in one study that investigated the efficacy of the parental compound pretomanid as well as a number of related analogues. In all cases, *M.tb* was more susceptible than *M.m in vitro* [180]. Nevertheless, the same study observed good *in vivo* efficacy when the free drugs were administered as a treatment to *M.m* infected zebrafish embryos. It is important to note that the embryos in that study were naturally infected by immersion, a practice our lab deems unreliable, and treatment was administered by adding dissolved drug to the water. Regardless, the peculiar observation of poor *in vitro* and good *in vivo* efficacy is not understood, and requires more examination. Currently, our group is working on analyzing nitric oxide (NO) release from the novel-drug analogues, *in vitro*, in *M.m* and BCG cultures. Preliminary results have indicated lower levels of NO release in *M.m* cultures compared to BCG. Our goal is to analyze NO generation and release *in vivo* using the zebrafish embryo. Perhaps this approach can provide a possible answer to the difference in susceptibility of *M.m* when in culture or in an animal, such as the zebrafish.

During the *in vivo* toxicity screen, drug A was found to be significantly more toxic against zebrafish embryos than drug B. Drug A resulted in severe toxicity in both free (45 mg/kg) and polymeric micelle NP (200 mg/kg) formulation. At 45 mg/kg in NP formulation, drug A had a similar toxic effect as drug B in NP formulation, where the dose was 200 mg/kg. In addition to identifying drug B as the compound of choice for more detailed studies, we also showed that NP encapsulation of these drugs significantly reduced toxicity. Reduction of toxicity is a key argument for NP-based treatments and has been shown multiple times, for instance in the study by Vibe et al. [181]. Therefore, it was important to establish that the polymeric micelle NP used in this thesis reduced the toxicity of the encapsulated drug.

An aspect worth mentioning regarding the free drugs is the problems we experienced in dissolving and injecting them into the zebrafish. All four drugs tested are hydrophobic, and therefore very challenging to dissolve and inject at relevant concentrations. Initially, we used dimethyl sulfoxide (DMSO) as the solvent, which is a commonly used agent for dissolving hydrophobic compounds. Before we started, there were hardly any data on administering DMSO for zebrafish drug delivery intravenously. We therefore needed to carry out a systematic testing to find the highest dose of DMSO that the zebrafish embryo could tolerate, when injected into blood circulation. This analysis showed that the embryos could tolerate as much as 10 nL of a solution comprising 60 % DMSO; a small number of deaths did occur within the first 24 h. However, the majority survived without severe signs of toxicity.

In the treatment studies all three (B, C and D) drugs had a significant therapeutic effect in *M.m* infected embryos, compared to the infected control group and the group given empty NP (drug A was not tested for therapy due to toxicity). These drugs had a similar efficacy, but drug D nevertheless stood out as the most potent one. Drug B in polymeric micelle NP formulation was tested at doses that ranged from 22.5 to 75 mg/kg. All doses had a protective effect and a clear dose response was observed, with 45 mg/kg being sufficient for high overall survival. Drugs C and D were only tested at a dose of 60 mg/kg, with excellent therapeutic outcome.

Due to mechanical difficulties injecting the free formulation of the drugs, drug B is the only compound thoroughly tested in its free form and compared to NP formulation in treatment experiments. Dissolved in DMSO, drug B had no therapeutic protection; rather we observed a synergistic negative effect of the free drug in combination with DMSO and infection. The situation drastically improved when PEG400 was used for dissolving and injecting the drug in combination with DMSO. In this formulation drug B displayed a therapeutic effect, nevertheless drug B when encapsulated in polymeric micelle NP was significantly better. Improved efficacy relative to free drug is another key argument for NP formulation, and it was therefore important to show this effect for at least one of the drugs in question. Further testing with drugs C and D needs to be carried out, in which free versus NP formulation is carefully compared.

It should be added that injections in human patients of free drugs, when dissolved in solutions comprising high concentrations of PEG400 or DMSO, are unlikely to be accepted. This is because both solvents have displayed toxicity in mice, below the concentrations that would be needed for effective drug delivery [182, 183]. Toxic response against high doses of PEG400 is a possible explanation for the three deaths amongst mice treated with free drug in the mouse treatment experiment performed by our collaborators. A systematic study in mice focusing on the toxicity of the most commonly used solvents for drug delivery via intravenous injection found that PEG400 at 5640 mg/kg, a dose comparable to that used in our mouse treatment experiment, had considerable toxic effects [184]. However, the use of such high doses of PEG400 was needed to be able to deliver free drug at the same dose as given in the NP formulation. A possible solution is to try PEG400-DMSO (4:1 ratio) as a vehicle instead. Our observation in zebrafish embryos is that this solution is well tolerated, as long as the injection volume does not exceed 4 nL. Additionally, the study mentioned above reported on less severe toxicity using this solution compared to PEG400 alone [184]. DMSO makes the solution much less viscous, thereby making the mixture easier and safer to inject. When injecting zebrafish embryos, pure PEG400 is too viscous for the small injection needle and not possible to be used alone.

Pretomanid, which is currently in clinical trials phase III, is well characterized regarding safety and efficacy doses against TB infection in mice [185] and humans [186, 187]. Daily oral administration of 100 mg/kg pretomanid has shown similar efficacy as monotherapies of moxifloxacin at 100 mg/kg, isoniazid at 25 mg/kg or rifampicin at 20 mg/kg, in mice infected with *M.tb* [188]. Combinatorial therapies involving pretomanid have a similar bactericidal effect in mice and humans [189-191], thereby strengthening the relevance of the mouse model when testing anti-TB drugs. Additionally, it has been shown in zebrafish embryos that concentrations of diverse compounds that cause toxicity are comparable to the toxicity in rodents, e.g. mice [192]. This is yet another piece of evidence supporting our hypothesis that data in zebrafish can be predictive of the situation occurring in mice. The work in this thesis further strengthens the link between the zebrafish and the mouse, as described next.

The therapeutic outcome and doses of novel-drug analogues tested in this thesis are indeed comparable between my experiments in zebrafish and in mice by our collaborators. The zebrafish received single therapeutic doses (22.5-75 mg/kg) one day post-infection. In the NP formulation, all doses displayed a protective effect against the fish-TB infection. The mice in the treatment experiment received four injections of drug B, in NP or free form. Here, one injection corresponded to a drug dose of 90 mg/kg, assuming an average weight of 20 grams for each mouse. This is only slightly higher than the doses given to zebrafish on an mg per kg body weight basis. Although no statistical significance was detected between mice in the untreated control group and groups receiving drug B, a decrease in CFU was evident. Additionally, statistical significance was detected between the day 24 day infection input group and mice treated with drug B in NP formulation, an improvement not seen in any other treatment group. Altogether, the data suggest that therapeutic outcome in mice can be predicted by preliminary zebrafish studies, therefore further strengthening the relevance of the embryonic zebrafish model as an intermediate screening system prior to mouse studies.

5.6 Fluorescent bacteria to study dynamics of the granuloma

Thanks to David G. Russell (Cornell University, USA), I had the opportunity to work with an exciting new plasmid in combination with *M.m*. This plasmid applied the Tet-On technology for the expression of a fluorescent protein, monomeric Kusabira Orange (mKO). Tet-On refers to a specific variant of a transcriptional activation system, which is controlled by the antibiotic tetracycline or a similar derivative, e.g. ATc. In the Tet-On system, gene transcription and subsequent protein expression is activated in the presence of a Tet-inducer [156].

The final aim of this thesis was therefore to establish a new model to study the fate of bacteria residing within a granuloma by taking advantage of the transcriptional control system. The first report on developing and applying the Tet-On system in mycobacteria for controlled protein expression in cell culture came in 2004 [161] while the use of Tet-On in transgenic zebrafish was first reported in 2005 [159]. Until now, there have been no studies using the Tet-On technology on transgenic *M.m* in zebrafish. In this thesis, we therefore focused on the latter, by infecting zebrafish embryos with genetically modified *M.m* having two fluorescent markers, where GFP (green) is constitutively expressed and mKO (red) is only expressed upon Tet induction. Therefore, when exposed to the inducer, only metabolically active bacteria will be able to express the red marker.

The results so far have provided proof of concept for visualizing the induction of mKO *in vivo*, where confocal microscopy has allowed to analyze the differences in metabolic state of bacteria residing within the same granuloma. Taken together these results encourage further development of the Tet-On system for *M.m* and suggest that this new tool could be used to assess the fitness of mycobacteria following treatment with our drugs encapsulated in NP or in free form.

6 Concluding remarks

There is a gap between *in vitro* cell analysis and more advanced models, e.g. the mouse, for preclinical drug testing today. This is especially true for nanomedicine, which requires extensive data on both drug and vehicle by themselves in addition to the combinatorial formulations. Therefore, the work provided in this thesis, where the embryonic zebrafish model is being introduced as an intermediate stage, is potentially of great relevance to the nanomedicine field.

We have shown that the embryonic zebrafish model is a useful screening system for anti-TB drugs prior to mice preclinical studies, both for drug safety and efficacy purposes. In this way, we contribute to the 3Rs principle by reducing the number of experimental mice needed. Our hypothesis of zebrafish relevance in anti-TB drug research is supported by our demonstration that screening of novel TB-drugs, in NP or free formulation, in the zebrafish, followed by mice studies by our collaborators, had comparable therapeutic outcome.

We have thoroughly examined the safety and efficacy of four novel-drug analogues of the parental drug pretomanid, both *in vitro* and *in vivo* following encapsulation by NP. Drug B was additionally tested in its free form, and NP formulation was superior in both safety and therapeutic outcome. In addition, we have identified the drug of choice to move forward with, namely drug D.

We have additionally been able to establish a new model, combining genetically modified *M.m* and zebrafish embryos that allow closer examination *in vivo* of the metabolic state of bacteria within a granuloma over time. Although, still in the early stages of refinement, it has so far revealed promise as a useful tool in practice.

7 Future perspectives

In April this year (2018), our group arranged a meeting in Oslo with all our collaborators on a joint project, which is tightly linked to the drugs tested in this thesis and other related compounds. The main goal of the project is to improve the treatment of TB by NP delivery in order to reduce adverse effects, increase efficacy and shorten treatment duration. The meeting set the stage for the future work ahead.

Refinement of the NP encapsulation process in order to achieve a higher degree of particle homogeneity and reduced level of non-encapsulated drug is a priority. In all cases, it is essential to make a thorough examination of the physical and chemical characteristics of the NP to be tested. An additional goal is the introduction of second-generation NP, where core-crosslinking and drug-particle covalent (reversible) conjugation is performed for increased particle stability and improved drug release kinetics.

Testing, in zebrafish embryos, of free drugs (C and D) using PEG400-DMSO as a solvent compared to NP formulation is a priority as well. A pilot experiment with neural tube infection and treatment with drug D has already been undertaken. Additionally, treatment administered at a later stage than 24 h post-infection is an intriguing concept. This approach would illustrate whether or not the novel-drugs could lead to granuloma regression rather than simply inhibition of granuloma formation and expansion.

The mortality associated with free drug delivery to mice in the preliminary experiment carried out by our collaborators at Cornell University needs to be clarified and dealt with. The most likely scenario would be to administer lower doses of drug so that reduced amounts of excipients is needed for dissolving the free drug. Hopefully, this will lead to safer administration of free drug as a comparative control to the NP formulations.

Finally, further development of the new model of GFP/mKO *M.m* within a granuloma is required. Specifically, new protocols will be made in order to better study how the infection progresses over time and how the bacteria respond, metabolically, to the infection and subsequent treatment.

8 Supplementary

8.1 Supplementary recipes

8.1.1 Maintenance of *M. marinum*

The following listed protocols were prepared as described by Gao and Manoranjan [153]. Deionized, distilled water was used, written as H_2O for simplicity.

ADC growth supplement

The following components were combined, under constant stirring at RT, in a 1 L glass bottle with a screw cap:

- 4.25 g NaCl
- 25 g bovine serum albumin fraction V
- 10 g D-glucose
- 15 mg catalase

H_2O was added until the final volume of 500 mL was reached. Subsequently, pH was adjusted to 7.0 using 1 M NaOH and the solution was then passed through a 0.20 µm filter for sterilization. The solution can be stored at 4 °C for up to one month. Catalase was added, due to its capability to degrade oxygen intermediates such as H_2O_2, produced by growing mycobacteria [153].

OADC growth supplement

In a 1 L glass bottle with a screw cap, 15 mL of oleic acid solution* were added to 485 mL of ADC while stirring. Subsequently, pH was adjusted to 7.0 using 1 M NaOH and the solution was then passed through a 0.20 µm filter for sterilization. The prepared mixture can be stored at 4 °C for up to one month.

*Oleic acid solution: Combine and mix 2.4 mL oleic acid and 2.4 mL of 6 M NaOH to 120 mL H_2O. Stored at 4 °C for up to one year.

***M.m* freezing medium**

The following components were combined, under constant stirring at RT, in a 250 mL glass bottle with a screw cap:

- 60 mL glycerol
- 1 mL 10 % (v/v) Tween 80

The solution was then passed through a 0.20 µm filter in order to sterilize and has to be stored at 4 °C for up to one month.

7H9 liquid culture medium

For 1 L of liquid medium, the following components were combined in a 1 L glass bottle with a screw cap:

- 891 mL H_2O
- 4.7 g Difco Middlebrook 7H9 broth
- 4 mL glycerol
- 5 mL 10 % (v/v) Tween 80
- 100 mL ADC growth supplement

The solution was passed through a 0.20 µm filter in order to sterilize. Another approach, commonly used in our lab, was to dissolve 7H9 broth powder and glycerol in water and store this at 4 °C. Then, when setting up bacterial cultures, appropriate amounts of ADC growth supplement and Tween 80 was added to 20 mL of 7H9 stock using a 0.20 µm filter.

7H10 agar plates

In a 2 L glass bottle with a screw cap, 19 g Difco Middlebrook 7H10 agar powder was dissolved in 895 mL of H_2O during constant stirring. The subsequent solution was heated until it reached the boiling point, was then autoclaved and left to cool. At a controlled temperature of 50 °C using a hot plate, 100 mL of OADC growth supplement were added while stirring. At this time point, antibiotics were introduced if needed. 20 mL solution was poured in each of the 10 cm petri dishes, and kept at room temperature for 2 days. The dishes were stored bottom-side-up in sealed plastic bags at 4 °C for up to two months.

8.1.2 Maintenance of zebrafish embryos

The following listed protocols were prepared as described in "The zebrafish book", written by Monte Westerfield [137]. Deionized, distilled water was used, written as H_2O for simplicity.

Zebrafish embryo water

For 1 L of embryo water, the following components were combined in a 1 L glass bottle with a screw cap:

- 10 mL Hank's Stock #1
- 1 mL Hank's Stock #2
- 10 mL Hank's Stock #4
- 10 mL Hank's Stock #5
- 10 mL fresh Hank's Stock #6
- 959 mL H_2O

The solution was adjusted to pH 7.2 using 1 M NaOH and subsequently autoclaved. The embryo water can be stored indefinitely at 4 °C and always needs to be pre-heated to 28.5 °C before use with zebrafish embryos.

Hank's Stock solutions

Stock #1

- 8.0 g NaCl
- 0.4 g KCl
- 100 mL H_2O

Stock #2

- 0.358 g Na_2HPO_4 anhydrous
- 0.600 g KH_2PO_4
- 100 mL H_2O

Stock #4

- 0.72 g $CaCl_2$
- 50 mL H_2O

Stock #5

- 0.601 g $MgSO_4$
- 50 mL H_2O

Stock #6

- 0.35 g $NaHCO_3$
- 10 mL H_2O

Tricaine stock solution

Tricaine methanesulfonate came in a powdered form. The solution was made by combining the following components in a 500 mL glass bottle with a screw cap:

- 400 mg tricaine powder
- 97.9 mL H_2O
- 2.1 mL 1 M TrisCl buffer (pH 9)*
- Adjust to pH 7.2

Stored at 4 °C for up to one month.

* TrisCl buffer:

a) 121.1 g Tris base (Sigma-Aldrich, St. Louis, MO, USA)

b) 700 mL H_2O

c) 70 mL 1 M HCl

Combine a) and b) by stirring, add c) to raise the pH until 7.2. Add b) until the total volume is 1 L.

Tricaine stock solution has a final concentration of 4 mg/mL. 1 mL of this mixture was added to 20 mL of embryo water, making the final tricaine concentration for sedation 190 µg/mL.

PTU stock solution

The solution was made by combining the following components in a 500 mL glass bottle with a screw cap:

- 120 mg N-Phenylthiourea (PTU)
- 200 mL zebrafish embryo water

PTU is difficult to completely dissolve, and require several hours with constant stirring. Store at 4 °C for up to one month.

8.2 Supplementary nanoparticle information

Table 8.1: *Complete list of polymeric micelles with corresponding information.*

Batch name	Drug loaded	Date of shipment (Germany to Norway)	Total concentration [mg/mL]
OSA.1	30485 (A)	~ 08.2016	66 (10 % drug)
OSA.3	30485 (A)	~ 08.2016	66 (30 % drug)
OSB.1	32625 (B)	~ 08.2016	66 (10 % drug)
OSB.3	32625 (B)	~ 08.2016	66 (30 % drug)
KS112B	32625 (B)	12.06.2017	25 (30 % drug)
KS117	-	28.06.2017	25 (polymer only)
KS125	32499 (D)	09.08.2017	20 (30 % drug)
KS124	31354 (C)	09.08.2017	20 (30 % drug)
KS132A	-	15.09.2017	50 (polymer only)
KS132B	32625 (B)	15.09.2017	50 (30 % drug)
KS135	-	17.10.2017	52 (polymer only)
KS136	32625 (B)	17.10.2017	60 (30 % drug)
KS137	AF647	17.10.2017	50 (4 % AF647)
KS149	32625 (B)	10.01.2018	25 (30 % drug)
KS150	31354 (C)	10.01.2018	25 (30 % drug)
KS151	32499 (D)	10.01.2018	25 (30 % drug)
KS152	-	10.01.2018	25 (polymer only)

8.3 Plasmid maps

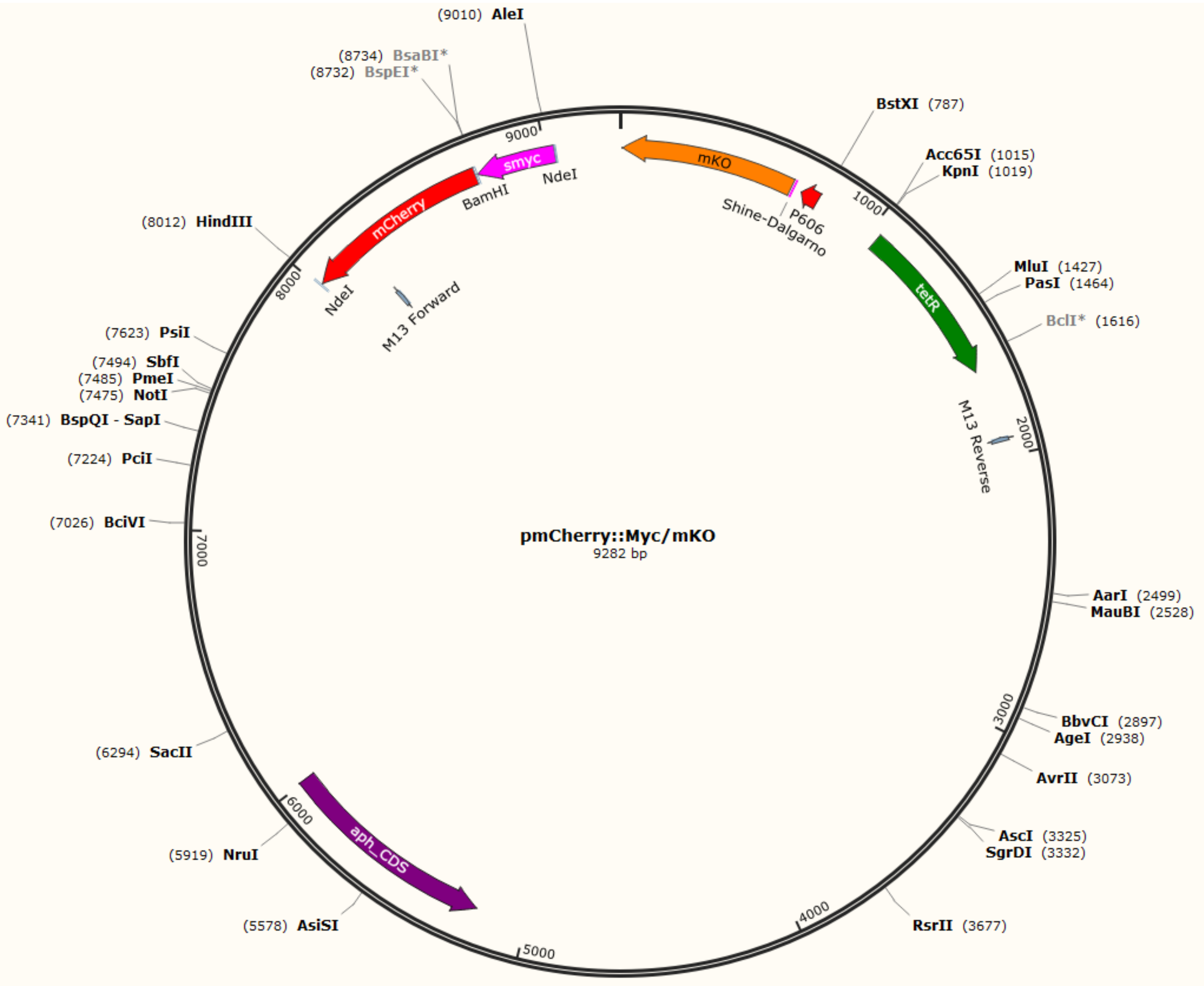

Figure 8.1: *Plasmid map of pmCherry::Myc/mKO, showing restriction sites and relevant genes. Provided by David G. Russell.*

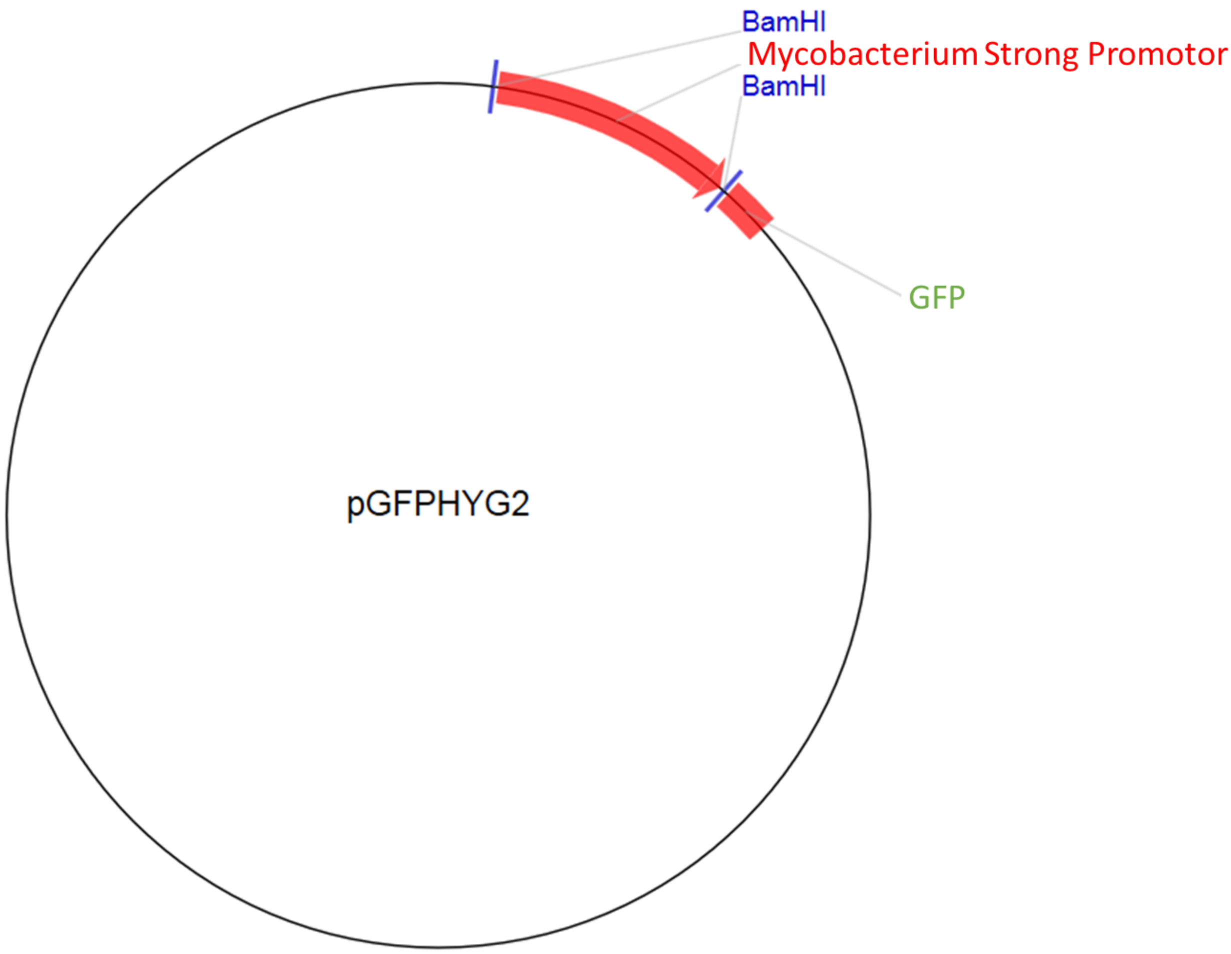

Figure 8.2: *Simplified plasmid map of pGFPHYG2, showing GFP and its promotor, plus restriction sites. Modified from https://www.addgene.org/30173/.*

8.4 Methodological considerations

Zebrafish embryos as a model system: The EU Directive 2010/63/EU on the protection of animals used for scientific purposes states that the ability of independent feeding is considered the stage from which experimental regulations apply to the zebrafish. This means that until independent feeding occurs, which is considered to be 120 h post-fertilization, the zebrafish embryo is not protected as an animal [193]. However, for experiments exceeding 120 h post-fertilization, a detailed application procedure and approval is required.

Although the zebrafish embryo possesses a large arsenal of qualities that make it a relevant and important model, it also has some drawbacks worth considering. The microinjection procedure is demanding and necessitates special equipment in addition to trained personnel to produce reliable data. A much simpler alternative to microinjection is natural infection by adding *M.m* directly into the water with the embryos. However, this results in a weak infection where the bacteria only colonize the gills and temporary the gut before being expelled. In addition, the infection does not kill the embryos so the experimental setup is dependent on fluorescent bacteria for measuring the therapeutic effect [180].

Controlling the therapeutic dose via measuring the size of the droplet is difficult, and a minor variation in size will change the injected dose (Fig. 3.3 and Table 3.2). This potential for variance therefore represents a technical variable that always ought to be considered. In addition, treatment experiments also contain two biological variables, the zebrafish embryo itself and the injected bacteria. The quality of the embryos can vary from batch to batch and the virulence of the bacteria varies from culture to culture. In practice, the experimenter is dependent on a healthy batch of embryos and a virulent bacteria culture for a successful experiment; we have had to terminate several experiments for these reasons.

Finally, there is an aspect about the fluorescent pixel count experiments worth mentioning. When using level of fluorescence as an indicator of bacterial burden and thereby therapeutic effect, it is important to be aware of the fact that this is an indirect approach. We kept record on day-to-day mortality in addition to measuring the fluorescence, thereby having a second set of data to compare and support the fluorescence data.

9 References

1. Hayman, J., *Mycobacterium ulcerans: an infection from Jurassic time?* Lancet, 1984. **2**(8410): p. 1015-6.
2. Stinear, T.P., et al., *Comparative genetic analysis of Mycobacterium ulcerans and Mycobacterium marinum reveals evidence of recent divergence.* J Bacteriol, 2000. **182**(22): p. 6322-30.
3. Alexander, K.A., et al., *Novel Mycobacterium tuberculosis complex pathogen, M. mungi.* Emerg Infect Dis, 2010. **16**(8): p. 1296-9.
4. Gutierrez, M.C., et al., *Ancient origin and gene mosaicism of the progenitor of Mycobacterium tuberculosis.* PLoS Pathog, 2005. **1**(1): p. e5.
5. Gutacker, M.M., et al., *Genome-wide analysis of synonymous single nucleotide polymorphisms in Mycobacterium tuberculosis complex organisms: resolution of genetic relationships among closely related microbial strains.* Genetics, 2002. **162**(4): p. 1533-43.
6. Sreevatsan, S., et al., *Restricted structural gene polymorphism in the Mycobacterium tuberculosis complex indicates evolutionarily recent global dissemination.* Proc Natl Acad Sci U S A, 1997. **94**(18): p. 9869-74.
7. Hughes, A.L., R. Friedman, and M. Murray, *Genomewide pattern of synonymous nucleotide substitution in two complete genomes of Mycobacterium tuberculosis.* Emerg Infect Dis, 2002. **8**(11): p. 1342-6.
8. Baker, O., et al., *Human tuberculosis predates domestication in ancient Syria.* Tuberculosis (Edinb), 2015. **95 Suppl 1**: p. S4-S12.
9. Hershkovitz, I., et al., *Detection and Molecular Characterization of 9000-Year-Old Mycobacterium tuberculosis from a Neolithic Settlement in the Eastern Mediterranean.* Plos One, 2008. **3**(10).
10. Nerlich, A.G., et al., *Molecular evidence for tuberculosis in an ancient Egyptian mummy.* Lancet, 1997. **350**(9088): p. 1404.
11. Salo, W.L., et al., *Identification of Mycobacterium tuberculosis DNA in a pre-Columbian Peruvian mummy.* Proc Natl Acad Sci U S A, 1994. **91**(6): p. 2091-4.
12. Murray, J.F., H.L. Rieder, and A. Finley-Croswhite, *The King's Evil and the Royal Touch: the medical history of scrofula.* Int J Tuberc Lung Dis, 2016. **20**(6): p. 713-6.
13. Daniel, T.M., *The history of tuberculosis.* Respir Med, 2006. **100**(11): p. 1862-70.
14. Daniel, T.M., *Rene Theophile Hyacinthe Laennec and the founding of pulmonary medicine.* Int J Tuberc Lung Dis, 2004. **8**(5): p. 517-8.
15. Koch, R., *Die Aetiologie der Tuberkulose.* Berliner Klinischen Wochenschrift, 1882(15): p. 221-230.
16. Kunst, H., *Diagnosis of latent tuberculosis infection: the potential role of new technologies.* Respir Med, 2006. **100**(12): p. 2098-106.
17. Calmette, A., *Preventive Vaccination Against Tuberculosis with BCG.* Proc R Soc Med, 1931. **24**(11): p. 1481-90.
18. Behr, M.A., et al., *Comparative genomics of BCG vaccines by whole-genome DNA microarray.* Science, 1999. **284**(5419): p. 1520-3.
19. Okkels, L.M. and P. Andersen, *Protein-protein interactions of proteins from the ESAT-6 family of Mycobacterium tuberculosis.* J Bacteriol, 2004. **186**(8): p. 2487-91.

20. Renshaw, P.S., et al., *Conclusive evidence that the major T-cell antigens of the Mycobacterium tuberculosis complex ESAT-6 and CFP-10 form a tight, 1 : 1 complex and characterization of the structural properties of ESAT-6, CFP-10, and the ESAT-6-CFP-10 complex - Implications for pathogenesis and virulence.* Journal of Biological Chemistry, 2002. **277**(24): p. 21598-21603.
21. Schatz, A., E. Bugie, and S.A. Waksman, *Streptomycin, a substance exhibiting antibiotic activity against gram positive and gram-negative bacteria.* Proceedings of the Society for Experimental Biology and Medicine, 1944. **55**(1): p. 66-69.
22. Vynnycky, E. and P.E. Fine, *Interpreting the decline in tuberculosis: the role of secular trends in effective contact.* Int J Epidemiol, 1999. **28**(2): p. 327-34.
23. *Global tuberculosis report 2017*. 2017, World Health Organization: Geneva.
24. Dye, C., et al., *Consensus statement. Global burden of tuberculosis: estimated incidence, prevalence, and mortality by country. WHO Global Surveillance and Monitoring Project.* JAMA, 1999. **282**(7): p. 677-86.
25. Lin, P.L. and J.L. Flynn, *Understanding latent tuberculosis: a moving target.* J Immunol, 2010. **185**(1): p. 15-22.
26. Andrews, J.R., et al., *Risk of progression to active tuberculosis following reinfection with Mycobacterium tuberculosis.* Clin Infect Dis, 2012. **54**(6): p. 784-91.
27. Comstock, G.W., V.T. Livesay, and S.F. Woolpert, *The prognosis of a positive tuberculin reaction in childhood and adolescence.* Am J Epidemiol, 1974. **99**(2): p. 131-8.
28. Zumla, A., et al., *Tuberculosis.* N Engl J Med, 2013. **368**(8): p. 745-55.
29. Selwyn, P.A., et al., *Clinical manifestations and predictors of disease progression in drug users with human immunodeficiency virus infection.* N Engl J Med, 1992. **327**(24): p. 1697-703.
30. Kaur, D., et al., *Chapter 2: Biogenesis of the cell wall and other glycoconjugates of Mycobacterium tuberculosis.* Adv Appl Microbiol, 2009. **69**: p. 23-78.
31. Dannenberg, A.M., *Pathogenesis of Human Pulmonary Tuberculosis: Insights from the Rabbit Model*. 2006: ASM Press.
32. Wells, W.F., H.L. Ratcliffe, and C. Grumb, *On the mechanics of droplet nuclei infection; quantitative experimental air-borne tuberculosis in rabbits.* Am J Hyg, 1948. **47**(1): p. 11-28.
33. Dannenberg, A.M., Jr., et al., *A histochemical study of phagocytic and enzymatic functions of rabbit mononuclear and polymorphonuclear exudate cells and alveolar macrophages. I. Survey and quantitation of enzymes, and states of cellular activation.* J Cell Biol, 1963. **17**: p. 465-86.
34. Shi, C. and E.G. Pamer, *Monocyte recruitment during infection and inflammation.* Nat Rev Immunol, 2011. **11**(11): p. 762-74.
35. Urdahl, K.B., S. Shafiani, and J.D. Ernst, *Initiation and regulation of T-cell responses in tuberculosis.* Mucosal Immunol, 2011. **4**(3): p. 288-93.
36. Lawrence, C.W. and T.J. Braciale, *Activation, differentiation, and migration of naive virus-specific CD8+ T cells during pulmonary influenza virus infection.* J Immunol, 2004. **173**(2): p. 1209-18.
37. Chackerian, A.A., et al., *Dissemination of Mycobacterium tuberculosis is influenced by host factors and precedes the initiation of T-cell immunity.* Infection and Immunity, 2002. **70**(8): p. 4501-4509.
38. Russell, D.G., *Who puts the tubercle in tuberculosis?* Nat Rev Microbiol, 2007. **5**(1): p. 39-47.
39. Ramakrishnan, L., *Revisiting the role of the granuloma in tuberculosis.* Nat Rev Immunol, 2012. **12**(5): p. 352-66.

40. Davis, J.M. and L. Ramakrishnan, *The role of the granuloma in expansion and dissemination of early tuberculous infection.* Cell, 2009. **136**(1): p. 37-49.
41. Volkman, H.E., et al., *Tuberculous granuloma formation is enhanced by a mycobacterium virulence determinant.* PLoS Biol, 2004. **2**(11): p. e367.
42. Davis, J.M., et al., *Real-time visualization of mycobacterium-macrophage interactions leading to initiation of granuloma formation in zebrafish embryos.* Immunity, 2002. **17**(6): p. 693-702.
43. Hunter, R.L., *Tuberculosis as a three-act play: A new paradigm for the pathogenesis of pulmonary tuberculosis.* Tuberculosis, 2016. **97**: p. 8-17.
44. Kumar, A., et al., *Redox homeostasis in mycobacteria: the key to tuberculosis control?* Expert Rev Mol Med, 2011. **13**: p. e39.
45. Ghon, A., *The seat, size and form of the primary lung rang among the infant and child tuberculosis.* Virchows Archiv Fur Pathologische Anatomie Und Physiologie Und Fur Klinische Medizin, 1925. **254**(3): p. 734-750.
46. Blacklock, J.W., *The Primary Lung Focus of Tuberculosis in Children.* Proc R Soc Med, 1932. **25**(5): p. 725-33.
47. Leong, F.J., Dartois, V., Dick, T., *A Color Atlas of Comparative Pathology of Pulmonary Tuberculosis*. 2011: CRC Press.
48. Hunter, R.L., *Pathology of post primary tuberculosis of the lung: an illustrated critical review.* Tuberculosis (Edinb), 2011. **91**(6): p. 497-509.
49. Barry, C.E., et al., *The spectrum of latent tuberculosis: rethinking the biology and intervention strategies.* Nature Reviews Microbiology, 2009. **7**(12): p. 845-855.
50. Rustad, T.R., et al., *Hypoxia: a window into Mycobacterium tuberculosis latency.* Cellular Microbiology, 2009. **11**(8): p. 1151-1159.
51. Singh, V., et al., *Mycobacterium tuberculosis-driven targeted recalibration of macrophage lipid homeostasis promotes the foamy phenotype.* Cell Host Microbe, 2012. **12**(5): p. 669-81.
52. Russell, D.G., et al., *Foamy macrophages and the progression of the human tuberculosis granuloma.* Nat Immunol, 2009. **10**(9): p. 943-8.
53. Hunter, R.L., C. Jagannath, and J.K. Actor, *Pathology of postprimary tuberculosis in humans and mice: contradiction of long-held beliefs.* Tuberculosis (Edinb), 2007. **87**(4): p. 267-78.
54. Mcdonough, K.A. and Y. Kress, *Cytotoxicity for Lung Epithelial-Cells Is a Virulence-Associated Phenotype of Mycobacterium-Tuberculosis.* Infection and Immunity, 1995. **63**(12): p. 4802-4811.
55. Levin, R., S. Grinstein, and J. Canton, *The life cycle of phagosomes: formation, maturation, and resolution.* Immunological Reviews, 2016. **273**(1): p. 156-179.
56. Ernst, J.D., *Macrophage receptors for Mycobacterium tuberculosis.* Infect Immun, 1998. **66**(4): p. 1277-81.
57. Armstrong, J.A. and P.D. Hart, *Response of cultured macrophages to Mycobacterium tuberculosis, with observations on fusion of lysosomes with phagosomes.* J Exp Med, 1971. **134**(3 Pt 1): p. 713-40.
58. Deretic, V., et al., *Mycobacterium tuberculosis inhibition of phagolysosome biogenesis and autophagy as a host defence mechanism.* Cell Microbiol, 2006. **8**(5): p. 719-27.
59. Sweet, L., et al., *Mannose Receptor-Dependent Delay in Phagosome Maturation by Mycobacterium avium Glycopeptidolipids.* Infection and Immunity, 2010. **78**(1): p. 518-526.
60. Rink, J., et al., *Rab conversion as a mechanism of progression from early to late endosomes.* Cell, 2005. **122**(5): p. 735-749.

61. Via, L.E., et al., *Arrest of mycobacterial phagosome maturation is caused by a block in vesicle fusion between stages controlled by rab5 and rab7.* Journal of Biological Chemistry, 1997. **272**(20): p. 13326-13331.
62. Armstrong, J.A. and P.D. Hart, *Phagosome-lysosome interactions in cultured macrophages infected with virulent tubercle bacilli. Reversal of the usual nonfusion pattern and observations on bacterial survival.* J Exp Med, 1975. **142**(1): p. 1-16.
63. Gomes, M.S., et al., *Survival of Mycobacterium avium and Mycobacterium tuberculosis in acidified vacuoles of murine macrophages.* Infect Immun, 1999. **67**(7): p. 3199-206.
64. Pethe, K., et al., *Isolation of Mycobacterium tuberculosis mutants defective in the arrest of phagosome maturation.* Proc Natl Acad Sci U S A, 2004. **101**(37): p. 13642-7.
65. Zumla, A., P. Nahid, and S.T. Cole, *Advances in the development of new tuberculosis drugs and treatment regimens.* Nat Rev Drug Discov, 2013. **12**(5): p. 388-404.
66. Espinal, M.A., et al., *Standard short-course chemotherapy for drug-resistant tuberculosis: treatment outcomes in 6 countries.* JAMA, 2000. **283**(19): p. 2537-45.
67. Bass, J.B., Jr., et al., *Treatment of tuberculosis and tuberculosis infection in adults and children. American Thoracic Society and The Centers for Disease Control and Prevention.* Am J Respir Crit Care Med, 1994. **149**(5): p. 1359-74.
68. Roy, A., et al., *Effect of BCG vaccination against Mycobacterium tuberculosis infection in children: systematic review and meta-analysis.* Bmj-British Medical Journal, 2014. **349**.
69. Andersen, P. and T.M. Doherty, *The success and failure of BCG - implications for a novel tuberculosis vaccine.* Nat Rev Microbiol, 2005. **3**(8): p. 656-62.
70. Lawrence, R. and E. Jeyakumar, *Antimicrobial resistance: a cause for global concern.* BMC Proc, 2013. **7**(Suppl 3): p. S1.
71. Chung-Delgado, K., et al., *Mortality among MDR-TB Cases: Comparison with Drug-Susceptible Tuberculosis and Associated Factors.* Plos One, 2015. **10**(3).
72. Chung-Delgado, K., et al., *Factors associated with anti-tuberculosis medication adverse effects: a case-control study in Lima, Peru.* PLoS One, 2011. **6**(11): p. e27610.
73. Suarez, P.G., et al., *Feasibility and cost-effectiveness of standardised second-line drug treatment for chronic tuberculosis patients: a national cohort study in Peru.* Lancet, 2002. **359**(9322): p. 1980-9.
74. Velayati, A.A., et al., *Emergence of new forms of totally drug-resistant tuberculosis bacilli: super extensively drug-resistant tuberculosis or totally drug-resistant strains in iran.* Chest, 2009. **136**(2): p. 420-425.
75. Eldholm, V. and F. Balloux, *Antimicrobial Resistance in Mycobacterium tuberculosis: The Odd One Out.* Trends Microbiol, 2016. **24**(8): p. 637-648.
76. Zhang, Y., *Persisters, persistent infections and the Yin-Yang model.* Emerg Microbes Infect, 2014. **3**(1): p. e3.
77. Adams, K.N., et al., *Drug tolerance in replicating mycobacteria mediated by a macrophage-induced efflux mechanism.* Cell, 2011. **145**(1): p. 39-53.
78. Sarathy, J.P., et al., *Extreme Drug Tolerance of Mycobacterium tuberculosis in Caseum.* Antimicrob Agents Chemother, 2018. **62**(2).
79. Agrawal, K.C., et al., *Potential radiosensitizing agents. Dinitroimidazoles.* J Med Chem, 1979. **22**(5): p. 583-6.
80. Nagarajan, K., et al., *Nitroimidazoles .21. 2,3-Dihydro-6-Nitroimidazo[2,1-B]Oxazoles with Antitubercular Activity.* European Journal of Medicinal Chemistry, 1989. **24**(6): p. 631-633.

81. Ashtekar, D.R., et al., *In vitro and in vivo activities of the nitroimidazole CGI 17341 against Mycobacterium tuberculosis.* Antimicrob Agents Chemother, 1993. **37**(2): p. 183-6.
82. Stover, C.K., et al., *A small-molecule nitroimidazopyran drug candidate for the treatment of tuberculosis.* Nature, 2000. **405**(6789): p. 962-6.
83. Manjunatha, U.H., et al., *Identification of a nitroimidazo-oxazine-specific protein involved in PA-824 resistance in Mycobacterium tuberculosis.* Proc Natl Acad Sci U S A, 2006. **103**(2): p. 431-6.
84. Manjunatha, U., H.I. Boshoff, and C.E. Barry, *The mechanism of action of PA-824: Novel insights from transcriptional profiling.* Commun Integr Biol, 2009. **2**(3): p. 215-8.
85. Singh, R., et al., *PA-824 kills nonreplicating Mycobacterium tuberculosis by intracellular NO release.* Science, 2008. **322**(5906): p. 1392-5.
86. Baptista, R., et al., *Untargeted metabolomics reveals a new mode of action of pretomanid (PA-824).* Sci Rep, 2018. **8**(1): p. 5084.
87. Palmer, B.D., et al., *Synthesis and structure-activity relationships for extended side chain analogues of the antitubercular drug (6S)-2-nitro-6-{[4-(trifluoromethoxy)benzyl]oxy}-6,7-dihydro-5H-imidazo[2,1-b][1, 3]oxazine (PA-824).* J Med Chem, 2015. **58**(7): p. 3036-59.
88. Palmer, B.D., et al., *Synthesis and structure-activity studies of biphenyl analogues of the tuberculosis drug (6S)-2-nitro-6-{[4-(trifluoromethoxy)benzyl]oxy}-6,7-dihydro-5H-imidazo[2,1-b][1, 3]oxazine (PA-824).* J Med Chem, 2010. **53**(1): p. 282-94.
89. Kmentova, I., et al., *Synthesis and structure-activity relationships of aza- and diazabiphenyl analogues of the antitubercular drug (6S)-2-nitro-6-{[4-(trifluoromethoxy)benzyl]oxy}-6,7-dihydro-5H-imidazo[2,1-b][1, 3]oxazine (PA-824).* J Med Chem, 2010. **53**(23): p. 8421-39.
90. Ntshangase, S., et al., *The downfall of TBA-354 - a possible explanation for its neurotoxicity via mass spectrometric imaging.* Xenobiotica, 2017: p. 1-7.
91. Panchagnula, R. and N.S. Thomas, *Biopharmaceutics and pharmacokinetics in drug research.* Int J Pharm, 2000. **201**(2): p. 131-50.
92. Chertok, B., et al., *Drug Delivery Interfaces in the 21st Century: From Science Fiction Ideas to Viable Technologies.* Molecular Pharmaceutics, 2013. **10**(10): p. 3531-3543.
93. Kreuter, J., *Nanoparticles--a historical perspective.* Int J Pharm, 2007. **331**(1): p. 1-10.
94. Khanna, S.C., T. Jecklin, and P. Speiser, *Bead polymerization technique for sustained-release dosage form.* J Pharm Sci, 1970. **59**(5): p. 614-8.
95. Birrenbach, G. and P.P. Speiser, *Polymerized Micelles and Their Use as Adjuvants in Immunology.* Journal of Pharmaceutical Sciences, 1976. **65**(12): p. 1763-1766.
96. Greish, K., Mathur, A., Bakhiet, M., Taurin, S., *Nanomedicine: is it lost in translation?* Therapeutic Delivery, 2018.
97. Watkins, R., et al., *Natural product-based nanomedicine: recent advances and issues.* Int J Nanomedicine, 2015. **10**: p. 6055-74.
98. Petros, R.A. and J.M. DeSimone, *Strategies in the design of nanoparticles for therapeutic applications.* Nat Rev Drug Discov, 2010. **9**(8): p. 615-27.
99. Harris, J.M. and R.B. Chess, *Effect of pegylation on pharmaceuticals.* Nat Rev Drug Discov, 2003. **2**(3): p. 214-21.
100. Lee, J.S., et al., *Circulation kinetics and biodistribution of dual-labeled polymersomes with modulated surface charge in tumor-bearing mice: comparison with stealth liposomes.* J Control Release, 2011. **155**(2): p. 282-8.

101. Matsumura, Y. and H. Maeda, *A new concept for macromolecular therapeutics in cancer chemotherapy: mechanism of tumoritropic accumulation of proteins and the antitumor agent smancs.* Cancer Res, 1986. **46**(12 Pt 1): p. 6387-92.
102. Maeda, H., H. Nakamura, and J. Fang, *The EPR effect for macromolecular drug delivery to solid tumors: Improvement of tumor uptake, lowering of systemic toxicity, and distinct tumor imaging in vivo.* Adv Drug Deliv Rev, 2013. **65**(1): p. 71-9.
103. Gao, W., et al., *Nanoparticle approaches against bacterial infections.* Wiley Interdiscip Rev Nanomed Nanobiotechnol, 2014. **6**(6): p. 532-47.
104. Blanco, E., H. Shen, and M. Ferrari, *Principles of nanoparticle design for overcoming biological barriers to drug delivery.* Nat Biotechnol, 2015. **33**(9): p. 941-51.
105. Kalluru, R., et al., *Poly(lactide-co-glycolide)-rifampicin nanoparticles efficiently clear Mycobacterium bovis BCG infection in macrophages and remain membrane-bound in phago-lysosomes.* Journal of Cell Science, 2013. **126**(14): p. 3043-+.
106. Kisich, K.O., et al., *Encapsulation of moxifloxacin within poly(butyl cyanoacrylate) nanoparticles enhances efficacy against intracellular Mycobacterium tuberculosis.* International Journal of Pharmaceutics, 2007. **345**(1-2): p. 154-162.
107. Anisimova, Y.V., et al., *Nanoparticles as antituberculosis drugs carriers: effect on activity against Mycobacterium tuberculosis in human monocyte-derived macrophages.* Journal of Nanoparticle Research, 2000. **2**(2): p. 165-171.
108. Datta, M., et al., *Anti-vascular endothelial growth factor treatment normalizes tuberculosis granuloma vasculature and improves small molecule delivery.* Proc Natl Acad Sci U S A, 2015. **112**(6): p. 1827-32.
109. Oehlers, S.H., et al., *Interception of host angiogenic signalling limits mycobacterial growth.* Nature, 2015. **517**(7536): p. 612-5.
110. Talelli, M., et al., *Core-Crosslinked Polymeric Micelles: Principles, Preparation, Biomedical Applications and Clinical Translation.* Nano Today, 2015. **10**(1): p. 93-117.
111. Moretton, M.A., et al., *Molecular implications in the nanoencapsulation of the anti-tuberculosis drug rifampicin within flower-like polymeric micelles.* Colloids and Surfaces B-Biointerfaces, 2010. **79**(2): p. 467-479.
112. Upadhyay, S., et al., *Conjugated and Entrapped HPMA-PLA Nano-Polymeric Micelles Based Dual Delivery of First Line Anti TB Drugs: Improved and Safe Drug Delivery against Sensitive and Resistant Mycobacterium Tuberculosis.* Pharm Res, 2017. **34**(9): p. 1944-1955.
113. Rao, J.P. and K.E. Geckeler, *Polymer nanoparticles: Preparation techniques and size-control parameters.* Progress in Polymer Science, 2011. **36**(7): p. 887-913.
114. Sharma, A., S. Sharma, and G.K. Khuller, *Lectin-functionalized poly (lactide-co-glycolide) nanoparticles as oral/aerosolized antitubercular drug carriers for treatment of tuberculosis.* J Antimicrob Chemother, 2004. **54**(4): p. 761-6.
115. Dutt, M. and G.K. Khuller, *Therapeutic efficacy of poly(DL-lactide-co-glycolide)-encapsulated antitubercular drugs against Mycobacterium tuberculosis infection induced in mice.* Antimicrobial Agents and Chemotherapy, 2001. **45**(1): p. 363-366.
116. Fenaroli, F., et al., *Nanoparticles as drug delivery system against tuberculosis in zebrafish embryos: direct visualization and treatment.* ACS Nano, 2014. **8**(7): p. 7014-26.
117. Russell, D.G., *The evolutionary pressures that have molded Mycobacterium tuberculosis into an infectious adjuvant.* Curr Opin Microbiol, 2013. **16**(1): p. 78-84.
118. Dharmadhikari, A.S. and E.A. Nardell, *What animal models teach humans about tuberculosis.* Am J Respir Cell Mol Biol, 2008. **39**(5): p. 503-8.

119. Kanesa-thasan, N., et al., *Ensuring the optimal safety of licensed vaccines: a perspective of the vaccine research, development, and manufacturing companies.* Pediatrics, 2011. **127 Suppl 1**: p. S16-22.
120. Via, L.E., et al., *Tuberculous granulomas are hypoxic in guinea pigs, rabbits, and nonhuman primates.* Infect Immun, 2008. **76**(6): p. 2333-40.
121. Bose, M., *Natural reservoir, zoonotic tuberculosis & interface with human tuberculosis: an unsolved question.* Indian J Med Res, 2008. **128**(1): p. 4-6.
122. Myllymaki, H., et al., *Animal models in tuberculosis research - where is the beef?* Expert Opin Drug Discov, 2015. **10**(8): p. 871-83.
123. Kramnik, I., P. Demant, and B.B. Bloom, *Susceptibility to tuberculosis as a complex genetic trait: analysis using recombinant congenic strains of mice.* Genetics and Tuberculosis, 1998. **217**: p. 120-137.
124. Driver, E.R., et al., *Evaluation of a mouse model of necrotic granuloma formation using C3HeB/FeJ mice for testing of drugs against Mycobacterium tuberculosis.* Antimicrob Agents Chemother, 2012. **56**(6): p. 3181-95.
125. Lenaerts, A., C.E. Barry, 3rd, and V. Dartois, *Heterogeneity in tuberculosis pathology, microenvironments and therapeutic responses.* Immunol Rev, 2015. **264**(1): p. 288-307.
126. Padilla-Carlin, D.J., D.N. McMurray, and A.J. Hickey, *The guinea pig as a model of infectious diseases.* Comp Med, 2008. **58**(4): p. 324-40.
127. Smith, T., *A Comparative Study of Bovine Tubercle Bacilli and of Human Bacilli from Sputum.* J Exp Med, 1898. **3**(4-5): p. 451-511.
128. Lurie, M.B., *The Fate of Human and Bovine Tubercle Bacilli in Various Organs of the Rabbit.* J Exp Med, 1928. **48**(2): p. 155-82.
129. Manabe, Y.C., et al., *Different strains of Mycobacterium tuberculosis cause various spectrums of disease in the rabbit model of tuberculosis.* Infect Immun, 2003. **71**(10): p. 6004-11.
130. Mendez, S., et al., *Susceptibility to tuberculosis: composition of tuberculous granulomas in Thorbecke and outbred New Zealand White rabbits.* Vet Immunol Immunopathol, 2008. **122**(1-2): p. 167-74.
131. Capuano, S.V., 3rd, et al., *Experimental Mycobacterium tuberculosis infection of cynomolgus macaques closely resembles the various manifestations of human M. tuberculosis infection.* Infect Immun, 2003. **71**(10): p. 5831-44.
132. Walsh, G.P., et al., *The Philippine cynomolgus monkey (Macaca fascicularis) provides a new nonhuman primate model of tuberculosis that resembles human disease.* Nature Medicine, 1996. **2**(4): p. 430-436.
133. Spence, R., et al., *The behaviour and ecology of the zebrafish, Danio rerio.* Biological Reviews, 2008. **83**(1): p. 13-34.
134. Streisinger, G., et al., *Production of clones of homozygous diploid zebra fish (Brachydanio rerio).* Nature, 1981. **291**(5813): p. 293-6.
135. Lieschke, G.J. and P.D. Currie, *Animal models of human disease: zebrafish swim into view.* Nat Rev Genet, 2007. **8**(5): p. 353-67.
136. Ali, S., H.G. van Mil, and M.K. Richardson, *Large-scale assessment of the zebrafish embryo as a possible predictive model in toxicity testing.* PLoS One, 2011. **6**(6): p. e21076.
137. Westerfield, M., *The zebrafish book*. 5 ed. 2007, University of Oregon Press.
138. Tonjum, T., et al., *Differentiation of Mycobacterium ulcerans, M. marinum, and M. haemophilum: mapping of their relationships to M. tuberculosis by fatty acid profile analysis, DNA-DNA hybridization, and 16S rRNA gene sequence analysis.* J Clin Microbiol, 1998. **36**(4): p. 918-25.

139. Aronson, J.D., *Spontaneous tuberculosis in salt water fish.* Journal of Infectious Diseases, 1926. **39**: p. 315-320.
140. Clark, H.F. and C.C. Shepard, *Effect of Environmental Temperatures on Infection with Mycobacterium Marinum (Balnei) of Mice and a Number of Poikilothermic Species.* J Bacteriol, 1963. **86**: p. 1057-69.
141. Ramakrishnan, L., et al., *Mycobacterium marinum causes both long-term subclinical infection and acute disease in the leopard frog (Rana pipiens).* Infection and Immunity, 1997. **65**(2): p. 767-773.
142. Cosma, C.L., D.R. Sherman, and L. Ramakrishnan, *The secret lives of the pathogenic mycobacteria.* Annu Rev Microbiol, 2003. **57**: p. 641-76.
143. Stinear, T.P., et al., *Insights from the complete genome sequence of Mycobacterium marinum on the evolution of Mycobacterium tuberculosis.* Genome Res, 2008. **18**(5): p. 729-41.
144. Cosma, C.L., et al., *Zebrafish and frog models of Mycobacterium marinum infection.* Curr Protoc Microbiol, 2006. **Chapter 10**: p. Unit 10B 2.
145. Willett, C.E., et al., *Early hematopoiesis and developing lymphoid organs in the zebrafish.* Dev Dyn, 1999. **214**(4): p. 323-36.
146. Herbomel, P., B. Thisse, and C. Thisse, *Ontogeny and behaviour of early macrophages in the zebrafish embryo.* Development, 1999. **126**(17): p. 3735-45.
147. Swaim, L.E., et al., *Mycobacterium marinum infection of adult zebrafish causes caseating granulomatous tuberculosis and is moderated by adaptive immunity.* Infect Immun, 2006. **74**(11): p. 6108-17.
148. Saunders, B.M. and A.M. Cooper, *Restraining mycobacteria: Role of granulomas in mycobacterial infections.* Immunology and Cell Biology, 2000. **78**(4): p. 334-341.
149. Avdesh, A., et al., *Regular care and maintenance of a zebrafish (Danio rerio) laboratory: an introduction.* J Vis Exp, 2012(69): p. e4196.
150. Kimmel, C.B., et al., *Stages of embryonic development of the zebrafish.* Dev Dyn, 1995. **203**(3): p. 253-310.
151. Harris, J.R., *Negative staining of thinly spread biological samples.* Methods Mol Biol, 2007. **369**: p. 107-42.
152. Dubochet, J. and A.W. Mcdowall, *Vitrification of Pure Water for Electron-Microscopy.* Journal of Microscopy-Oxford, 1981. **124**(Dec): p. Rp3-Rp4.
153. Gao, L.Y. and J. Manoranjan, *Laboratory maintenance of Mycobacterium marinum.* Curr Protoc Microbiol, 2005. **Chapter 10**: p. Unit 10B 1.
154. Vibe, C.B., *Master's thesis: Nanoparticle-based delivery of efflux pump inhibitors and antibiotics to treat mycobacterial infections*, in *Department of Molecular Biosciences* 2014, University of Oslo: http://www.duo.uio.no.
155. Lawson, N.D. and B.M. Weinstein, *In vivo imaging of embryonic vascular development using transgenic zebrafish.* Dev Biol, 2002. **248**(2): p. 307-18.
156. Gossen, M., et al., *Transcriptional activation by tetracyclines in mammalian cells.* Science, 1995. **268**(5218): p. 1766-9.
157. Campbell, L.J., J.J. Willoughby, and A.M. Jensen, *Two types of Tet-On transgenic lines for doxycycline-inducible gene expression in zebrafish rod photoreceptors and a gateway-based tet-on toolkit.* PLoS One, 2012. **7**(12): p. e51270.
158. Gu, Q., et al., *Generation and characterization of a transgenic zebrafish expressing the reverse tetracycline transactivator.* J Genet Genomics, 2013. **40**(10): p. 523-31.
159. Huang, C.J., et al., *Conditional expression of a myocardium-specific transgene in zebrafish transgenic lines.* Dev Dyn, 2005. **233**(4): p. 1294-303.
160. Blokpoel, M.C., et al., *Tetracycline-inducible gene regulation in mycobacteria.* Nucleic Acids Res, 2005. **33**(2): p. e22.

161. Ehrt, S., et al., *Controlling gene expression in mycobacteria with anhydrotetracycline and Tet repressor.* Nucleic Acids Res, 2005. **33**(2): p. e21.
162. Tan, S.M., et al., *Mycobacterium tuberculosis Responds to Chloride and pH as Synergistic Cues to the Immune Status of its Host Cell.* Plos Pathogens, 2013. **9**(4).
163. Raschke, W.C., et al., *Functional macrophage cell lines transformed by Abelson leukemia virus.* Cell, 1978. **15**(1): p. 261-7.
164. Falzari, K., et al., *In vitro and in vivo activities of macrolide derivatives against Mycobacterium tuberculosis.* Antimicrob Agents Chemother, 2005. **49**(4): p. 1447-54.
165. White, R.M., et al., *Transparent adult zebrafish as a tool for in vivo transplantation analysis.* Cell Stem Cell, 2008. **2**(2): p. 183-189.
166. Trousil, J., et al., *System with embedded drug release and nanoparticle degradation sensor showing efficient rifampicin delivery into macrophages.* Nanomedicine, 2017. **13**(1): p. 307-315.
167. Chopra, I. and M. Roberts, *Tetracycline antibiotics: mode of action, applications, molecular biology, and epidemiology of bacterial resistance.* Microbiol Mol Biol Rev, 2001. **65**(2): p. 232-60 ; second page, table of contents.
168. Wallace, R.J., Jr. and K. Wiss, *Susceptibility of Mycobacterium marinum to tetracyclines and aminoglycosides.* Antimicrob Agents Chemother, 1981. **20**(5): p. 610-2.
169. Oliva, B., et al., *Evidence That Tetracycline Analogs Whose Primary Target Is Not the Bacterial Ribosome Cause Lysis of Escherichia-Coli.* Antimicrobial Agents and Chemotherapy, 1992. **36**(5): p. 913-919.
170. Evers, P., *Nanotechnology in Medical Applications: The Global Market*. 2017, bcc Research.
171. Griffiths, G., et al., *Nanobead-based interventions for the treatment and prevention of tuberculosis.* Nat Rev Microbiol, 2010. **8**(11): p. 827-34.
172. Venditto, V.J. and F.C. Szoka, *Cancer nanomedicines: So many papers and so few drugs!* Advanced Drug Delivery Reviews, 2013. **65**(1): p. 80-88.
173. Werner, M.E., et al., *Preclinical Evaluation of Genexol-PM, a Nanoparticle Formulation of Paclitaxel, as a Novel Radiosensitizer for the Treatment of Non-Small Cell Lung Cancer.* International Journal of Radiation Oncology Biology Physics, 2013. **86**(3): p. 463-468.
174. Simon, J.A. and E.S. Grp, *Estradiol in micellar nanoparticles: the efficacy and safety of a novel transdermal drug-delivery technology in the management of moderate to severe vasomotor symptoms.* Menopause-the Journal of the North American Menopause Society, 2006. **13**(2): p. 222-231.
175. Ragelle, H., et al., *Nanoparticle-based drug delivery systems: a commercial and regulatory outlook as the field matures.* Expert Opinion on Drug Delivery, 2017. **14**(7): p. 851-864.
176. Barenholz, Y., *Doxil (R) - The first FDA-approved nano-drug: Lessons learned.* Journal of Controlled Release, 2012. **160**(2): p. 117-134.
177. Tannenbaum, J. and B.T. Bennett, *Russell and Burch's 3Rs Then and Now: The Need for Clarity in Definition and Purpose.* Journal of the American Association for Laboratory Animal Science, 2015. **54**(2): p. 120-132.
178. Johnston, H.J., et al., *Adoption of in vitro systems and zebrafish embryos as alternative models for reducing rodent use in assessments of immunological and oxidative stress responses to nanomaterials.* Crit Rev Toxicol, 2018. **48**(3): p. 252-271.
179. Tiberi, S., et al., *New drugs and perspectives for new anti-tuberculosis regimens.* Pulmonology, 2018. **24**(2): p. 86-98.

180. Dalton, J.P., et al., *Screening of anti-mycobacterial compounds in a naturally infected zebrafish larvae model.* J Antimicrob Chemother, 2016.
181. Vibe, C.B., et al., *Thioridazine in PLGA nanoparticles reduces toxicity and improves rifampicin therapy against mycobacterial infection in zebrafish.* Nanotoxicology, 2016. **10**(6): p. 680-8.
182. Pellegrini, G., et al., *Intraperitoneal administration of high doses of polyethylene glycol (PEG) causes hepatic subcapsular necrosis and low-grade peritonitis with a rise in hepatic biomarkers.* Toxicology, 2013. **314**(2-3): p. 262-266.
183. Hanslick, J.L., et al., *Dimethyl sulfoxide (DMSO) produces widespread apoptosis in the developing central nervous system.* Neurobiology of Disease, 2009. **34**(1): p. 1-10.
184. Thackaberry, E.A., et al., *Solvent-based formulations for intravenous mouse pharmacokinetic studies: tolerability and recommended solvent dose limits.* Xenobiotica, 2014. **44**(3): p. 235-241.
185. Tyagi, S., et al., *Bactericidal activity of the nitroimidazopyran PA-824 in a murine model of tuberculosis.* Antimicrob Agents Chemother, 2005. **49**(6): p. 2289-93.
186. Diacon, A.H., et al., *Early bactericidal activity and pharmacokinetics of PA-824 in smear-positive tuberculosis patients.* Antimicrob Agents Chemother, 2010. **54**(8): p. 3402-7.
187. Ginsberg, A.M., et al., *Safety, tolerability, and pharmacokinetics of PA-824 in healthy subjects.* Antimicrob Agents Chemother, 2009. **53**(9): p. 3720-5.
188. Lenaerts, A.J., et al., *Preclinical testing of the nitroimidazopyran PA-824 for activity against Mycobacterium tuberculosis in a series of in vitro and in vivo models.* Antimicrob Agents Chemother, 2005. **49**(6): p. 2294-301.
189. Diacon, A.H., et al., *14-day bactericidal activity of PA-824, bedaquiline, pyrazinamide, and moxifloxacin combinations: a randomised trial.* Lancet, 2012. **380**(9846): p. 986-93.
190. Tasneen, R., et al., *Enhanced bactericidal activity of rifampin and/or pyrazinamide when combined with PA-824 in a murine model of tuberculosis.* Antimicrob Agents Chemother, 2008. **52**(10): p. 3664-8.
191. Nuermberger, E., et al., *Powerful bactericidal and sterilizing activity of a regimen containing PA-824, moxifloxacin, and pyrazinamide in a murine model of tuberculosis.* Antimicrob Agents Chemother, 2008. **52**(4): p. 1522-4.
192. Ducharme, N.A., et al., *Comparison of toxicity values across zebrafish early life stages and mammalian studies: Implications for chemical testing.* Reprod Toxicol, 2015. **55**: p. 3-10.
193. Strahle, U., et al., *Zebrafish embryos as an alternative to animal experiments-A commentary on the definition of the onset of protected life stages in animal welfare regulations.* Reproductive Toxicology, 2012. **33**(2): p. 128-132.